TIDAL INTERACTIONS IN BINARY ASTEROID SYSTEMS

A Dissertation

Presented to the Faculty of the Graduate School

of Cornell University

in Partial Fulfillment of the Requirements for the Degree of

Doctor of Philosophy

by

Patrick Alan Taylor

May 2009

TIDAL INTERACTIONS

IN BINARY ASTEROID SYSTEMS

Patrick Alan Taylor, Ph.D.

Cornell University 2009

Tidal evolution in binary asteroid systems is examined with the dynamics extended to systems with close orbits within 5 radii of the primary component, non-negligibly eccentric mutual orbits, and a non-spherical primary component. The use of tidal evolution to determine the material properties of asteroids in terms of the product of the rigidity (shear modulus) and specific tidal dissipation function shows binary systems in the main belt with 100-km scale primary components are consistent with monolithic or fractured rock. Near-Earth binaries must either be much weaker mechanically than their main belt cousins, as one would expect for heavily fractured or rubble pile bodies, or have been formed in the main belt prior to injection to the near-Earth region. The most important factor in determining material properties of an asteroid in this manner is uncertainty in the age of the binary. The formation of contact binary systems where the two components are in physical contact and rotate as a single body is shown to be caused by the lack of a valid, stable, fully despun, double synchronous mutual orbit. Whether this lack of a tidal end state is caused during the formation process, with non-spherical components, or through the reduction of the angular momentum of the system via a spin-down mechanism, contact binaries are preferentially produced with components of similar size as is observed by radar. Radar observations of near-Earth asteroid 2004 DC show it to be a binary system with an eccentric mutual orbit and an asynchronous secondary that may be tumbling chaotically. The spin state, shape, angular momentum content, and mutual orbit of 2004 DC all indicate that the system was produced via a

spin-up mechanism such as the YORP effect. The 2004 DC binary likely formed in essentially its current configuration and has not evolved significantly due to tides.

BIOGRAPHICAL SKETCH

Patrick Alan Taylor was born on November 25, 1981 in Annapolis, Maryland to Linda and James Taylor. His early education took him to such exotic locales near the Chesapeake Bay as Cape St. Claire Elementary School, Magothy River Middle School, Severn River Junior High School, and Broadneck Senior High School, graduating in 1999, before trekking westward into the wilderness to The University of Maryland at College Park. There, his interest in astronomy, specifically in celestial mechanics, grew as he earned a double degree with high honors in astronomy and physics in 2003, writing a senior thesis entitled "Orbital Evolution of Asteroidal Dust" summarizing his research with Dr. Sergei Ipatov at the National Aeronautics and Space Administration Goddard Space Flight Center under the advisement of University of Maryland at College Park faculty members Dr. Douglas P. Hamilton and Dr. Douglas C. Hamilton of the astronomy and physics departments, respectively. From Maryland, Patrick ventured northward to the frozen tundra of Ithaca, New York to attend graduate school in the Astronomy Department at Cornell University, where, after one year of studies, he began working with Dr. Jean-Luc Margot. His graduate work includes the first detection of the asteroidal YORP effect (a thermal torque due to sunlight), the discovery of binary asteroid 2004 DC with radar, and research on the dynamics of binary asteroids via tidal interactions. From Cornell, Patrick will endure a stark change in weather upon moving to La Isla del Encanto of Puerto Rico in the Caribbean to work as a Postdoctoral Associate in the Astronomy Department at the National Astronomy and Ionosphere Center's Arecibo Observatory.

To all those who believed in me.

ACKNOWLEDGEMENTS

This work was supported by NASA Planetary Astronomy grants NNG04GN31G and NNX07AK68G to Jean-Luc Margot. We thank the staffs of the Arecibo Observatory and the Goldstone Solar System Radar for their support in performing the observational portion of this work. The Arecibo Observatory is part of the National Astronomy and Ionosphere Center, which is operated by Cornell University under a cooperative agreement with the National Science Foundation. The Goldstone Solar System Radar is operated by the Jet Propulsion Laboratory under contract with NASA. I also wish to acknowledge the author of my favorite joke, whoever he or she may be:

Two nuns walk into a bar; the third one ducks.

TABLE OF CONTENTS

Biographical Sketch . . . iii
Dedication . . . iv
Acknowledgements . . . v
Table of Contents . . . vi
List of Tables . . . viii
List of Figures . . . ix

1 Introduction 1

2 Separated Binary Systems 5
2.1 Angular Momentum Content . . . 5
2.2 Contact Binary and Angular Momentum Limits . . . 7
2.3 Fully Despun, Double Synchronous Orbits . . . 8
2.4 Stability Limit of Synchronous Orbits . . . 11
2.5 Summary of Main Belt and Jupiter Trojan Binaries . . . 16
2.6 Summary of Near-Earth Binaries . . . 17
2.7 Synchronous Orbits About a Non-Spherical Primary . . . 23
2.7.1 Oblate Primary, $\alpha_3 < \alpha_2 = \alpha_1$ . . . 24
2.7.2 Prolate Primary, $\alpha_3 = \alpha_2 < \alpha_1$ . . . 29

3 Tidal Evolution of Close Binary Systems 33
3.1 Tidal Potential of Arbitrary Order . . . 33
3.2 Roche Limit . . . 36
3.3 External Potential of Arbitrary Order . . . 36
3.4 Tidal Torques on the Components . . . 40
3.5 Tidal Dissipation Function Q . . . 41
3.6 Orbit Expansion and Despinning for Close Orbits . . . 42

4 Material Properties of Binary Asteroids 47
4.1 Caveats . . . 47
4.2 Estimation of μQ for Binary Systems . . . 48
4.3 Main Belt and Jupiter Trojan Binaries . . . 49
4.4 Near-Earth Binaries . . . 53
4.5 Correction for Close Orbits . . . 61
4.6 Effect of Initial Separation . . . 62
4.7 Effect of Unequal Component Densities . . . 64
4.8 Effect of Solar Tides . . . 66
4.9 Effect of Unequal Material Properties . . . 67
4.10 Summary of Tidal Evolution in Circular Orbits . . . 68

5 Tidal Evolution with Non-negligible Eccentricity **69**
5.1 Tidal Evolution to Fourth Order in Eccentricity 69
5.2 Typical Signs for Lag Terms 73
5.3 The Eccentricity Problem 74

6 Contact Binary Formation and Disruption **79**
6.1 Contact Binary Population 79
6.2 Angular Momentum Content 80
6.3 Critical Rotation of a Contact Binary 82
6.4 Density Estimation of Contact Binaries 83
6.5 Formation Mechanisms 85
6.5.1 No Synchronous Orbit 86
6.5.2 Formation Through Spin-Down 87
6.6 Timescales for Recollapse 91

7 Physical Characterization of Near-Earth Binary Asteroid 2004 DC **96**
7.1 Radar Observations 96
7.2 Reflection Properties 101
7.3 Mutual Orbit 105
7.4 Mutual Event 107
7.5 Spin States of the Components 107
7.6 Is the Secondary Tumbling? 112
7.7 Shape Model 114
7.8 Tidal Evolution 118

8 Discussion **123**

A Integrals for Synchronous Orbits About Non-Spherical Primaries **127**

LIST OF TABLES

2.1 Physical properties of main belt and Jupiter Trojan binaries 18
2.2 Physical properties of near-Earth binaries 21

3.1 Necessary expansion orders for separations under $5R_{\rm p}$ 35

4.1 μQ values for main belt and Jupiter Trojan binaries 52
4.2 μQ values for near-Earth binaries 58

5.1 Lag angles and corresponding frequencies for eccentric tides 72

6.1 Lower limits on densities of candidate contact binaries 86

7.1 Radar observation masterlog for 2004 DC 98
7.2 Radar reflection properties of 2004 DC 106

LIST OF FIGURES

2.1 Synchronous orbits for various J/J' values 10
2.2 Direction of tidal evolution for systems with a specific J/J' value . . . 12
2.3 q vs. a/R_p for main belt and Jupiter Trojan binaries 19
2.4 q vs. a/R_p for near-Earth binaries 22
2.5 Synchronous orbits for an oblate shape with $J/J' = 0.5$ 26
2.6 Synchronous orbits for an oblate shape with $\gamma = 0.9$ 28
2.7 Synchronous orbits for a prolate shape (long axis) with $J/J' = 0.5$ . . . 30
2.8 Synchronous orbits for a prolate shape (intermediate axis) with $J/J' = 0.5$ 31

4.1 q vs. a/R_p with tidal timescales for main belt and Jupiter Trojan binaries 51
4.2 Tidal evolution of a $q = 0.001$ main belt binary 54
4.3 Tidal evolution of nearly equal-mass binary (90) Antiope 55
4.4 q vs. a/R_p with tidal timescales for near-Earth binaries 57
4.5 Tidal evolution of a $q = 0.1$ near-Earth binary 60
4.6 Effect of close orbit correction on calculation of μQ 63
4.7 Effect of initial separation on calculation of μQ 65

5.1 Regions where $\omega_p > n$, $\omega_p > 3n/2$, and $\omega_p > 2n$ for eccentric orbits . . 75

6.1 Rigidly rotating contact binary system 81
6.2 J/J' required to separate a contact binary 84
6.3 $\Delta J/J'$ required to collapse a binary to contact 90
6.4 Recollapse of a $q = 1$ binary to contact 93
6.5 Recollapse of a $q = 0.1$ binary to contact 94

7.1 Arecibo high-resolution delay-Doppler images of 2004 DC 102
7.2 Continuous wave spectra of 2004 DC (1 of 2) 103
7.3 Continuous wave spectra of 2004 DC (2 of 2) 104
7.4 2004 DC mutual event observed from Goldstone 108
7.5 Best-fit pole positions of 2004 DC primary 110
7.6 Data, fit, and sky projection of 2004 DC primary shape model 115
7.7 Shape model of the 2004 DC primary 116
7.8 Shape model of the 2004 DC secondary 117
7.9 Tidal evolution of 2004 DC with similar μQ values 120

CHAPTER 1

INTRODUCTION

Twenty years ago, Weidenschilling et al. (1989) asked "do asteroids have satellites?" Today, binary asteroids have been discovered in every dynamical class of small solar system bodies from near-Earth asteroids to Mars-crossers and main belt asteroids, among the Jupiter Trojans, and in the outer solar system in the Kuiper belt. Beginning with the Galileo spacecraft's serendipitous discovery of tiny moon Dactyl orbiting (243) Ida (Chapman et al., 1995) in 1993 while on its cruise to Jupiter and continuing with the success of radar, ground-based adaptive optics imaging, Hubble space telescope imaging, and high-precision lightcurve photometry, reviewed by Merline et al. (2002), Richardson and Walsh (2006),and Noll et al. (2008), now over 160 small solar system bodies are suspected to be binary or multiple sytems (compiled at http://www.johnstonsarchive.net/astro/asteroidmoons.html from references therein).

The Keplerian orbit of the two components of a binary systems about the common center of mass allows one to determine the mass of the system and, with an estimate of the component sizes, the (assumed equal) densities of the bodies. Density estimates combined with taxonomic classifications hint at the internal structure of the asteroids (Britt et al., 2002) where low densities of rocky bodies when compared to similarly classified meteorites with known bulk densities imply porous, fractured bodies or even rubblized gravitational aggregates of material rather than monolithic bodies. Such fundamental knowledge is otherwise unattainable without spacecraft missions to individual asteroids.

The binary fraction among near-Earth asteroids larger than 200 m in diameter is a substantial ~16% based on radar (Margot et al., 2002) and photometric (Pravec et al., 2006) observations meaning one in six near-Earth asteroids observed is, in fact, a binary

system. Such an observed binary fraction agrees with the ~15% binary fraction deduced by Bottke and Melosh (1996a,b) required to explain the number of doublet craters on the surfaces of Earth and Venus. The binary fraction in the main belt among 100-km scale asteroids is much lower at ~2% (Merline et al., 2002), but for small main belt asteroids under 10 km in diameter, the binary fraction may be comparable to that of near-Earth asteroids (Pravec et al., 2007). The binary fraction in the Kuiper belt appears to vary from as high as ~20% in the cold classical disk (Stephens and Noll, 2006) to as low as ~5% among the other dynamical classes (Petit and Mousis, 2004; Stephens and Noll, 2006).

The most probable binary formation mechanism differs for each population with near-Earth binaries forming through rotational disruption via spin-up by thermal torques due to sunlight (the YORP effect; Bottke et al., 2002; Walsh et al., 2008) or close planetary encounters (Richardson et al., 1998; Walsh and Richardson, 2006), 100 km-scale main belt binaries forming through subcatastrophic impacts (Durda et al., 2004), though 1 to 10 km-scale binaries in the inner main belt may form through YORP spin-up (Pravec and Harris, 2007), and Kuiper belt binaries forming through collisions or by a flavor of dynamical capture (see Noll et al. (2008) for a review). The observation of the YORP effect altering the spins of ~100 m near-Earth asteroid (54509) YORP (Taylor et al., 2007; Lowry et al., 2007), so named for its role in the confirmation of the YORP effect (Rubincam, 2000, and references therein), and the known binary (1862) Apollo (Kaasalainen et al., 2007) along with the inability of tidal disruption during close planetary encounters to account for more than 2% of the observed 16% near-Earth binary fraction (Walsh and Richardson, 2008), suggests the ubiquitous YORP torques could dominate the formation of near-Earth binaries. Studying the formation and subsequent evolution of binary asteroids is an indespensible method of learning about the past, present, and future of the asteroidal population and dynamical environment.

For well over 100 years, the question of how tides from the differential gravity between two objects affect the state of the system has fascinated scientists. Since the pioneering work by Darwin (1879, 1880) on the interaction between the Earth and Moon, the study of tides has experienced its own ebb and flow, resurging in the mid-20th century with more general works on the rotation of Earth by Munk and MacDonald (1960), the effect of tides on small eccentricities in planet-satellite systems by Jeffreys (1961) and Goldreich (1963), improved tidal formulations for studying the evolution of the Earth-Moon system by MacDonald (1964), Kaula (1964), and Goldreich (1966), and on generalized tidal interactions between the planets and their satellites that led to advances in the understanding of planetary interiors by Goldreich and Soter (1966) among many others. With the discovery in the last 15 years that minor planets from asteroids to Kuiper belt objects can have moons, interest in the tidal problem has resurged once more (Taylor and Margot, 2007; Marchis et al., 2008a,b) to understand the interior structure of minor planets where the problem has scaled down to a smaller size, but the same physics act on these binary systems.

The tidal interaction between the components of binary minor planet systems is examined in terms of dynamical evolution of the mutual orbit. Chapter 2 introduces the basic dynamics of a binary asteroid system and the possible end states of the tidal interaction between the components. Chapter 3 discusses in depth the tidal evolution of the mutual orbit of a binary asteroid with special attention paid to close orbits within a handful of radii of the primary component. Chapter 4 applies tidal evolution to well-characterized binary systems to gain insight toward the internal properties of asteroids in terms of rigidity and energy dissipation. Chapter 5 discusses how a non-negligible eccentricity for the mutual orbit of a binary can affect its evolution. Chapter 6 analyzes how tidal evolution can lead to the formation of contact binaries with a preference for similarly-sized components. Chapter 7 describes the properties of near-Earth binary as-

teroid 2004 DC including its eccentric mutual orbit and attempts to decipher how the system evolved to its present state and how it will subsequently evolve in the future.

CHAPTER 2

SEPARATED BINARY SYSTEMS

We describe the angular momentum distribution in binary asteroid systems and introduce the subsets of main belt and near-Earth binaries that will be examined in later chapters. We also place dynamical and stability limits on the evolution of binary systems via tides and derive the location of fully despun, double synchronous tidal end states where the rotation rates of both components equal the mean motion of the mutual orbit for both spherical and non-spherical components.

2.1 Angular Momentum Content

The most important quantity in describing the interaction between the components of a binary system is the angular momentum. It is the distribution and transfer of angular momentum through the system that ultimately give one information on the formation and evolution of the system. The dynamics of a binary system with primary and secondary components of masses $M_{\rm p}$ and $M_{\rm s}$, repectively, in a mutual orbit about their common center of mass can be described equivalently by a system where a secondary of mass $M_{\rm p}M_{\rm s}/(M_{\rm p}+M_{\rm s})$ orbits a stationary primary mass, $M_{\rm p}+M_{\rm s}$. The orbital angular momentum of such a system is $L = M_{\rm p}M_{\rm s}/(M_{\rm p}+M_{\rm s})\sqrt{G(M_{\rm p}+M_{\rm s})a(1-e^2)}$ where G is the gravitational constant and a and e are the semimajor axis and eccentricity of the mutual orbit, respectively. Rewriting the orbital angular momentum in terms of the component mass ratio $q = M_{\rm s}/M_{\rm p} \leq 1$ and the volumetric equivalent primary radius $R_{\rm p}$ (the radius of the primary if its volume were cast into the shape of a sphere) we have

$$L = \frac{q}{(1+q)^{1/2}}\left(\frac{a}{R_{\rm p}}\right)^{1/2}\left(1-e^2\right)^{1/2}\sqrt{GM_{\rm p}^3R_{\rm p}}. \tag{2.1}$$

In terms of the total mass $M_{\rm tot} = M_{\rm p}+M_{\rm s}$ and effective system radius $R_{\rm eff} = (R_{\rm p}^3+R_{\rm s}^3)^{1/3} = \left(1+\frac{\rho_{\rm p}}{\rho_{\rm s}}q\right)^{1/3} R_{\rm p}$, where $R_{\rm s}$ is the volumetric equivalent radius of the secondary and $\rho_{\rm p}$ and $\rho_{\rm s}$ are the uniform mass densities of the components derived from the ratio of the individual masses and volumes, the orbital angular momentum is re-written as

$$L = \frac{q}{(1+q)^2}\left(1+\frac{\rho_{\rm p}}{\rho_{\rm s}}q\right)^{-1/6}\left(\frac{a}{R_{\rm p}}\right)^{1/2}\left(1-e^2\right)^{1/2}\sqrt{GM_{\rm tot}^3 R_{\rm eff}}. \tag{2.2}$$

Using Kepler's Third Law, $n^2a^3 = G\left(M_{\rm p}+M_{\rm s}\right)$, the orbital angular momentum may also be written in terms of the mean motion n as

$$L = \frac{q}{(1+q)^2}M_{\rm tot}a^2n\left(1-e^2\right)^{1/2} = \frac{q}{1+q}M_{\rm p}a^2n\left(1-e^2\right)^{1/2}. \tag{2.3}$$

The spin angular momentum is given by the moments of inertia $I = \alpha MR^2$ of the components and their spin rates ω as

$$S = I_{\rm p}\omega_{\rm p} + I_{\rm s}\omega_{\rm s} = \alpha_{\rm p}M_{\rm p}R_{\rm p}^2\omega_{\rm p}\left(1+\frac{\alpha_{\rm s}}{\alpha_{\rm p}}\left(\frac{\rho_{\rm p}}{\rho_{\rm s}}\right)^{2/3}q^{5/3}\frac{\omega_{\rm s}}{\omega_{\rm p}}\right). \tag{2.4}$$

The coefficient α is 2/5 for a uniform density, rotating sphere, but varies with the shape of the body and the density profile of the interior.

For comparison, suppose a rapidly-spinning parent body sheds mass in such a way to conserve angular momentum and produce the aforementioned mutually-orbiting binary system. If the spherical body with radius R, mass M, and uniform density spins at the breakup rate $\omega_{\rm break}$ without cohesion among its constituent particles, the inward force per unit mass of gravity at the equator, $F_g = GM/R^2$, is balanced by the outward centrifugal force per unit mass, $F_c = \omega_{\rm break}^2 R$, due to rotation such that $\omega_{\rm break} = \sqrt{GM/R^3}$. The angular momentum contained in the critically-rotating sphere is $I_{\rm sphere}\omega_{\rm break}$ or

$$J = \frac{2}{5}\sqrt{GM_{\rm tot}^3 R_{\rm eff}}, \tag{2.5}$$

where the mass and radius of the parent body have been written as the total mass and effective radius of the binary system produced by the breakup of the parent body. Subsequently, the total angular momentum of a binary system $J = L + S$ is often normalized by $J' = \sqrt{GM_{\rm tot}^3 R_{\rm eff}}$ (*e.g.*, Canup (2005); Noll et al. (2008)) such that $J/J' \sim 0.4$ indicates that the binary could have formed by mass shedding from the spin-up of a single spherical strengthless parent body. Pravec and Harris (2007) normalize the total angular momentum by that of the critically-rotating sphere (Equation 2.5) such that their scaling parameter $\alpha_{\rm L} = (J/J')/0.4$, and $\alpha_{\rm L} = 1$ has the same implication for binary formation. We will use the J' normalization throughout the following text.

2.2 Contact Binary and Angular Momentum Limits

The minimum and maximum separations of two components in a binary system are limited by the physical size of the components and the total angular momentum of the system, respectively. The separation of two components is naturally bounded from below by the contact condition where, at a separation of $R_{\rm p} + R_{\rm s}$, the components are resting against one another. In terms of the semimajor axis and the radius of the primary, the contact binary limit is

$$\left(\frac{a}{R_{\rm p}}\right)_{\rm min} = 1 + \frac{R_{\rm s}}{R_{\rm p}} = 1 + \left(\frac{\rho_{\rm p}}{\rho_{\rm s}}\, q\right)^{1/3}. \tag{2.6}$$

For components of similar density, the contact limit ranges from $a/R_{\rm p} = 1$ to 2, akin to a pea resting on the surface of a beach ball and two beach balls in contact, respectively.

An upper bound is placed on the separation of the components by the total angular momentum content of the system. If the entire budget of angular momentum $J = (J/J') \sqrt{GM_{\rm tot}^3 R_{\rm eff}}$ is transferred to the mutual orbit of the components, which are no longer spinning ($S \rightarrow 0$), the maximum attainable separation according to Equation (2.2) with $e = 0$ is

$$\left(\frac{a}{R_{\rm p}}\right)_{\rm max} = (J/J')^2 \frac{(1+q)^4}{q^2} \left(1 + \frac{\rho_{\rm p}}{\rho_{\rm s}} q\right)^{1/3}, \tag{2.7}$$

which increases quickly with decreasing q, allowing for binaries with smaller secondaries to have much wider separations than binaries with similarly-sized components.

2.3 Fully Despun, Double Synchronous Orbits

The natural evolution of a binary system is through mutual tidal interaction. The differential gravity across each body due to the proximity of its companion acts to evolve the rotation states of the individual bodies as well as their physical separation; tides tend to evolve rapidly rotating components in close proximity to a more widely separated system with more slowly rotating components. Prior to delving into the tidal mechanism, we can examine the tidal end state of the fully despun, double synchronous system, where the mean motion in the mutual orbit n equals the spin rates of the components, $\omega_{\rm p}$ and $\omega_{\rm s}$. The classic example of such an end state is in the Pluto-Charon system where the bodies are face-locked (Christy and Harrington, 1978), meaning they keep the same sides facing one another because the periods of revolution and rotation have synchronized.

The scaled angular momentum of the system at any time is given by the sum of

Equations (2.3) and (2.4) divided by J'. After setting the spin rates ω_p and ω_s equal to the mean motion n, replacing n with a function of the semimajor axis a via Kepler's Third Law, and some rearranging, the locations of the synchronous orbits a_{sync}/R_p are the solutions to the quasi-quadratic equation

$$\frac{1}{\alpha_p}\frac{q}{1+q}\frac{1}{1+\frac{\alpha_s}{\alpha_p}\left(\frac{\rho_p}{\rho_s}\right)^{2/3}q^{5/3}}\left(\frac{a_{sync}}{R_p}\right)^2 - \frac{J/J'}{\alpha_p}\frac{\left(1+\frac{\rho_p}{\rho_s}q\right)^{1/6}(1+q)}{1+\frac{\alpha_s}{\alpha_p}\left(\frac{\rho_p}{\rho_s}\right)^{2/3}q^{5/3}}\left(\frac{a_{sync}}{R_p}\right)^{3/2} + 1 = 0. \tag{2.8}$$

If the components are spherical and have similar uniform densities, the condition for a synchronous orbit reduces to

$$\frac{5}{2}\frac{q}{1+q}\frac{1}{1+q^{5/3}}\left(\frac{a_{sync}}{R_p}\right)^2 - \frac{5}{2}\frac{(1+q)^{7/6}}{1+q^{5/3}}(J/J')\left(\frac{a_{sync}}{R_p}\right)^{3/2} + 1 = 0. \tag{2.9}$$

Depending on the total angular momentum of the system, J/J', and the mass ratio q, the equation above may have two, one, or zero solutions corresponding to inner and outer synchronous orbits, a single synchronous orbit, or the absence of a valid fully despun, double synchronous orbit, respectively, for the system. Solutions to Equation (2.9) for all q are shown in Figure 2.1 for various values of J/J' where the number of solutions for a specific q is given by the number of intersections between the curve of the relevant J/J' value for the system and the horizontal line of constant mass ratio q that the system will tidally evolve along. From Figure 2.1, clearly binary systems with smaller secondaries can attain much wider separations than binary systems with components of similar size.

The general trends of tidal evolution when the spins of the components have the same sense of rotation as the motion in the mutual orbit are illustrated by Figure 2.2. If the system is between the two solutions to the synchronous orbit equation for the q of

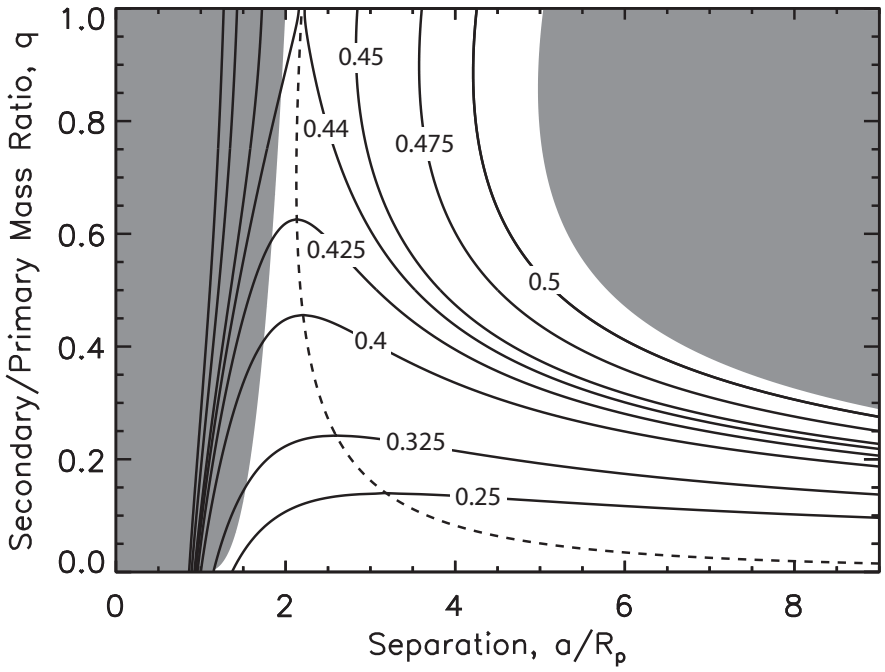

Figure 2.1: Binary component separation in terms of the primary radius $a/R_{\rm p}$ for the fully despun, double synchronous orbits of binary systems of given mass ratio q and scaled angular momentum J/J'. The solid lines indicate the synchronous orbits for $J/J' = 0.25$, 0.325, 0.4, 0.425, 0.44, 0.45, 0.475, and 0.5. The shaded regions indicate separations that are inaccessible to the binary components. The region at left requires the components to be in contact while the region at right is disallowed by angular momentum conservation (shown for $J/J' = 0.5$). The dashed line indicates the synchronous stability limit (see Section 2.4) that divides the two solutions for each mass ratio, if they exist, into an unstable inner synchronous orbit and a stable outer synchronous orbit. In most cases, the unstable inner synchronous orbit is within the contact binary limit.

the system, as systems with small secondaries and/or close separations are, meaning it visually appears "below" its synchronous orbit curve in $\left(q, a/R_{\rm p}\right)$-space, the system will evolve outward as spin angular momentum is transferred to the mutual orbit via the tidal interaction ($\omega_{\rm p} > n$, $\omega_{\rm s} \sim n$). If the system is above its synchronous orbit curve, due to having a large secondary or wide separation, the orbital angular momentum increases such that the angular momentum available in the spins of the components requires that $\omega_{\rm p} < n$ (for $\omega_{\rm s} \sim n$), and the system will evolve inward as angular momentum from the orbit is transferred to the spins of the components. For systems with constant angular momentum, the cases of inward evolution require a binary formation mechanism that initially produces well-separated components with rotation rates slower than the mean motion because tidal evolution cannot have evolved a system outward to these configuration above the synchronous orbit curve.

Note that binaries with equal mass components, $q = 1$, in Figure 2.1 only have fully despun, double synchronous end states if $J/J' > 0.44$. This fact, along with the case where the synchronous orbit equation has no solution because q lies entirely above the synchronous orbit curve for the relevant J/J' for the system (the uppermost arrow in Figure 2.2), will be important in the context of contact binary formation discussed in Chapter 6.

2.4 Stability Limit of Synchronous Orbits

The synchronous orbit solutions to Equation (2.8) are equivalently thought of as contours of constant J/J' in (q, $a/R_{\rm p}$)-space satisfying

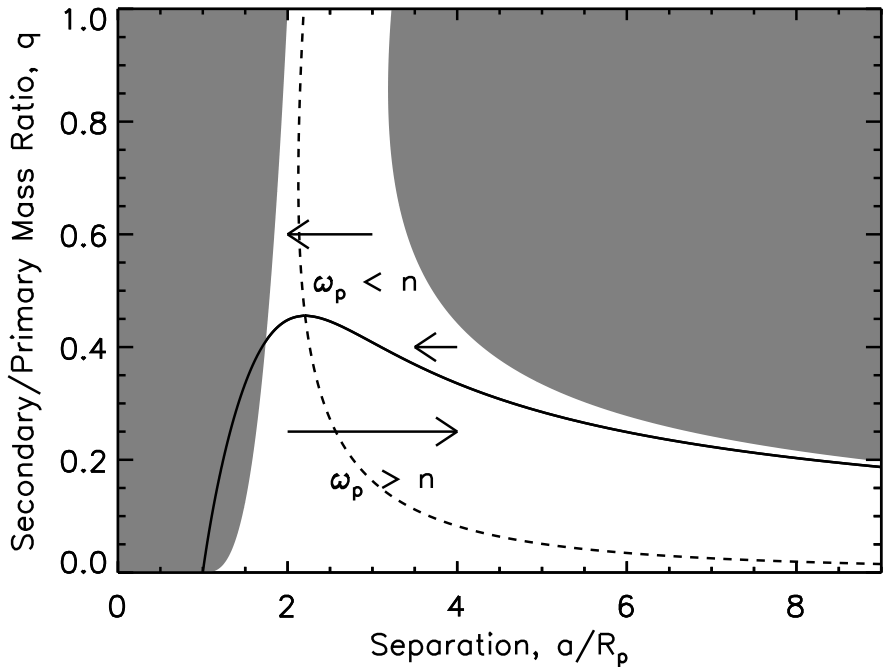

Figure 2.2: Directions of tidal evolution for systems with $J/J' = 0.4$. For binaries dominated by the primary mass, systems under the synchronous orbit curve will evolve outward as angular momentum is transferred from the rapid spin of the primary to the orbit ($\omega_p > n$). Systems above the synchronous orbit curve evolve inward as angular momentum is transferred from the orbit to the spins of the components ($\omega_p < n$) until either the outer synchronous orbit is reached or the orbit collapses to contact. The shaded regions indicate separations that are inaccessible to the binary components due to the contact and angular momentum limits. The dashed line indicates the synchronous stability limit (see Section 2.4).

$$\frac{J}{J'} = \frac{1}{\left(1+\frac{\rho_p}{\rho_s}q\right)^{1/6}}\frac{q}{(1+q)^2}\left(\frac{a}{R_p}\right)^{1/2} + \alpha_p\frac{1+\frac{\alpha_s}{\alpha_p}\left(\frac{\rho_p}{\rho_s}\right)^{2/3}q^{5/3}}{\left(1+\frac{\rho_p}{\rho_s}q\right)^{1/6}(1+q)}\left(\frac{a}{R_p}\right)^{-3/2}. \quad (2.10)$$

The maxima of the set of contour curves for a continuous range of J/J' are traced out by taking the derivative of Equation (2.10) with respect to a/R_p giving

$$\frac{a}{R_p} = \left[3\alpha_p\left(1+\frac{\alpha_s}{\alpha_p}\left(\frac{\rho_p}{\rho_s}\right)^{2/3}q^{5/3}\right)\frac{1+q}{q}\right]^{1/2}. \quad (2.11)$$

For spherical components with similar densities,

$$\frac{a}{R_p} = \left[\frac{6}{5}\frac{1+q}{q}\left(1+q^{5/3}\right)\right]^{1/2}, \quad (2.12)$$

which is the dashed curve in Figure 2.1 that splits the synchronous orbit curves into inner and outer solutions when there are two synchronous solutions.

Harris and Ward (1982) showed that Equation (2.11) is also a stability limit against perturbations to the system, splitting the synchronous orbit solutions into an unstable inner solution and a stable outer solution. To illustrate this, take a binary system to be in a fully despun, double synchronous state with $\omega_p = \omega_s = \omega = n$ when it is perturbed such that $n' = n + \Delta n$ or $\omega' = n + \Delta\omega$; a change in one parameter will cause tidal torques to change the other. For a circular orbit, to conserve angular momentum between the initial and final configurations

$$\left(I_p + I_s\right)n + \frac{q}{(1+q)^{1/3}}G^{2/3}M_p^{5/3}n^{-1/3} = \left(I_p + I_s\right)(n+\Delta\omega) + \frac{q}{(1+q)^{1/3}}G^{2/3}M_p^{5/3}(n+\Delta n)^{-1/3}, \quad (2.13)$$

where a was rewritten in terms of n via Kepler's Third Law. For $\Delta\omega$, $\Delta n \ll n$, $(n + \Delta n)^{-1/3} \simeq n^{-1/3}\left(1 - \frac{1}{3}\frac{\Delta n}{n}\right)$, and thus

$$\Delta n = 3\frac{I_\mathrm{p} + I_\mathrm{s}}{M_\mathrm{p} a^2}\frac{1+q}{q}\Delta\omega = 3\frac{I_\mathrm{p} + I_\mathrm{s}}{\mu a^2}\Delta\omega, \tag{2.14}$$

where a is the semimajor axis of the initial synchronous orbit, and $\mu = M_\mathrm{p} M_\mathrm{s}/\left(M_\mathrm{p} + M_\mathrm{s}\right)$ is the reduced mass of the system. Expanding the moments of inertia, the equivalent expression is

$$\Delta n = 3\alpha_\mathrm{p}\left(1 + \frac{\alpha_\mathrm{s}}{\alpha_\mathrm{p}}\left(\frac{\rho_\mathrm{p}}{\rho_\mathrm{s}}\right)^{2/3} q^{5/3}\right)\frac{1+q}{q}\left(\frac{a}{R_\mathrm{p}}\right)^{-2}\Delta\omega. \tag{2.15}$$

If $\mu a^2 = 3\left(I_\mathrm{p} + I_\mathrm{s}\right)$, the frequencies change by the same amount, and the synchronous state is preserved. Rearranging Equation (2.15) in this case reproduces Equation (2.11). If $\mu a^2 < 3\left(I_\mathrm{p} + I_\mathrm{s}\right)$, corresponding to the inner synchronous orbit, $\Delta n > \Delta\omega$. If the secondary moves inside the inner synchronous orbit, the spin rate does not increase rapidly enough to re-synchronize the system resulting in the orbit decaying until a collision occurs (Weidenschilling et al., 1989). If the secondary moves outside the inner synchronous orbit, the system will evolve outward until the outer synchronous orbit is reached and the system is stabilized. Thus, the stability condition is that $\mu a^2 > 3\left(I_\mathrm{p} + I_\mathrm{s}\right)$ or

$$\frac{a}{R_\mathrm{p}} > \left[3\alpha_\mathrm{p}\left(1 + \frac{\alpha_\mathrm{s}}{\alpha_\mathrm{p}}\left(\frac{\rho_\mathrm{p}}{\rho_\mathrm{s}}\right)^{2/3} q^{5/3}\right)\frac{1+q}{q}\right]^{1/2} \tag{2.16}$$

or, for spherical components with similar densities,

$$\frac{a}{R_{\rm p}} > \left[\frac{6}{5}\frac{1+q}{q}\left(1+q^{5/3}\right)\right]^{1/2}. \quad (2.17)$$

For $\alpha_{\rm p,s} \neq 2/5$, one may use the nonsphericity parameter $\lambda_{\rm p,s} = 5\alpha_{\rm p,s}/2$ introduced by Descamps and Marchis (2008) such that

$$\frac{a}{R_{\rm p}} > \left[\frac{6}{5}\frac{1+q}{q}\left(\lambda_{\rm p}+\lambda_{\rm s}q^{5/3}\right)\right]^{1/2}, \quad (2.18)$$

which is a correction to the formula and direction of the inequality given in Marchis et al. (2008a,b).

The stability of the synchronous orbit is further illustrated by the arrows in Figure 2.2. If the system is perturbed inward from the inner synchronous orbit, the system will evolve inward; if the system is perturbed outward from the inner synchronous orbit, the system will evolve outward. In both cases, evolution is away from the synchronous point indicating that the inner synchronous orbit is unstable. The opposite is true for the outer synchronous orbit. The arrows in Figure 2.2 show that perturbation of the system from the outer synchronous orbit will allow the system to return to the outer synchronous orbit, which indicates that the orbit is stable to tidal perturbation.

With the definition of the stability limit in hand, Equation (2.11) gives the minimum separation, and minimum angular momentum using Equation (2.10), that allows for a stable synchronous end state of tidal evolution for a given mass ratio q. Satisfying the stability condition is thus a necessary, but not sufficient condition for the end of tidal evolution. Systems that do not satisfy the stability condition must continue to evolve tidally, while systems that do satisfy the stability condition may or may not continue their evolution depending on the angular momentum of the system. At the minimum angular momentum, the synchronous orbit equation, Equation (2.8), only has one solu-

tion, which is simply the stability limit, and tidal evolution may cease. If the angular momentum is larger than the minimum, the synchronous orbit equation has two solutions and the system will continue to evolve to the outer synchronous orbit. Of course, having below the minimum angular momentum needed for a synchronous orbit would cause the system to collapse as the synchronous orbit equation has no solution.

2.5 Summary of Main Belt and Jupiter Trojan Binaries

In our study, we consider binary systems in the main asteroid belt and among the Jupiter Trojans with 100 km-scale primary components that have been characterized by direct adaptive optics imaging and lightcurve photometry. To be included in this study, orbital properties must be known and some estimate of the size must be available. Imaging of large main belt asteroids and Jupiter Trojans mostly finds secondaries roughly one tenth the size of their primaries ($q \sim 0.001$) or smaller (Merline et al., 2002). These secondaries are likely the result of a subcatastrophic impact on the parent body (*i.e.*, SMATS, smashed target satellites, as described by Durda et al. (2004)), which is supported by the angular momentum budget of the systems. With the exception of (90) Antiope and (617) Patroclus, which have nearly equal-sized components, the 100 km-scale main belt binaries have J/J' values well below the $J/J' \sim 0.4$ regime of binaries formed via a spin-up mechanism (see Table 2.1). Among the $q < 0.1$ binaries, the primary component spins with a period of roughly 6 hours, twice the rotational breakup period, yet accounts for 98% of the angular momentum of the system due to the large mass disparity between the components. Equal mass binary (90) Antiope (Merline et al., 2000a,b) has $J/J' = 0.488$ that is more similar to a binary formed through spin-up than through a collision. However, the sheer size of the components at almost 90 km in diameter each and its location in the main belt make it difficult for the YORP effect or close planetary

encounters to explain how (90) Antiope originally formed. If size estimates are correct, (617) Patroclus has $J/J' = 0.757$, far larger than any other binary considered among our sample, but near the upper limit for giant impacts of $J/J' < 0.8$ (Canup, 2005). Such a high angular momentum content is more similar to many of the Kuiper belt binaries whose main formation mechanism is likely *n*-body capture rather than spin-up or collisions (see Noll et al. (2008) for a review).

The $q < 0.1$ binaries in the main belt are in the midst of a lengthy tidal evolution. As shown by Figure 2.3, none of the $q < 0.1$ binaries have reached the synchronous stability limit and are very far from reaching the outer synchronous orbit that nearly coincides with the angular momentum limit for these systems. The inner synchronous orbit for $J/J' = 0.2$ lies above the contact binary limit, so these binaries must have begun their tidal evolution from an initial orbit of roughly $a/R_{\rm p} = 2$ or more to evolve outward due to tides. Of the main belt binaries listed in Table 2.1, only (130) Elektra and (283) Emma have mutual orbits that are not roughly circular, each having an eccentricity $e \sim 0.1$ likely caused by tidal excitation (Marchis et al., 2008b). (90) Antiope is in the fully despun, double synchronous tidal end state (Michałowski et al., 2004; Descamps et al., 2007) where the rotational periods of the components equal the period of the mutual orbit. The mutual orbit of (617) Patroclus is also roughly circular, but it is not clear whether the system has reached its tidal end state (Marchis et al., 2006).

2.6 Summary of Near-Earth Binaries

We also consider binary systems in the near-Earth region well-characterized by radar and lightcurve observations, all of which have primaries on the 1 km scale. These systems are most likely the result of a spin-up mechanism (Margot et al., 2002) as evidenced

Table 2.1: Physical properties of select main belt and Jupiter trojan binary asteroids with primary radii of order 100 km. R_p is the radius of the primary. R_s/R_p is the size ratio of the components. q is the mass ratio, taken to be the size ratio cubed by assuming the components have equal densities. ρ is the density used for both components. a/R_p is the semimajor axis of the mutual orbit in terms of the radius of the primary. J/J' is the normalized angular momentum whose average value of roughly 0.2 for $q \ll 1$ indicates a subcatastrophic collisional origin rather than formation through spin-up. For the triple systems of (45) Eugenia and (87) Sylvia, only properties of the larger satellite are considered.

	Name	R_p [km]	R_s/R_p	q	ρ [g/cm^3]	a/R_p	J/J'
22	Kalliope	91	0.198	0.0077	2.37	11.7	0.230
45	Eugenia	108	0.059	0.0002	1.12	11.0	0.220
87	Sylvia	143	0.063	0.0003	1.2	9.48	0.233
90	Antiope	44	0.954	0.8695	1.25	3.90	0.488
107	Camilla	112	0.040	0.00006	1.88	11.0	0.199
121	Hermione	105	0.086	0.0006	1.8	7.57	0.179
130	Elektra	91	0.022	0.00001	3.8	13.8	0.130
283	Emma	74	0.081	0.0005	0.87	8.05	0.207
617	Patroclus	61	0.934	0.8159	0.8	11.2	0.757
702	Alauda	97	0.029	0.00002	1.6	12.6	0.125
762	Pulcova	69	0.145	0.0030	1.8	11.7	0.178

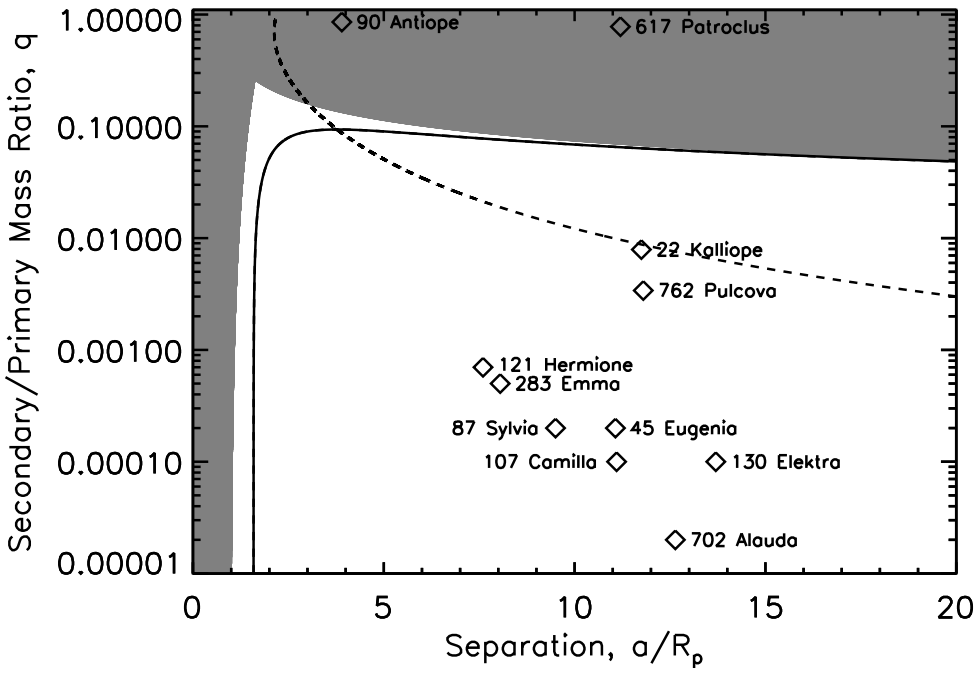

Figure 2.3: Mass ratio q and primary-secondary separation in terms of the primary radius $a/R_{\rm p}$ for select main belt and Jupiter Trojan binaries along with the synchronous orbit curve and shaded angular momentum limit for $J/J' = 0.2$. Clearly, all of the main belt binaries besides (90) Antiope and perhaps (617) Patroclus are presently tidally evolving. (90) Antiope and (617) Patroclus plot beyond the angular momentum limit because $J/J' > 0.2$ and they must have formed via another mechanism than the main belt binaries with $q < 0.1$. Of the binaries with small secondary components, only (22) Kalliope lies near the stability limit, and all of these binaries are far from completing their tidal evolution at a fully despun, double synchronous orbit that falls essentially at the angular momentum limit.

by the $J/J' \sim 0.4$ values for the near-Earth binaries in Table 2.2. Since the detection of the asteroidal YORP effect (Taylor et al., 2007; Lowry et al., 2007; Kaasalainen et al., 2007), spin-up via thermal re-radiation of absorbed sunlight has become the preferred binary formation mechanism among km-scale parent bodies in the near-Earth region and perhaps the inner main belt (Pravec and Harris, 2007). Further evidence of spin-up comes from the rapid rotation of the primaries that, ignoring equal mass binary (69230) Hermes, spin at 95% of the rubble-pile breakup period and contain about 88% of the angular momentum of the system in their spin. Though they spin faster than their main belt counterparts, the primaries of near-Earth binaries contain a smaller fraction of the angular momentum of the system because the secondaries are larger among the near-Earth binaries.

With the exception of equal mass binary (69230) Hermes that has reached its fully despun, double synchronous end state (Margot et al., 2006), the binaries in the near-Earth region are also in the midst of a lengthy tidal evolution. As shown by Figure 2.4, only 1991 VH and 2000 DP_{107} have passed the synchronous stability limit, but are far from reaching the outer synchronous orbit for $J/J' = 0.4$ that lies near the angular momentum limit. 1991 VH is believed to be an asynchronous binary as three periods are detected in lightcurves (Pravec et al., 2006), presumably the rotation of each component plus the mutual orbit period; the orbit and rotation periods of the secondary of 2000 DP_{107} suggest it has synchronized (Margot et al., 2002), but the primary has not been despun (Margot et al., 2002; Pravec et al., 2006) illustrating the necessary, but not sufficient nature of crossing the synchronous stability limit for completing tidal evolution. Because the inner synchronous orbit is buried within the contact binary limit for the $q \sim 0.1$ binaries with $J/J' = 0.4$, the secondaries have evolved outward since the binary was formed. Of the near-Earth binaries listed in Table 2.2, only 2004 DC (Taylor et al., 2008) and 2003 YT_1 (Nolan et al., 2004) have moderate eccentricities of $e > 0.1$.

Table 2.2: Physical properties of select near-Earth binary asteroids with primary radii of order 1 km. Note that J/J' in each case roughly satisfies the condition for binary formation from the spin-up of a single parent body.

	Name	R_p [km]	R_s/R_p	q	ρ [g/cm^3]	a/R_p	J/J'
3671	Dionysus	0.75	0.2	0.008	1.6	4.8	0.397
5381	Sekhmet	0.7	0.214	0.0098	2	2.2	0.355
35107	1991 VH	0.6	0.417	0.0723	1.6	5.33	0.499
65803	Didymos	0.4	0.188	0.0066	1.7	2.75	0.454
66391	1999 KW_4	0.66	0.342	0.0402	1.97	3.87	0.392
69230	Hermes	0.31	0.898	0.7236	1.8	3.90	0.484
137170	1999 HF_1	1.87	0.214	0.0098	2	3.74	0.415
	1996 FG_3	0.7	0.31	0.030	1.4	3.43	0.348
	2000 DP_{107}	0.4	0.375	0.0527	1.7	6.55	0.455
	2000 UG_{11}	0.12	0.417	0.0723	0.8	2.83	0.402
	2002 CE_{26}	1.74	0.086	0.0006	0.9	2.70	0.424
	2003 YT_1	0.53	0.189	0.0067	2.01	6.42	0.410
	2004 DC	0.17	0.207	0.0089	1.70	4.41	0.406

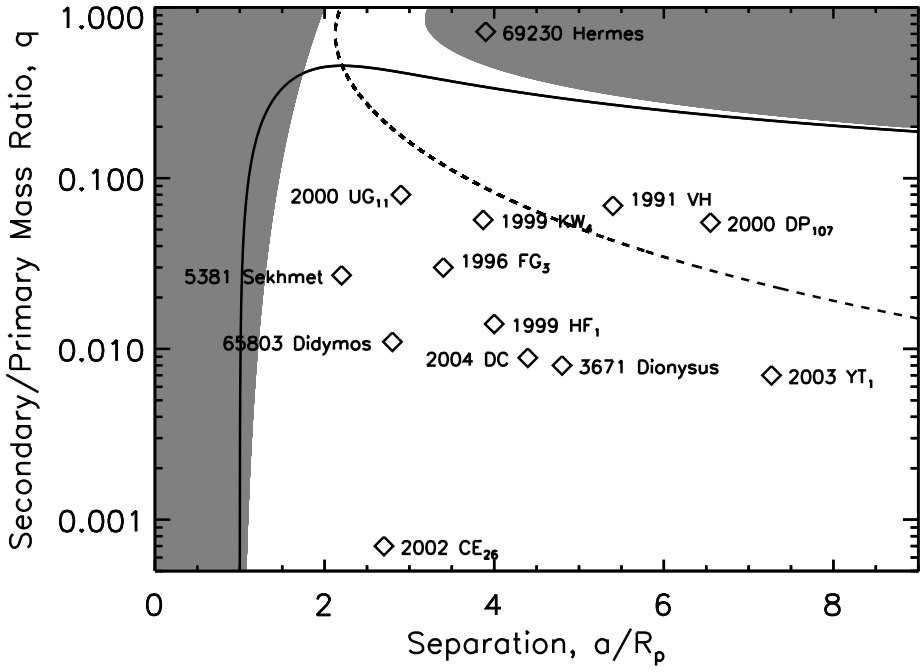

Figure 2.4: Mass ratio q and primary-secondary separation in terms of the primary radius $a/R_{\rm p}$ for select near-Earth binaries along with the synchronous orbit curve and shaded angular momentum limit for $J/J' = 0.4$. Clearly, all of the near-Earth binaries besides (69230) Hermes are presently tidally evolving. (69230) Hermes plots beyond the angular momentum limit because its $J/J' > 0.4$ and has reached its tidal end state. Although 1991 VH and 2000 $\rm DP_{107}$ fall to the right of the synchronous stability curve, they have yet to reach a fully despun, double synchronous tidal end state.

2.7 Synchronous Orbits About a Non-Spherical Primary

Because an asteroid in a binary system will not be an idealized spherical body as assumed thus far, the next step is to deform the primary to an oblate or prolate shape and examine the effect of a non-spherical primary on the location of the fully despun, double synchronous tidal end states. Let the primary component of the binary system be ellipsoidal in shape with principal semi-axes $\alpha_1 \geq \alpha_2 \geq \alpha_3 > 0$ such that the equivalent radius of the primary is $R_\mathrm{p} = (\alpha_1\alpha_2\alpha_3)^{1/3}$. For rotation about the shortest principal axis, the ratio of the moment of inertia of the ellipsoid to that of its equivalent sphere with radius R_p is the nonsphericity parameter λ (Descamps and Marchis, 2008),

$$\lambda = \frac{1+\beta^2}{2\left(\beta\gamma\right)^{2/3}}, \tag{2.19}$$

where $\beta = \alpha_2/\alpha_1$ and $\gamma = \alpha_3/\alpha_1$. The spin angular momentum of the system when synchronized is then

$$S = \frac{2}{5}\left(\lambda_\mathrm{p} + q^{5/3}\right) M_\mathrm{p} R_\mathrm{p}^2 \omega. \tag{2.20}$$

The secondary is assumed to remain spherical and the definition of the mass ratio q remains unchanged for equal density components. To retain orbital relative equilibrium, the sphere must lie along one of the principal axes of the ellipsoid and the system must rotate about another principal axis of the ellipsoid at a specific rate (Scheeres, 2006) given by

$$n^2 = \frac{3}{2} G(M_\mathrm{p} + M_\mathrm{s}) \int_{r^2-\alpha_i^2}^{\infty} \frac{\mathrm{d}u}{\left(\alpha_i^2 + u\right)\Delta(u)}, \tag{2.21}$$

where $\Delta(u) = \sqrt{\left(\alpha_1^2 + u\right)\left(\alpha_2^2 + u\right)\left(\alpha_3^2 + u\right)}$, α_i is the semi-major principal axis the secondary lies along, r is the orbital separation of the bodies ($r = a$ for a circular orbit), and the spin rate and mean motion are synchronized. For two spheres, the above equation simplifies to Kepler's Third Law, but as one component's shape departs from a sphere, the result becomes more complicated. The orbital angular momentum for a circular orbit is given by Equation (2.3) and J' for the system is $(1+q)^{5/3} M_\mathrm{p} R_\mathrm{p}^2 \sqrt{G M_\mathrm{p} / R_\mathrm{p}^3}$. Thus, for an ellipsoid and a sphere in a fully synchronous binary system,

$$\frac{J}{J'} = \frac{\sqrt{3/2}}{(1+q)^{7/6}} R_\mathrm{p}^{3/2} \left[\frac{q}{1+q} \left(\frac{a}{R_\mathrm{p}} \right)^2 + \frac{2}{5} \left(\lambda_\mathrm{p} + q^{5/3} \right) \right] \left(\int_{r^2 - \alpha_i^2}^{\infty} \frac{\mathrm{d}u}{\left(\alpha_i^2 + u\right) \Delta(u)} \right)^{1/2} . \quad (2.22)$$

The integral in the above equation is non-trivial, and the results given in the following sections include simplifications to the nominal output from the symbolic integrator *Mathematica*. The interested reader may consult Appendix A for details.

2.7.1 Oblate Primary, $\alpha_3 < \alpha_2 = \alpha_1$

Oblate shapes are of particular interest in the case of near-Earth binary systems where the primaries tend to spin near the breakup limit. As the spin rate increases, the potential low moves from the poles to the equator (Guibout and Scheeres, 2003) producing oblate shapes where loose regolith builds up a circular equatorial belt such as that seen in shape models of the primary components of near-Earth binaries (66391) 1999 KW_4 (Ostro et al., 2006; Scheeres et al., 2006) and 2004 DC, discussed in Chapter 7, based on radar observations, as well as in simulations of rapidly-spinning rubble piles (Walsh et al., 2008).

For an oblate primary with two equivalent equatorial principal axes rotating about

the shortest principal axis, $\alpha_3 < \alpha_2 = \alpha_1$ ($\gamma < \beta = 1$) and $\lambda = \gamma^{-2/3}$. Simplifying the integral for the secondary along α_1, actually anywhere in the equator plane of the primary because of the symmetry of the oblate shape, the necessary spin rate for orbital relative equilibrium is

$$n^2 = \frac{3}{2} G M_{\rm p} (1+q) \alpha_1^{-3} \int_{\alpha^2-1}^{\infty} \frac{{\rm d}u'}{(1+u')^2 (\gamma^2+u')^{1/2}} \tag{2.23}$$

where $\alpha = a/\alpha_1$ and $u' = u/\alpha_1^2$, and the fully despun, double synchronous orbit satisfies the angular momentum equation

$$\begin{aligned} J/J' &= \sqrt{\frac{3}{2}} \frac{\gamma^{1/2}}{(1+q)^{7/6}} \left[\frac{q}{1+q} \bar{a}^2 + \frac{2}{5} \left(\gamma^{-2/3} + q^{5/3} \right) \right] \left[\int_{\gamma^{2/3}\bar{a}^2-1}^{\infty} \frac{{\rm d}u'}{(1+u')^2 (\gamma^2+u')^{1/2}} \right]^{1/2} \\ &= \frac{\sqrt{3/2}}{(1+q)^{7/6}} \left(\frac{\gamma}{1-\gamma^2} \right)^{1/2} \left[\frac{q}{1+q} \bar{a}^2 + \frac{2}{5} \left(\gamma^{-2/3} + q^{5/3} \right) \right] \\ &\quad \times \left[\frac{1}{(1-\gamma^2)^{1/2}} \left(\frac{\pi}{2} - \tan^{-1} \sqrt{\frac{\gamma^{2/3}\bar{a}^2 + \gamma^2 - 1}{1-\gamma^2}} \right) - \frac{\sqrt{\gamma^{2/3}\bar{a}^2 + \gamma^2 - 1}}{\gamma^{2/3}\bar{a}^2} \right]^{1/2} \end{aligned} \tag{2.24}$$

where $\bar{a} = a/R_{\rm p}$. The above expression describes the synchronous orbits as contours of constant J/J' in the same way as Equation (2.10).

For a given angular momentum J/J' value such as $J/J' = 0.5$ in Figure 2.5, decreasing γ from 1 makes the primary more oblate and pinches the synchronous orbit curves together, in this case near $q \sim 0.85$, until the inner and outer synchronous curves intersect at a single solution. Then it is possible to have synchronous orbits for $q \sim 1$ and $q < 1$ with a gap at mass ratios in between where there is no solution such that synchronous orbits do not exist and the binary would have to collapse back into contact. Further increase in the oblateness eventually causes the synchronous orbits for $q \sim 1$ to no longer exist, and the remaining curves look like those for two spherical components

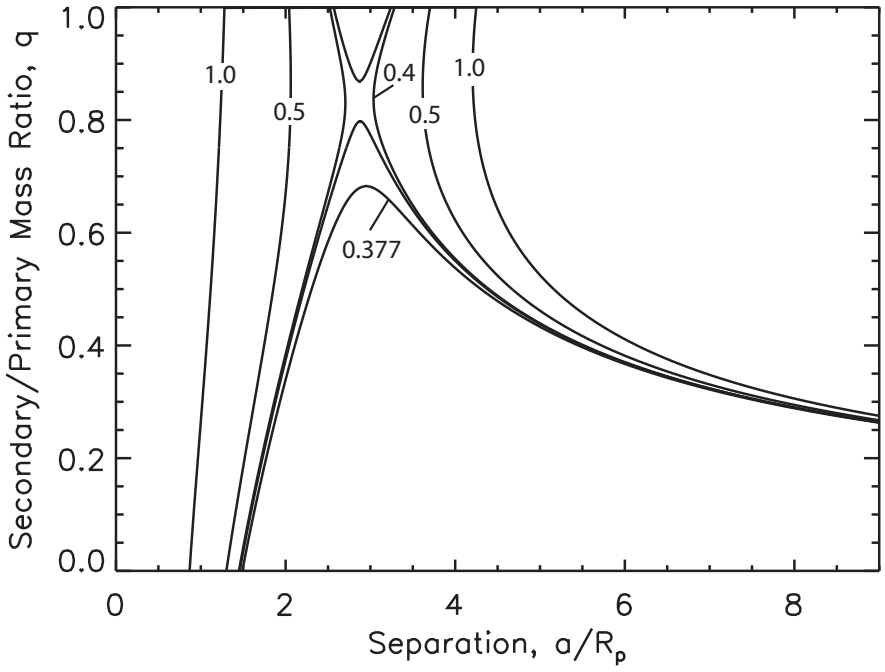

Figure 2.5: Binary component separation in terms of the primary radius $a/R_{\rm p}$ for the fully despun, double synchronous orbits of binary systems of given mass ratio q, scaled angular momentum $J/J' = 0.5$ (chosen for clarity of the curves), and primary oblateness γ. The curves indicate the inner and outer synchronous orbits for $\gamma = 1.0$ (spherical), 0.5, 0.4, 0.395, and 0.377. Increasing the oblateness pushes the inner and outer synchronous solutions closer to each other, eventually pinching off around $q = 0.85$ for $\gamma = 0.395$. The upper branch of solutions disappears at $\gamma = 0.377$. The contact limit is not shown as it is a function of oblateness: $\gamma^{-1/3} + q^{1/3}$.

from Figure 2.1, but in this case, the shapes of the curves are solely due to increasing the oblateness of the primary rather than decreasing J/J'. For $J/J' = 0.5$, the primary must have an oblateness of $\gamma < 0.4$ (more than a 2:1 axial ratio), which implies severe flattening to a disk-like shape, for the $q \sim 1$ synchronous solutions to disappear. For comparison, the primary of 1999 KW_4 has $\gamma = 0.9$. For $J/J' = 0.45$, similar to that of the near-Earth binaries created via spin-up, the oblateness condition is less restrictive and synchronous solutions disappear for $q \sim 1$ for a more reasonable oblateness of $\gamma < 0.85$.

The net result of having an oblate primary is that, for a given mass ratio q, the system requires more angular momentum than a system with a spherical primary to have a fully despun, double synchronous end state (see Figure 2.6). Take two similar binary systems, each with mass ratio q and effective spherical primary radius R_p, where the only difference is one primary is spherical and the other primary is oblate. Oblateness is characterized by an increase of girth at the equator such that the moment of inertia of an oblate shape is greater than that of a sphere. Thus, if the primaries spin at the same rate, the oblate primary contains more angular momentum in its spin than the spherical primary. Because the orbital angular momentum is independent of the shape of the primary, if the systems have the same orbital configuration and same rotation rates, the system with the oblate primary must have a greater amount of angular momentum. Therefore, as oblateness increases, for a fixed amount of angular momentum, a binary system with an oblate primary cannot support the same secondary that a spherical primary can. Oblate primaries can only support secondaries with smaller q as the reduced spin and orbital angular momentum of the secondary are necessary to balance the increased spin angular momentum of the oblate primary.

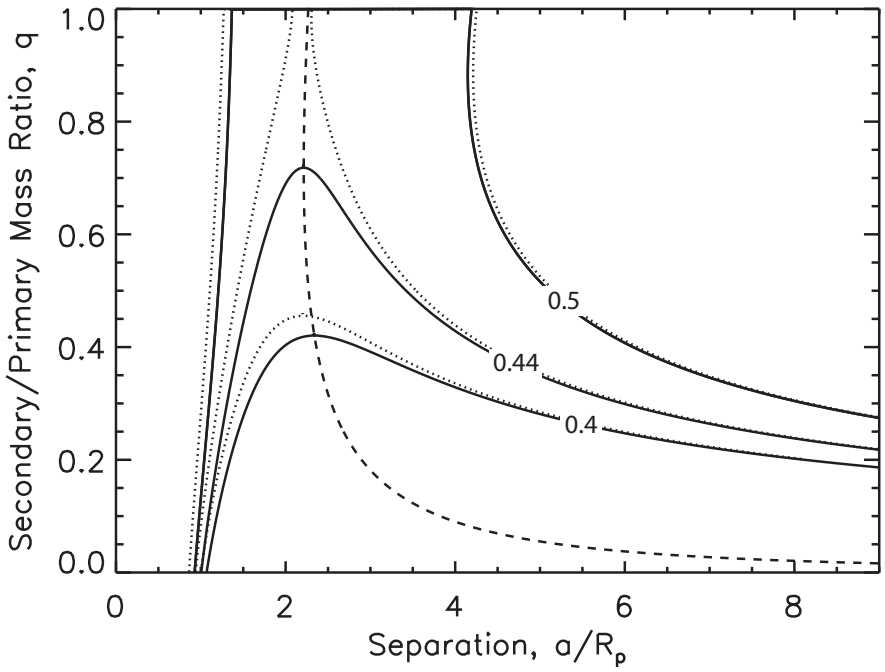

Figure 2.6: Binary component separation in terms of the primary radius $a/R_{\rm p}$ for the fully despun, double synchronous orbits of binary systems of given mass ratio q and primary oblateness $\gamma = 0.9$ (solid), similar to 1999 KW_4, and for a spherical primary (dotted). The dashed curve is the stability limit for $\gamma = 0.9$. The curves indicate the inner and outer synchronous orbits for $J/J' = 0.4, 0.44$, and 0.5 where the curves for the spherical primary always surround the curves for the oblate primary. While a binary system with a spherical primary has synchronous orbits for $q = 1$ and $J/J' = 0.44$, a binary system with a slightly oblate primary can only have a synchronous orbit for $q \sim 0.7$ for the same amount of angular momentum.

2.7.2 Prolate Primary, $\alpha_3 = \alpha_2 < \alpha_1$

Angular momentum equations follow similarly for the prolate cases. For a prolate primary with two equivalent shorter principal axes, one of which is aligned with the spin axis, $\alpha_3 = \alpha_2 < \alpha_1$ ($\gamma = \beta < 1$) and $\lambda = \left(1+\gamma^2\right)/2\gamma^{4/3}$. Further details of the integrals are provided in Appendix A.

Secondary Along Longest Axis

If the secondary lies along the longest principal axis α_1, the fully despun, double synchronous orbit satisfies the angular momentum equation

$$\begin{aligned}\frac{J}{J'} &= \sqrt{\frac{3}{2}}\frac{\gamma}{(1+q)^{7/6}}\left[\frac{q}{1+q}\bar{a}^2+\frac{2}{5}\left(\frac{1+\gamma^2}{2\gamma^{4/3}}+q^{5/3}\right)\right]\left[\int_{\gamma^{4/3}\bar{a}^2-1}^{\infty}\frac{\mathrm{d}u'}{(1+u')^{3/2}\left(\gamma^2+u'\right)}\right]^{1/2} \\ &= \frac{\sqrt{3}}{(1+q)^{7/6}}\frac{\gamma}{(1-\gamma^2)^{1/2}}\left[\frac{q}{1+q}\bar{a}^2+\frac{2}{5}\left(\frac{1+\gamma^2}{2\gamma^{4/3}}+q^{5/3}\right)\right] \\ &\quad\times\left[\frac{\tanh^{-1}\left(\frac{\sqrt{1-\gamma^2}}{\gamma^{2/3}\bar{a}}\right)}{(1-\gamma^2)^{1/2}}-\frac{1}{\gamma^{2/3}\bar{a}}\right]^{1/2}. \end{aligned} \tag{2.25}$$

For $J/J' = 0.5$ in Figure 2.7, decreasing γ to increase how prolate the shape is has the same effect as for oblate shapes. The synchronous orbit curves pinch together creating a gap without solutions at $q \sim 0.85$ at $\gamma = 0.541$. Below $\gamma = 0.533$ (nearly a 2:1 axial ratio), synchronous solutions no longer exist for $q \sim 1$. For $J/J' = 0.45$, synchronous solutions no longer exist for $q \sim 1$ when $\gamma < 0.88$.

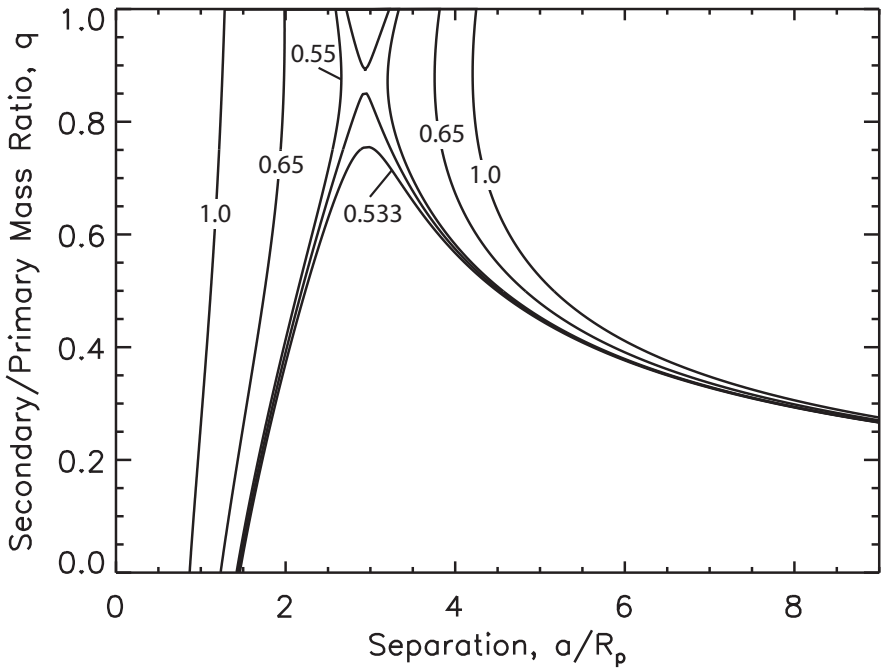

Figure 2.7: Binary component separation in terms of the primary radius $a/R_{\rm p}$ for the fully despun, double synchronous orbits of binary systems of given mass ratio q, scaled angular momentum $J/J' = 0.5$ and primary prolateness γ with the secondary along the longest principal axis of the primary. The curves indicate the inner and outer synchronous orbits for $\gamma = 1.0$ (spherical), 0.65, 0.55, 0.541, and 0.533. Increasing the nonsphericity pushes the inner and outer synchronous solutions closer to each other, eventually pinching off around $q = 0.85$ for $\gamma = 0.541$. The upper branch of solutions disappears at $\gamma = 0.533$. The contact limit is not shown as it is a function of γ: $\gamma^{-2/3} + q^{1/3}$.

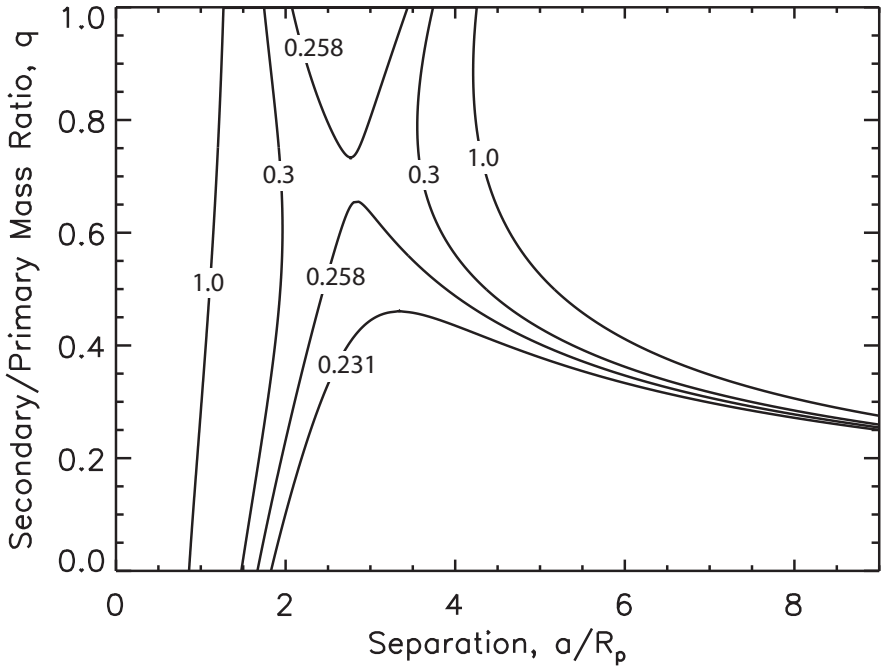

Figure 2.8: Binary component separation in terms of the primary radius $a/R_{\rm p}$ for the fully despun, double synchronous orbits of binary systems of given mass ratio q, scaled angular momentum $J/J' = 0.5$ and primary prolateness γ with the secondary along the intermediate principal axis of the primary. The curves indicate the inner and outer synchronous orbits for $\gamma = 1.0$ (spherical), 0.3, 0.258, and 0.231. Increasing the non-sphericity pushes the inner and outer synchronous solutions closer to each other, eventually pinching off around $q = 0.7$ for $\gamma = 0.258$. The upper branch of solutions disappears at $\gamma = 0.231$. The contact limit is not shown as it is a function of γ: $\gamma^{1/3} + q^{1/3}$.

Secondary Along Intermediate Axis

If, instead, the secondary lies along the shorter equatorial axis α_2, the fully despun, double synchronous orbit satisfies the angular momentum equation

$$\begin{aligned}\frac{J}{J'} &= \sqrt{\frac{3}{2}}\frac{\gamma}{(1+q)^{7/6}}\left[\frac{q}{1+q}\overline{a}^2+\frac{2}{5}\left(\frac{1+\gamma^2}{2\gamma^{4/3}}+q^{5/3}\right)\right]\left[\int_{\gamma^{4/3}\overline{a}^2-\gamma^2}^{\infty}\frac{\mathrm{d}u'}{(1+u')^{1/2}\left(\gamma^2+u'\right)^2}\right]^{1/2} \\ &= \frac{\sqrt{3/2}}{(1+q)^{7/6}}\frac{\gamma}{(1-\gamma^2)^{1/2}}\left[\frac{q}{1+q}\overline{a}^2+\frac{2}{5}\left(\frac{1+\gamma^2}{2\gamma^{4/3}}+q^{5/3}\right)\right] \\ &\quad\times\left[\frac{\sqrt{1+\gamma^{4/3}\overline{a}^2-\gamma^2}}{\gamma^{4/3}\overline{a}^2}-\frac{\tanh^{-1}\left(\sqrt{\frac{1-\gamma^2}{1+\gamma^{4/3}\overline{a}^2-\gamma^2}}\right)}{(1-\gamma^2)^{1/2}}\right]^{1/2}. \end{aligned} \tag{2.26}$$

For $J/J' = 0.5$ in Figure 2.8, decreasing γ to increase how prolate the shape is has a lesser effect than the case with the secondary along the long axis. The synchronous orbit curves pinch together creating a gap without solutions at a smaller mass ratio of $q \sim 0.7$ and at a more extreme cigar shape with $\gamma = 0.258$ (axial ratio of 4:1). Below $\gamma = 0.231$, synchronous solutions no longer exist for $q \sim 1$. For $J/J' = 0.45$, synchronous solutions no longer exist for $q \sim 1$ when $\gamma < 0.47$ (more than 2:1 axial ratio), still a strong deviation from a spherical shape.

Prolate shapes with the secondary along the intermediate axis can more easily accomodate a synchronous end state for $q \sim 1$ than prolate shapes with the secondary along the long axis. On the other hand, it is possible for oblate primaries and prolate primaries with the secondary along the long axis to be unable to support a $q \sim 1$ secondary in a fully despun, double synchronous orbit for reasonable values of nonsphericity, $\gamma \sim 0.8$, and angular momentum $J/J' = 0.45$. In these cases, the system must collapse back to contact. We will return to the idea of forming contact binaries through the lack of a viable fully despun, double synchronous orbit in Chapter 6.

CHAPTER 3

TIDAL EVOLUTION OF CLOSE BINARY SYSTEMS

The equations of tidal evolution including tidal torques, the changes in spin rates of the components, and the change in orbital separation are derived for binary systems with circular mutual orbits. The tidal potential due to the presence of a satellite about a primary body is expanded in terms of Legendre polynomials to arbitrary order, rather than truncated at leading order as is typically done in studies of well-separated systems like the Earth and Moon, to allow for accurate reproduction of the tidal evolution at separations less than $5R_\mathrm{p}$.

3.1 Tidal Potential of Arbitrary Order

The potential V at a point on the surface of the primary due to the secondary of mass M_s orbiting on a circular path with semimajor axis a is

$$V = -G\frac{M_\mathrm{s}}{\Delta}, \tag{3.1}$$

where Δ is the distance between the center of the secondary and the point of interest given by

$$\Delta = a\left[1 - 2\left(\frac{R_\mathrm{p}}{a}\right)\cos\psi + \left(\frac{R_\mathrm{p}}{a}\right)^2\right]^{1/2}, \tag{3.2}$$

where ψ is measured from the line joining the centers of the primary and secondary (*e.g.*, Murray and Dermott (1999)). In a spherical polar coordinate system (r, θ, ϕ) with the polar angle θ measured from the rotation axis of the primary, the separation angle ψ

between the secondary and the point of interest is

$$\cos\psi \;=\; \cos\theta_{\rm p}\cos\theta_{\rm s} + \sin\theta_{\rm p}\sin\theta_{\rm s}\cos\left(\phi_{\rm p} - \phi_{\rm s}\right). \tag{3.3}$$

For widely separated binary systems where the separation of the bodies a is much larger than the radius of the primary $R_{\rm p}$, the potential is expanded in powers of the small term $R_{\rm p}/a$ such that

$$V = -G\,\frac{M_{\rm s}}{a}\left[1 + \left(\frac{R_{\rm p}}{a}\right)\cos\psi + \left(\frac{R_{\rm p}}{a}\right)^2\,\frac{1}{2}\left(3\cos^2\psi - 1\right) + \ldots\right]. \tag{3.4}$$

The first term produces no force on the primary, and the second term provides the force necessary to retain the secondary in orbit. The third term is the most important term in the tidal potential

$$U = -G\,\frac{M_{\rm s}R_{\rm p}^2}{a^3}\,\frac{1}{2}\left(3\cos^2\psi - 1\right) \tag{3.5}$$

and is the focus of past studies of tidal evolution where the the bodies are widely separated such as in the Earth-Moon system. However, truncation of the expansion of V in Equation (3.4) at three terms accurately estimates the true potential in Equation (3.1) only for separations exceeding $5R_{\rm p}$. For smaller separations, as are often found among binary asteroids, higher orders in the expansion of V are necessary.

The full expansion of the potential V may be written concisely as the sum over Legendre polynomials $P_\ell(\cos\psi)$, zonal harmonics or azimuthally independent surface harmonic functions, as

$$V = -G\frac{M_s}{a}\sum_{\ell=0}^{\infty}\left(\frac{R_p}{a}\right)^{\ell} P_\ell(\cos\psi), \tag{3.6}$$

where $\ell = 2$ is the dominant tidal term of Equation (3.5). The full tidal potential U becomes

$$U = -G\frac{M_s}{a}\sum_{\ell=2}^{\infty}\left(\frac{R_p}{a}\right)^{\ell} P_\ell(\cos\psi). \tag{3.7}$$

Table 3.1 lists the order of the expansion necessary for accurate reproduction of the tidal potential at small separations. At $2R_p$, the potential must be expanded to at least $\ell = 6$, and proceeding any closer the the primary requires the addition of an unwieldy number of terms to the expansion.

Table 3.1: Order ℓ of Legendre polynomials necessary in the expansion of the gravitational potential of a binary system (with $\psi = 0$) to accurately reproduce the full potential to within 1% at separations under $a/R_p \simeq 5$. Such small separations are common among near-Earth asteroid binaries (see Table 2.2 and Figure 2.4). Recall that the hydrostatic Roche limit is $a/R_p = 2.46$. The Legendre polynomials are given in terms of $\cos m\psi$ rather than the more common $\cos^m\psi$, where m is an integer.

ℓ	a/R_p	Legendre Polynomial
2	4.64	$\frac{1}{4}(1 + 3\cos 2\psi)$
3	3.16	$\frac{3}{8}(3\cos\psi + 5\cos 3\psi)$
4	2.51	$\frac{1}{64}(9 + 20\cos 2\psi + 35\cos 4\psi)$
5	2.15	$\frac{1}{128}(30\cos\psi + 35\cos 3\psi + 63\cos 5\psi)$
6	1.93	$\frac{1}{512}(50 + 105\cos 2\psi + 126\cos 4\psi + 231\cos 6\psi)$

3.2 Roche Limit

The hydrostatic Roche limit is located at $a/R_p = 2.46$ (Chandrasekhar, 1969) for equal density components, so if one considers secondaries just above the Roche limit, one must include the Legendre polynomials of orders $\ell \leq 4$ in the potential expansion. Aggarwal and Oberbeck (1974) calculated that a secondary with tensile strength T of

$$T \geq \frac{8}{57}\pi G \rho_p \rho_s R_s^2 \tag{3.8}$$

could orbit its primary within the Roche limit. For the rough properties of an near-Earth binary of $\rho_{p,s} = 2$ g/cm^3 and $R_s = 100$ m, a non-zero tensile strength (of order 1 N/m^2) is enough to hold the secondary together even at the surface of the primary. For comparison, the tensile strength of snow at a density of 2 g/cm^3 is of order 10^6 N/m^2; at a density of 0.1 g/cm^3, the tensile strength of snow is of order 10^3 N/m^2 (Petrovic, 2003; Button, 2008). For a main belt binary with $\rho_{p,s} = 2$ g/cm^3 and $R_s = 10$ km, the secondary requires a tensile strength of order 10^5 N/m^2, less than that of a snowball of comparable density. Therefore, in the tidal field of the primary, the secondary can stably exist within the Roche limit. Since we are not bounded by the Roche limit, we choose to work with tidal evolution from an initial separation of $a/R_p = 2$, which requires the potential to be expanded to order $\ell = 6$.

3.3 External Potential of Arbitrary Order

The tidal potential U_ℓ of arbitrary order ℓ felt by the primary, taken from Equation (3.7), may be written as

$$U_\ell \;=\; -\,\zeta_{\ell,\mathrm{p}}\, g_\mathrm{p}\, P_\ell\,(\cos\psi)\,, \tag{3.9}$$

where

$$\zeta_{\ell,\mathrm{p}} \;=\; \frac{M_\mathrm{s}}{M_\mathrm{p}}\left(\frac{R_\mathrm{p}}{a}\right)^{\ell+1} R_\mathrm{p}. \tag{3.10}$$

The combination $\zeta_{\ell,\mathrm{p}} P_\ell\,(\cos\psi)$ is the equilibrium tide height on the surface of the primary for the tidal potential of order ℓ, and $g_\mathrm{p} = GM_\mathrm{p}/R_\mathrm{p}^2$ is the surface gravity on the primary.

The tidal potential U_ℓ deforms the surface of the primary by a small amount $\lambda_{\ell,\mathrm{p}} R_\mathrm{p} S_\ell$, where S_ℓ is a surface harmonic function. Love (1944) (p. 257-259) lays the groundwork for showing that, in general, the deformation of a homogeneous density incompressible sphere

$$\lambda_{\ell,\mathrm{p}}\, R_\mathrm{p}\, S_\ell \;=\; h_{\ell,\mathrm{p}}\,\frac{U_\ell}{g_\mathrm{p}} \;=\; h_{\ell,\,\mathrm{p}}\,\zeta_{\ell,\,\mathrm{p}}\, P_\ell\,(\cos\psi)\,, \tag{3.11}$$

is given in terms of one of the Love numbers $h_{\ell,\mathrm{p}}$ (Munk and MacDonald, 1960),

$$h_{\ell,\mathrm{p}} \;=\; \frac{2\ell+1}{2\,(\ell-1)}\,\frac{1}{1+\frac{(2\ell^2+4\ell+3)\mu_\mathrm{p}}{\ell g_\mathrm{p}\rho_\mathrm{p} R_\mathrm{p}}}, \tag{3.12}$$

introducing μ_p as the rigidity or shear modulus of the primary.

Of particular interest is the external potential felt by the secondary now that the primary has been deformed. It is this external potential that will produce the tidal

torque that transfers angular momentum through the system. The surface of the nearly-spherical primary is now given by

$$R \;=\; R_{\rm p}\left(1 + \sum_{\ell=2}^{\infty} \lambda_{\ell,{\rm p}} P_\ell\left(\cos\psi\right)\right). \tag{3.13}$$

The total potential felt at a point external to the primary is the sum of the potential of a spherical primary with radius $R_{\rm p}$ and that of the deformed shell. However, only that due to the deformed shell, called the non-central potential by Murray and Dermott (1999), will contribute to the torque.

Here, we slightly alter our spherical coordinate system such that θ now measures the polar angle from the axis of symmetry of the tidal bulge. The reciprocal of the distance between the external point P located at (r, θ, ϕ) and some point on the surface of the primary P' at (r', θ', ϕ') that are separated by an angle ψ is

$$\frac{1}{\Delta} \;=\; \frac{1}{r}\sum_{\ell=0}^{\infty}\left(\frac{R_{\rm p}}{r}\right)^{\ell} P_\ell\left(\cos\psi\right) \;+\; O\left(\lambda_{\ell'}\right). \tag{3.14}$$

The use of ℓ' denotes terms based upon the surface deformation rather than the expansion of the distance between the points of interest. The non-central potential at the external point due to the deformed shell with mass element $\rho_{\rm p} R_{\rm p}^3 \sum_{\ell'=2}^{\infty} \lambda_{\ell',{\rm p}} P_{\ell'}\left(\cos\theta'\right) d\left(\cos\theta'\right) d\phi'$ is

$$U_{\rm nc} \;=\; -G\rho_{\rm p} R_{\rm p}^2 \left(\frac{R_{\rm p}}{r}\right) \sum_{\ell'=2}^{\infty}\sum_{\ell=0}^{\infty} \lambda_{\ell',{\rm p}} \left(\frac{R_{\rm p}}{r}\right)^{\ell} \int\int P_{\ell'}\left(\cos\theta'\right) P_\ell\left(\cos\psi\right) d\left(\cos\theta'\right) d\phi', \tag{3.15}$$

where the double integral goes over the surface of the primary. The integral of the

product of two surface harmonics like the Legendre polynomials over a surface is zero unless $\ell = \ell'$ such that for a specific order $\ell \geq 2$,

$$\begin{aligned} U_{\ell,\mathrm{nc}} &= -G\rho_\mathrm{p} R_\mathrm{p}^2 \left(\frac{R_\mathrm{p}}{r}\right) \lambda_{\ell,\mathrm{p}} \times \frac{4\pi}{2\ell+1} \left(\frac{R_\mathrm{p}}{r}\right)^\ell P_\ell(\cos\theta) \\ &= -\frac{3}{2\ell+1} h_{\ell,\mathrm{p}} \zeta_{\ell,\mathrm{p}} g_\mathrm{p} \left(\frac{R_\mathrm{p}}{r}\right)^{\ell+1} P_\ell(\cos\theta). \end{aligned} \tag{3.16}$$

By defining the more familiar Love number

$$k_{\ell,\mathrm{p}} = \frac{3}{2\ell+1} h_{\ell,\mathrm{p}} = \frac{3}{2(\ell-1)} \frac{1}{1 + \frac{(2\ell^2+4\ell+3)\mu_\mathrm{p}}{\ell g_\mathrm{p} \rho_\mathrm{p} R_\mathrm{p}}}, \tag{3.17}$$

the non-central potential is written in the form

$$U_{\ell,\mathrm{nc}} = -k_{\ell,\mathrm{p}} \zeta_{\ell,\mathrm{p}} g_\mathrm{p} \left(\frac{R_\mathrm{p}}{r}\right)^{\ell+1} P_\ell(\cos\theta). \tag{3.18}$$

For $R < 200$ km, as is the case for all of the main belt and near-Earth primaries and secondaries, μ dominates $g\rho R$ (Weidenschilling et al., 1989) and

$$k_{\ell,\mathrm{p}} \simeq \frac{3}{2(\ell-1)} \frac{\ell}{2\ell^2+4\ell+3} \frac{g_\mathrm{p}\rho_\mathrm{p} R_\mathrm{p}}{\mu_\mathrm{p}} = \frac{2\pi}{\ell-1} \frac{\ell}{2\ell^2+4\ell+3} \frac{G\rho_\mathrm{p}^2 R_\mathrm{p}^2}{\mu_\mathrm{p}}. \tag{3.19}$$

The complete non-central potential that perturbs the secondary orbiting a distance a from the primary is thus given by

$$U_\mathrm{nc} = -g_\mathrm{p} \sum_{\ell=2}^{\infty} k_{\ell,\mathrm{p}} \zeta_{\ell,\mathrm{p}} \left(\frac{R_\mathrm{p}}{a}\right)^{\ell+1} P_\ell(\cos\theta). \tag{3.20}$$

The θ term in the Legendre polynomial accounts for the angular separation between the secondary and the tidal bulge of the primary.

3.4 Tidal Torques on the Components

Returning to the notation where the angle ψ measures the angle from the axis of symmetry of one component's tidal bulge, the torque $\Gamma_{\ell,\mathrm{p}}$ that transfers angular momentum between the spin of the primary and the mutual orbit with semimajor axis a is

$$\Gamma_{\ell,\mathrm{p}} = -M_{\mathrm{s}}\frac{\partial U_{\ell,\mathrm{nc}}}{\partial \psi} = k_{\ell,\mathrm{p}}\zeta_{\ell,\mathrm{p}}g_{\mathrm{p}}M_{\mathrm{s}}\left(\frac{a}{R_{\mathrm{p}}}\right)^{-(\ell+1)}\left.\frac{\partial P_{\ell}\left(\cos\psi_{\mathrm{p}}\right)}{\partial \psi_{\mathrm{p}}}\right|_{\psi_{\mathrm{p}}=\epsilon_{\mathrm{p}}}, \tag{3.21}$$

where ϵ_{p} is the tidal lag angle between the tidal bulge of the primary and the line connecting the centers of the two components. Note that the torque actually scales as $\left(a/R_{\mathrm{p}}\right)^{-2(\ell+1)}$ by the definition of $\zeta_{\ell,\mathrm{p}}$. A similar torque arises from tides raised on the secondary. By the symmetry of motion about the center of mass, the torque that transfers angular momentum between the spin of the secondary and the mutual orbit is given by swapping the subscripts p and s in Equation (3.21) such that

$$\begin{aligned}\Gamma_{\ell,\mathrm{s}} &= k_{\ell,\mathrm{s}}\zeta_{\ell,\mathrm{s}}g_{\mathrm{s}}M_{\mathrm{p}}\left(\frac{a}{R_{\mathrm{s}}}\right)^{-(\ell+1)}\left.\frac{\partial P_{\ell}\left(\cos\psi_{\mathrm{s}}\right)}{\partial \psi_{\mathrm{s}}}\right|_{\psi_{\mathrm{s}}=\epsilon_{\mathrm{s}}} \\ &= k_{\ell,\mathrm{p}}\zeta_{\ell,\mathrm{p}}g_{\mathrm{p}}M_{\mathrm{s}}\left(\frac{a}{R_{\mathrm{p}}}\right)^{-(\ell+1)}\frac{\mu_{\mathrm{p}}}{\mu_{\mathrm{s}}}\left(\frac{R_{\mathrm{s}}}{R_{\mathrm{p}}}\right)^{2\ell-3}\left.\frac{\partial P_{\ell}\left(\cos\psi_{\mathrm{s}}\right)}{\partial \psi_{\mathrm{s}}}\right|_{\psi_{\mathrm{s}}=\epsilon_{\mathrm{s}}},\end{aligned} \tag{3.22}$$

and ϵ_{s} is the tidal lag angle between the tidal bulge of the secondary and the line of centers. Both torques weaken for higher orders of ℓ, and the torque due to the distortion of the secondary is weakened further for smaller secondaries.

3.5 Tidal Dissipation Function Q

In addition to the rigidity μ, the response of a homogeneous incompressible sphere to a disturbing potential is characterized by the specific tidal dissipation function Q defined by

$$Q^{-1} = \frac{1}{2\pi E^*} \oint \left(-\frac{dE}{dt} \right) dt, \tag{3.23}$$

where E^* is the maximum energy stored in the tidal distortion and the integral is the energy dissipated over one cycle (see *e.g.*, Goldreich (1963)). This definintion is akin to the quality factor in a linear, damped oscillator and does not depend on the details of how the energy is dissipated. Friction in the response of the body to the tide-raising potential plus the rotation of the body itself lead to the misalignment of the tidal bulge and line connecting the centers of the components of the binary by the tidal lag angle ϵ. For weak energy dissipation ($Q \gg 1$), the dissipation function and lag angle relate as $Q^{-1} = 2\epsilon$ (Goldreich, 1963). The tidal lag angle ϵ is always taken to be positive such that Q is also positive. To indicate whether the tidal bulge leads or lags the tide raising component of the binary, we append $\text{sign}(\omega - n)$ to our equations, where ω relates to the tidally distorted component.

The Legendre polynomials in Table 3.1 are written as sums of terms of the form $\cos m\psi$ where m is an integer. Thus, the derivative $\partial P_\ell / \partial \psi|_{\psi=\epsilon}$ is a sum of terms of the form $\sin m\epsilon$. For small tidal lag angles, $\partial P_\ell / \partial \psi|_{\psi=\epsilon} \leq 0$ and $\sin m\epsilon \simeq m\epsilon$ such that $-\partial P_\ell / \partial \psi|_{\psi=\epsilon} \propto Q^{-1}$.

3.6 Orbit Expansion and Despinning for Close Orbits

During tidal evolution, angular momentum is transferred between the spins of the components and the mutual orbit. The torque on the distorted primary alters its spin with time at a rate $\dot{\omega}_{\rm p} = \Gamma_{\rm p}/I_{\rm p}$,

$$\dot{\omega}_{\ell,{\rm p}} = \frac{\Gamma_{\ell,{\rm p}}}{\alpha_{\rm p} M_{\rm p} R_{\rm p}^2} = -\frac{k_{\ell,{\rm p}}}{\alpha_{\rm p}} \frac{q^2}{1+q} \left(\frac{a}{R_{\rm p}}\right)^{-2\ell+1} n^2 \left(-\left. \frac{\partial P_\ell\left(\cos\psi_{\rm p}\right)}{\partial \psi_{\rm p}} \right|_{\psi_{\rm p}=\epsilon_{\rm p}} \right) {\rm sign}\left(\omega_{\rm p} - n\right), \tag{3.24}$$

recalling that $\partial P_\ell/\partial\psi \leq 0$ for small angles. For rapidly spinning primaries with $\omega_{\rm p} > n$, $\dot{\omega}_{\ell,{\rm p}} < 0$ and the torque will slow the rotation. To conserve the total angular momentum of the system, the change in spin angular momentum of the primary due to the torque, $\dot{S}_{\ell,{\rm p}} = \Gamma_{\ell,{\rm p}}$, must be balanced by the change in the orbital angular momentum of the system. Equating $-\Gamma_{\ell,{\rm p}}$ to the change in orbital angular momentum $\dot{L}$ from Equation 2.1 for a circular orbit, $(q/2)\left[GM_{\rm p}^3/(1+q)a\right]^{1/2}\dot{a}$, gives the rate of change of the orbital separation due to the change in rotation of the primary as

$$\left(\frac{\dot{a}}{R_{\rm p}}\right)_{\ell,{\rm p}} = 2k_{\ell,{\rm p}}\, q \left(\frac{a}{R_{\rm p}}\right)^{-2\ell} n \left(-\left. \frac{\partial P_\ell\left(\cos\psi_{\rm p}\right)}{\partial \psi_{\rm p}} \right|_{\psi_{\rm p}=\epsilon_{\rm p}} \right) {\rm sign}\left(\omega_{\rm p} - n\right). \tag{3.25}$$

For rapidly spinning primaries, the orbit will expand as angular momentum is transferred from the spin of the primary to the mutual orbit.

Although the total angular momentum of the system is conserved, energy is dissipated in the primary's interior as heat at a rate of $\dot{E}_{\rm p} = \Gamma_{\rm p}\left(\omega_{\rm p} - n\right) < 0$ since the change in rotational energy due to the tidal torque is not equal to the change in orbital energy required by angular momentum conservation. In other words, the work done by the torque

to change the orbital energy is not equal to the work done to change the rotational energy unless $\omega_{\rm p}$ equals n, which is the synchronous end state where tidal evolution ceases.

Similarly, the torque on the distorted secondary alters its spin with time at a rate $\dot{\omega}_{\rm s} = \Gamma_{\rm s}/I_{\rm s}$,

$$\begin{aligned}\dot{\omega}_{\ell,{\rm s}} &= -\frac{k_{\ell,{\rm s}}}{\alpha_{\rm s}}\frac{1}{q\,(1+q)}\left(\frac{R_{\rm s}}{R_{\rm p}}\right)^{2\ell-1}\left(\frac{a}{R_{\rm p}}\right)^{-2\ell+1} n^2\left(-\left.\frac{\partial P_\ell\,(\cos\psi_{\rm s})}{\partial\psi_{\rm s}}\right|_{\psi_{\rm s}=\epsilon_{\rm s}}\right)\mathrm{sign}\,(\omega_{\rm s}-n) \quad (3.26)\\ &= -\frac{k_{\ell,{\rm p}}}{\alpha_{\rm p}}\frac{q}{1+q}\left(\frac{R_{\rm s}}{R_{\rm p}}\right)^{2\ell-5}\left(\frac{a}{R_{\rm p}}\right)^{-2\ell+1} n^2\,\frac{\mu_{\rm p}}{\mu_{\rm s}}\,\frac{\alpha_{\rm p}}{\alpha_{\rm s}}\left(-\left.\frac{\partial P_\ell\,(\cos\psi_{\rm s})}{\partial\psi_{\rm s}}\right|_{\psi_{\rm s}=\epsilon_{\rm s}}\right)\mathrm{sign}\,(\omega_{\rm s}-n)\,,\end{aligned}$$

and alters the semimajor axis at a rate of

$$\left(\frac{\dot{a}}{R_{\rm p}}\right)_{\ell,{\rm s}} = 2k_{\ell,{\rm p}}\,q\left(\frac{R_{\rm s}}{R_{\rm p}}\right)^{2\ell-3}\left(\frac{a}{R_{\rm p}}\right)^{-2\ell} n\,\frac{\mu_{\rm p}}{\mu_{\rm s}}\left(-\left.\frac{\partial P_\ell\,(\cos\psi_{\rm s})}{\partial\psi_{\rm s}}\right|_{\psi_{\rm s}=\epsilon_{\rm s}}\right)\mathrm{sign}\,(\omega_{\rm s}-n) \quad (3.27)$$

while dissipating energy as heat in the interior of the secondary at a rate of $\dot{E}_{\rm s} = \Gamma_{\rm s}\,(\omega_{\rm s} - n)$.

Using the fact that Q^{-1} is proportional to the derivative of the Legendre polynomials, only the size ratio of the components and their material properties in terms of μQ determine the relative strength of the torques and the relative contributions to the orbit expansion,

$$\left|\frac{\Gamma_{\ell,{\rm s}}}{\Gamma_{\ell,{\rm p}}}\right| = \left|\frac{\dot{a}_{\ell,{\rm s}}}{\dot{a}_{\ell,{\rm p}}}\right| = \frac{\mu_{\rm p}Q_{\rm p}}{\mu_{\rm s}Q_{\rm s}}\left(\frac{R_{\rm s}}{R_{\rm p}}\right)^{2\ell-3}, \quad (3.28)$$

with the contribution of the secondary decreasing at higher orders of ℓ and for smaller secondaries. Note that the relative strength of the torques is independent of the mass and

density, depending only on the size ratio. For classic $\ell = 2$ tides, the torque due to the distorted secondary is a factor of the size ratio weaker than the torque on the distorted primary. The changes in the spin rates compare as

$$\left|\frac{\dot{\omega}_{\ell,\mathrm{s}}}{\dot{\omega}_{\ell,\mathrm{p}}}\right| = \frac{\mu_\mathrm{p} Q_\mathrm{p}}{\mu_\mathrm{s} Q_\mathrm{s}} \frac{\alpha_\mathrm{p}}{\alpha_\mathrm{s}} \frac{1}{q} \left(\frac{R_\mathrm{s}}{R_\mathrm{p}}\right)^{2\ell-5} . \tag{3.29}$$

At the dominant orders, $\ell = 2$ and 3, with similar material properties, shapes, and densities, the spin rate of the secondary changes faster than the primary. Interestingly, for $\ell = 4$ and similar densities, the changes in spin rates are equal, and for $\ell > 4$, the spin rate of the primary changes faster than the secondary.

Evaluating $\partial P_\ell / \partial \psi$ explicitly for orders $\ell \leq 6$, assuming small tidal lag angles, and replacing $2\epsilon_\mathrm{p}$ with Q_p^{-1}, the spin of the primary changes as

$$\begin{aligned} \dot{\omega}_\mathrm{p} = & -\frac{8}{19} \frac{1}{\alpha_\mathrm{p}} \frac{\pi^2 G^2 \rho_\mathrm{p}^3 R_\mathrm{p}^2}{\mu_\mathrm{p} Q_\mathrm{p}} q^2 \left(\frac{a}{R_\mathrm{p}}\right)^{-6} \mathrm{sign}\left(\omega_\mathrm{p} - n\right) \\ & \times \left[1 + \frac{19}{22}\left(\frac{a}{R_\mathrm{p}}\right)^{-2} + \frac{380}{459}\left(\frac{a}{R_\mathrm{p}}\right)^{-4} + \frac{475}{584}\left(\frac{a}{R_\mathrm{p}}\right)^{-6} + \frac{133}{165}\left(\frac{a}{R_\mathrm{p}}\right)^{-8}\right], \end{aligned} \tag{3.30}$$

where n has been replaced with Kepler's Third Law to show the full dependence upon the separation of the components a/R_p. Using Equation (3.29), the spin of the secondary changes as

$$\begin{aligned} \dot{\omega}_\mathrm{s} = & -\frac{8}{19} \frac{1}{\alpha_\mathrm{s}} \frac{\pi^2 G^2 \rho_\mathrm{p}^3 R_\mathrm{p}^2}{\mu_\mathrm{s} Q_\mathrm{s}} q \left(\frac{R_\mathrm{s}}{R_\mathrm{p}}\right)^{-1} \left(\frac{a}{R_\mathrm{p}}\right)^{-6} \mathrm{sign}\left(\omega_\mathrm{s} - n\right) \\ & \times \left[1 + \frac{19}{22}\left(\frac{R_\mathrm{s}}{R_\mathrm{p}}\right)^{2}\left(\frac{a}{R_\mathrm{p}}\right)^{-2} + \frac{380}{459}\left(\frac{R_\mathrm{s}}{R_\mathrm{p}}\right)^{4}\left(\frac{a}{R_\mathrm{p}}\right)^{-4} \right. \\ & \left. + \frac{475}{584}\left(\frac{R_\mathrm{s}}{R_\mathrm{p}}\right)^{6}\left(\frac{a}{R_\mathrm{p}}\right)^{-6} + \frac{133}{165}\left(\frac{R_\mathrm{s}}{R_\mathrm{p}}\right)^{8}\left(\frac{a}{R_\mathrm{p}}\right)^{-8}\right]. \end{aligned} \tag{3.31}$$

For close orbits, the separation of the components changes as angular momentum is transferred to or from the spin of the primary according to

$$\left(\frac{\dot{a}}{R_\mathrm{p}}\right)_\mathrm{p} = \frac{8\sqrt{3}}{19}\frac{\pi^{3/2}G^{3/2}\rho_\mathrm{p}^{5/2}R_\mathrm{p}^2}{\mu_\mathrm{p}Q_\mathrm{p}}\,q\,(1+q)^{1/2}\left(\frac{a}{R_\mathrm{p}}\right)^{-11/2}\mathrm{sign}\left(\omega_\mathrm{p}-n\right) \times\left[1+\frac{19}{22}\left(\frac{a}{R_\mathrm{p}}\right)^{-2}+\frac{380}{459}\left(\frac{a}{R_\mathrm{p}}\right)^{-4}+\frac{475}{584}\left(\frac{a}{R_\mathrm{p}}\right)^{-6}+\frac{133}{165}\left(\frac{a}{R_\mathrm{p}}\right)^{-8}\right]. \quad (3.32)$$

The contribution to the change in the orbital separation due to the secondary follows similarly from Equation (3.28) as

$$\left(\frac{\dot{a}}{R_\mathrm{p}}\right)_\mathrm{s} = \frac{8\sqrt{3}}{19}\frac{\pi^{3/2}G^{3/2}\rho_\mathrm{p}^{5/2}R_\mathrm{p}^2}{\mu_\mathrm{s}Q_\mathrm{s}}\,q\,(1+q)^{1/2}\left(\frac{a}{R_\mathrm{p}}\right)^{-11/2}\mathrm{sign}\left(\omega_\mathrm{s}-n\right) \times\left[\frac{R_\mathrm{s}}{R_\mathrm{p}}+\frac{19}{22}\left(\frac{R_\mathrm{s}}{R_\mathrm{p}}\right)^{3}\left(\frac{a}{R_\mathrm{p}}\right)^{-2}+\frac{380}{459}\left(\frac{R_\mathrm{s}}{R_\mathrm{p}}\right)^{5}\left(\frac{a}{R_\mathrm{p}}\right)^{-4} +\frac{475}{584}\left(\frac{R_\mathrm{s}}{R_\mathrm{p}}\right)^{7}\left(\frac{a}{R_\mathrm{p}}\right)^{-6}+\frac{133}{165}\left(\frac{R_\mathrm{s}}{R_\mathrm{p}}\right)^{9}\left(\frac{a}{R_\mathrm{p}}\right)^{-8}\right]. \quad (3.33)$$

The overall change in the orbital separation is the sum of the contributions from each component, $\dot{a} = \dot{a}_\mathrm{p} + \dot{a}_\mathrm{s}$,

$$\frac{\dot{a}}{R_\mathrm{p}} = \frac{8\sqrt{3}}{19}\frac{\pi^{3/2}G^{3/2}\rho_\mathrm{p}^{5/2}R_\mathrm{p}^2}{\mu_\mathrm{p}Q_\mathrm{p}}\,q\,(1+q)^{1/2}\left(\frac{a}{R_\mathrm{p}}\right)^{-11/2} \times\left[\mathrm{sign}\left(\omega_\mathrm{p}-n\right)+\left(\frac{R_\mathrm{s}}{R_\mathrm{p}}\right)\frac{\mu_\mathrm{p}Q_\mathrm{p}}{\mu_\mathrm{s}Q_\mathrm{s}}\mathrm{sign}\left(\omega_\mathrm{s}-n\right) +\frac{19}{22}\left(\frac{a}{R_\mathrm{p}}\right)^{-2}\left(\mathrm{sign}\left(\omega_\mathrm{p}-n\right)+\left(\frac{R_\mathrm{s}}{R_\mathrm{p}}\right)^{3}\frac{\mu_\mathrm{p}Q_\mathrm{p}}{\mu_\mathrm{s}Q_\mathrm{s}}\mathrm{sign}\left(\omega_\mathrm{s}-n\right)\right) +\frac{380}{459}\left(\frac{a}{R_\mathrm{p}}\right)^{-4}\left(\mathrm{sign}\left(\omega_\mathrm{p}-n\right)+\left(\frac{R_\mathrm{s}}{R_\mathrm{p}}\right)^{5}\frac{\mu_\mathrm{p}Q_\mathrm{p}}{\mu_\mathrm{s}Q_\mathrm{s}}\mathrm{sign}\left(\omega_\mathrm{s}-n\right)\right) +\frac{475}{584}\left(\frac{a}{R_\mathrm{p}}\right)^{-6}\left(\mathrm{sign}\left(\omega_\mathrm{p}-n\right)+\left(\frac{R_\mathrm{s}}{R_\mathrm{p}}\right)^{7}\frac{\mu_\mathrm{p}Q_\mathrm{p}}{\mu_\mathrm{s}Q_\mathrm{s}}\mathrm{sign}\left(\omega_\mathrm{s}-n\right)\right)$$

$$+\frac{133}{165}\left(\frac{a}{R_{\rm p}}\right)^{-8}\left[\text{sign}\left(\omega_{\rm p}-n\right)+\left(\frac{R_{\rm s}}{R_{\rm p}}\right)^{9}\frac{\mu_{\rm p}Q_{\rm p}}{\mu_{\rm s}Q_{\rm s}}\text{sign}\left(\omega_{\rm s}-n\right)\right]. \qquad (3.34)$$

Obviously, the contribution of the secondary is most important when the components are of similar size. Note that any difference in density between the components is accounted for in the mass ratio q; otherwise, only the size ratio of the components is involved in the terms due to the secondary. Not only is the contribution of the secondary weakened because of its smaller size, it should also be despun faster than the primary at the dominant orders of ℓ such that its contribution turns off when $\omega_{\rm s} = n$ long before the primary does the same. Higher orders in ℓ are only needed at small separations as the strength of these extra terms falls off by an additional square of the separation for each order of ℓ. With the framework in place, we can now use tidal evolution as a means of discerning the material properties μQ of asteroids in binary systems in Chapter 4.

CHAPTER 4

MATERIAL PROPERTIES OF BINARY ASTEROIDS

Calculations of material strength based on limiting the tidal evolution time to the age of the solar system indicate that binaries with 100 km-scale primaries are consistent with being made of monolithic or fractured rock as expected for binaries likely formed from sub-catastrophic impacts in the early solar system. To tidally evolve in their dynamical lifetime, near-Earth binaries with 1 km-scale primaries created via a spin-up mechanism must be mechanically weaker than their main belt counterparts or else be formed in the main belt prior to injection into the near-Earth region. Several issues affecting the calculation are considered with uncertainty in the age of binary systems having the strongest effect on the determination of material strength.

4.1 Caveats

In estimating the material properties of binary asteroids, we assume that tides are the dominant method of evolution in these systems, specifically in the evolution of the separation between the components. It has recently been argued that the binary YORP effect (BYORP; Ćuk and Burns, 2005), where a synchronous secondary acts to asymmetrically reradiate sunlight with respect to its orbital velocity (similar to how the YORP effect is an asymmetric reradition of sunlight with respect to the rotational velocity) so that the orbit is expanded or contracted, can act on timescales faster than tidal evolution in the near-Earth region (Goldreich and Sari, 2009). However, unlike the YORP effect, BYORP has yet to be proven observationally. Furthermore, BYORP requires a synchronous secondary and, thus, could not be the dominant evolution mechanism for systems with asynchronous secondaries like 2004 DC (discussed in Chapter 7). Also of interest for rapidly spinning primaries is the idea of mass lofting (Harris et al., 2008),

where particles at the equator of a rapidly-spinning primary become weightless due to the gravitational presence of the secondary passing overhead, causing the particles to briefly enter orbit, transferring angular momentum to the orbit of the secondary before falling back to the surface of the primary. This method has also been argued to expand the mutual orbit more quickly than tidal evolution (Fahnestock and Scheeres, 2008). It may be a combination of effects, also including close planetary flybys, that evolve the separation of near-Earth binary components, but tides are the only mechanism one can say at this time must act on all systems. For main belt binaries with 100-km scale primaries, tides are the dominant mechanism because planetary encounters are not feasible in the main belt, the thermal YORP and BYORP effects are weakened by the increased heliocentric distance to the main belt (and the increased sizes of the bodies involved), and the primaries do not rotate rapidly enough nor are are the secondaries close enough to produce mass lofting.

4.2 Estimation of μQ for Binary Systems

Material properties, in terms of the product of the rigidity and tidal dissipation function μQ, and the time over which tidal evolution has taken place Δt are inherent unknowns in a binary system. However, the ratio $\mu Q/\Delta t$ is fully determined by the current separation of the binary system $a_{\rm f}/R_{\rm p}$, the physical sizes and masses of the components, and the assumption of an initial separation of the components after the formation of the binary. Here we use $a_{\rm i}/R_{\rm p} = 2$, so that solving for the semimajor axis of the mutual orbit as a function of time for the classical tidal formulation with $\ell = 2$ gives

$$\frac{\mu Q}{\Delta t} = \frac{8\sqrt{3}}{19}\pi^{3/2} G^{3/2} \rho_{\rm p}^{5/2} R_{\rm p}^2 \, q \, (1+q)^{1/2} \left[\int_2^{a_{\rm f}/R_{\rm p}} \left(\frac{a}{R_{\rm p}} \right)^{11/2} {\rm d}\left(a/R_{\rm p} \right) \right]^{-1} \qquad (4.1)$$

for $\omega_p > n$ and only accounting for tides raised on the primary. To estimate either μQ or Δt, the other must be assumed where varying one by, say, an order of magnitude varies the other parameter by the same amount. With a judicious assumption of the age of the binary, one can estimate μQ for the binary or at least place bounds on the value of μQ. Such an analysis was done for the martian moon Phobos by Yoder (1981) who estimated μQ is of order 10^{11} N/m^2 based on the inward evolution of Phobos' orbit from its inner synchronous orbit about Mars.

Because the above equation has only accounted tides raised on the primary, it represents a lower bound on μQ of the system for the timescale Δt because the tide raised on the secondary will assist in the expansion until the secondary is despun to synchronous rotation. Taking $\mu_s Q_s = \mu_p Q_p$, $\omega_s > n$, and allowing the secondary to contribute for the entire evolution gives an upper limit on μQ for the system, which is a factor of $1 + R_s/R_p$, or $1 + q^{1/3}$ for equal density components, greater than the lower limit found using only the primary. If Δt is correct, the actual μQ for the system should lie between the two bounds. Ideally, one would know the initial spin states of the components, integrate the spin rates for $\ell = 2$ in Equations (3.24) and (3.27) and include both tides until the secondary is despun, then include only the tide on the primary for the remainder of Δt. Our ignorance of the secondary's initial spin state cannot change the estimate of μQ by more than a factor of two, far less critical than the choice of Δt, the age of the binary.

4.3 Main Belt and Jupiter Trojan Binaries

Assuming the value of μQ of 10^{11} N/m^2 for Phobos found by Yoder (1981) is applicable to the components of main belt binaries, timescales for tidal evolution are plotted in Figure 4.1. The main belt binaries with $q < 0.1$ cluster around ages of order one

billion years for this particular value of μQ. Solid rock has a rigidity μ of 10^{10} N/m^2 or greater (Weidenschilling et al., 1989), and we have assumed $Q \gg 1$ earlier such that the product μQ for solid rock would be of order 10^{12} N/m^2 or greater. A fractured rock would have a lower rigidity like that of Phobos.

To place a concrete upper limit on the μQ of these systems, we set Δt to 4.5 Gy, the age of the solar system and the maximum amount of time these systems could have been evolving, in Equation (4.1) and also include tides on the secondary for all of Δt by inserting a factor of $1 + R_s/R_p$. This is equivalent to saying the secondary has yet to despin or has reached synchroneity at this instant. Ignoring (90) Antiope and (617) Patroclus, which tidally evolve on timescales much more rapid than the age of the solar system due to having nearly equal-size components, the average upper bound on μQ from Table 4.1 for main belt binaries with 100 km-scale primaries is 10^{12} N/m^2. This is one order of magnitude larger than Yoder (1981) found for Phobos, but reasonable for solid or fractured rock. Lower bounds on μQ calculated from Equation (4.1) also average 10^{12} N/m^2 since the bounds must differ by less than a factor of 2.

The despinning timescales for the binary components of these systems, $\omega/\dot{\omega}$, are of order 1-10 My for the $q < 0.001$ secondaries and much, much longer than the age of the solar system for the primaries at their current separations. At smaller separations, the despinning timescales are shorter. Thus, one would expect the secondaries in collisional binaries to have synchronized their rotation to their mean motion in the mutual orbit even if the systems are much younger than 4.5 Gy. Because the despinning timescale of the primaries far exceed the age of the solar system, the fact the systems are still tidally evolving does not limit the age of the binaries.

An example of tidal evolution for a $q = 0.001$ binary is shown in Figure 4.2. The expansion of the mutual orbit and the despinning of the components are calculated with

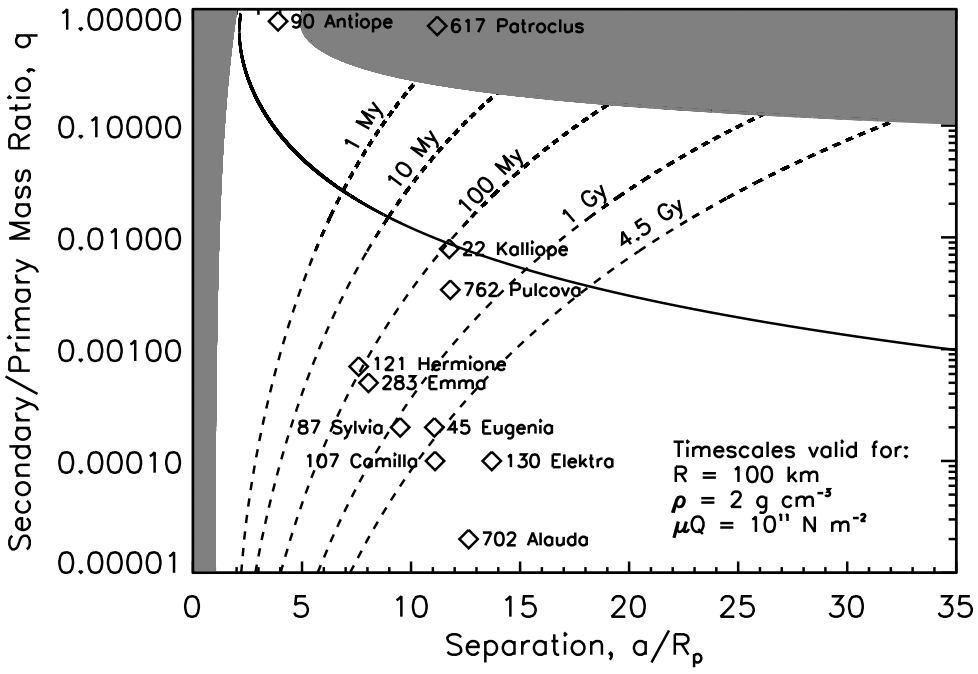

Figure 4.1: Mass ratio q and primary-secondary separation in terms of the primary radius $a/R_{\rm p}$ for select main belt and Jupiter Trojan binaries along with the angular momentum limit for $J/J' = 0.5$. Tidal evolution timescales are calculated assuming $\rho_{\rm p,s} = 2$ g/cm^3, $R_{\rm p} = 100$ km, and $\mu_{\rm p} Q_{\rm p} = \mu_{\rm s} Q_{\rm s} = 10^{11}$ N/m^2 and allowing tides from both components to contribute over the entire evolution from an initial separation of $2R_{\rm p}$. One expects (130) Elektra and (702) Alauda to have the smallest μQ for a 4.5 Gy evolution unless they have not evolved significantly in separation. With these parameters, (90) Antiope evolves far more rapidly than the other main belt binaries.

Table 4.1: Physical properties of select main belt and Jupiter trojan binary asteroids with primary radii of order 100 km. Lower and upper bounds on the product of rigidity and the specific tidal dissipation function μQ are given corresponding to primary tides only and primary plus secondary tides, respectively, acting over the 4.5 Gy age of the solar system. For (45) Eugenia and (87) Sylvia, only the larger satellite is considered.

† (90) Antiope is known to be in a fully despun, double synchronous state where tidal evolution has ceased. Because of the nearly equal-sized components, the tidal evolution occurred over much less than the age of the solar system.

‡ (617) Patroclus may have formed in a giant impact or via *n*-body capture with a larger initial separation than the value of $2R_p$ assumed here.

	Name	R_p [km]	R_s/R_p	q	ρ [g/cm^3]	a/R_p	J/J'	μQ [N/m^2]	
								Lower	Upper
22	Kalliope	91	0.198	0.0077	2.37	11.7	0.230	4.1×10^{12}	5.0×10^{12}
45	Eugenia	108	0.059	0.0002	1.12	11.0	0.220	3.6×10^{10}	3.8×10^{10}
87	Sylvia	143	0.063	0.0003	1.2	9.48	0.233	2.3×10^{11}	2.5×10^{11}
90	Antiope	44	0.954	0.8695	1.25	3.90	0.488	3.8×10^{16}	7.4×10^{16}†
107	Camilla	112	0.040	0.00006	1.88	11.0	0.199	4.3×10^{10}	4.4×10^{10}
121	Hermione	105	0.086	0.0006	1.8	7.57	0.179	3.8×10^{12}	4.1×10^{12}
130	Elektra	91	0.022	0.00001	3.8	13.8	0.130	6.6×10^{9}	6.7×10^{9}
283	Emma	74	0.081	0.0005	0.87	8.05	0.207	1.7×10^{11}	1.9×10^{11}
617	Patroclus	61	0.934	0.8159	0.8	11.2	0.757	2.4×10^{13}	4.6×10^{13}‡
702	Alauda	97	0.029	0.00002	1.6	12.6	0.125	3.1×10^{9}	3.2×10^{9}
762	Pulcova	69	0.145	0.0030	1.8	11.7	0.178	4.5×10^{11}	5.2×10^{11}

a simple fourth-order Runge-Kutta integration of Equations (3.34), (3.24), (3.27) for classical tides with $\ell = 2$ (the first term in brackets of each equation). The integration accounts for the synchronization of the components by turning off the tidal contributions when $\omega = n$. In this case, the secondary is rapidly despun, and the primary dominates the tidal evolution, retaining essentially its entire initial spin rate resulting in a binary system similar to (121) Hermione or (283) Emma. The quick synchronization of the secondary and the negligible despinning of the primary make our ignorance of the initial spin states unimportant for tidal evolution of binaries with small secondaries.

Taking the average μQ of 10^{12} N/m^2 found for the $q < 1$ main belt binaries, (90) Antiope needs less than 100,000 years to evolve from near-contact to its present separation, shown by Figure 4.3. If Antiope is heavily fractured, as a binary possibly formed by spin-up could be, the time needed to tidally evolve becomes even shorter by an order of magnitude for every order of magnitude less than 10^{12} N/m^2 the material strength of Antiope is. Though Antiope is clearly tidally evolved, because the system can evolve to its observed end state rapidly for any reasonable μQ value, one cannot constrain the material properties of Antiope well through tidal evolution.

4.4 Near-Earth Binaries

The dynamical lifetime of an asteroid in the near-Earth region is of order 10 My (Gladman et al., 1997, 2000), so the spread of data beyond the generic 10 My evolution curve in Figure 4.4 implies either the actual μQ values are much weaker than the assumed 10^{11} N/m^2 or that the systems must be older than 10 My, having formed in the main belt prior to injection into the near-Earth region. Assuming all the binaries have tidally evolved for 10 My, the average lower limit on μQ in Table 4.2 is 5×10^9 N/m^2, nearly

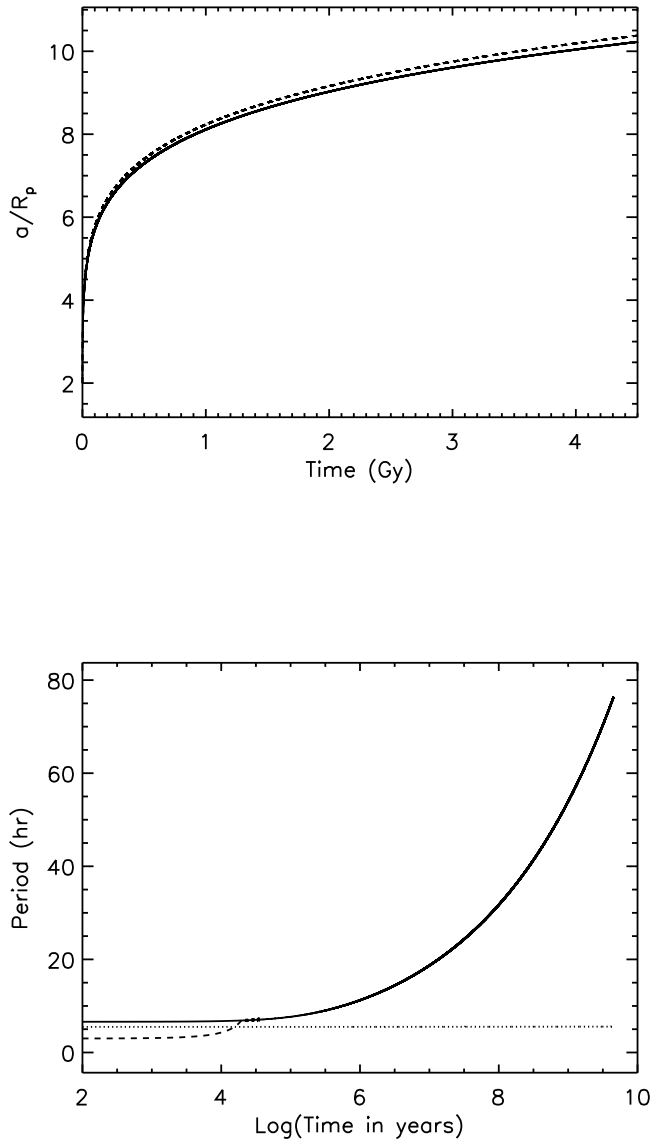

Figure 4.2: Tidal evolution of a main belt binary system (R_p = 100 km, ρ = 2 g/cm^3, $\mu_p Q_p = \mu_s Q_s = 10^{12}$ N/m^2) with q = 0.001 in terms of the orbit expansion (top) and the rotation and orbit periods (bottom) over 4.5 Gy. The orbit expands (solid line, top) rapidly from $2R_p$ to $8R_p$ in the first billion years. The dashed line (top) represents the orbit expansion if the secondary contributed over the entire age of the solar system. The secondary (dashed line, bottom) is despun to the orbital period (solid line) in less than 100,000 years making the tidal evolution essentially due to tides raised on the primary only. The dominance of the primary is illustrated by the negligible amount of despinning of the primary (dotted line) over the age of the solar system.

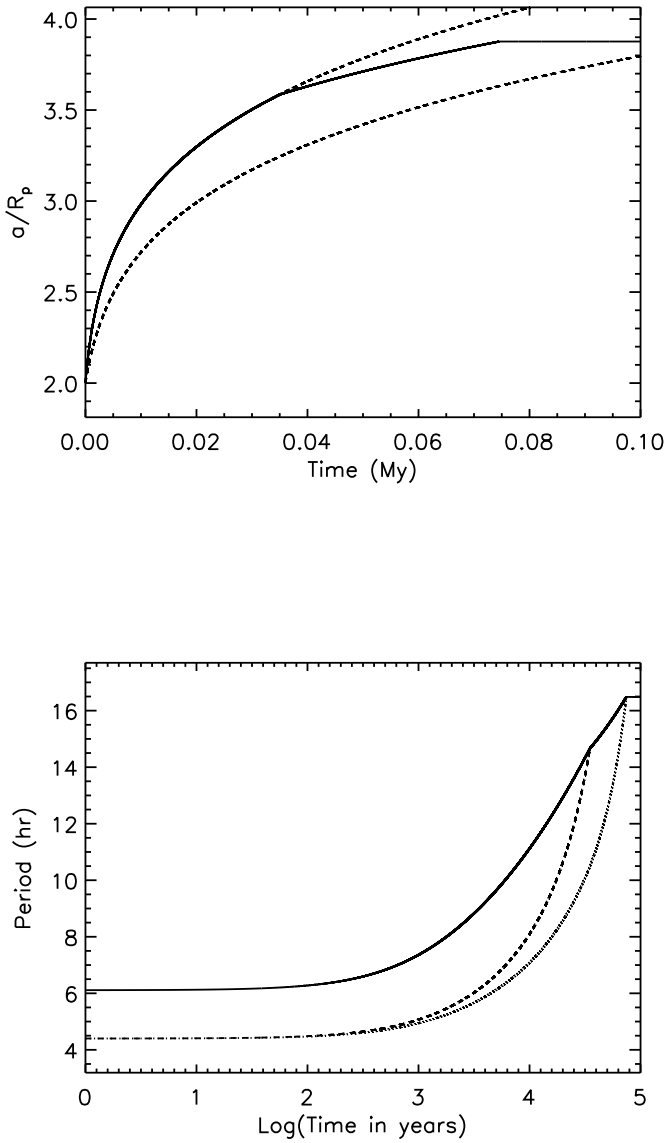

Figure 4.3: Tidal evolution of $q = 0.8695$ binary (90) Antiope using the parameters in Table 4.1 and $\mu_p Q_p = \mu_s Q_s = 10^{12}$ N/m^2. The initial spin period of 4.4 hours for both components is necessary to satisfy $J/J' = 0.488$. The system reaches the fully despun, double synchronous end state (bottom) as the orbital period (solid), spin period of the secondary (dashed), and spin period of the primary (dotted) coincide in less than 80,000 years. The orbit expansion (solid line, top) is bracketed by dashed lines representing tidal evolution for just the primary (below) and both components (above). The kinks in the orbit expansion illustrate where the contribution from the secondary turns off as it synchronizes and then where the primary synchronizes halting the tidal evolution.

three orders of magnitude smaller than the average main belt binary μQ of 10^{12} N/m^2. However, we note that if the near-Earth binaries are 4.5 Gy old, the average μQ is of order 10^{12} N/m^2 meaning the near-Earth binaries can have the same material properties as the main belt binaries if the binaries all have the same age! This fact illustrates the inherent difficulty in deriving material properties from tidal evolution as the choice of the binary's age strongly affects the result for material properties and vice versa.

Though far less rigid than solid rock, μ as low as 10^7 N/m^2 for a 1 km body (10^6 N/m^2 for a 100 m body) remain reasonable within the description of Goldreich and Sari (2009) for rubble pile conglomerations of small, identical spheres or irregularly shaped pieces. Void space between the constituent particles, each of which has the rigidity of solid rock of order 10^{10} N/m^2, and the increased stress at contact points lower the equivalent rigidity of the rubble pile as a whole compared to monolithic rock and can easily account for μQ values of order 10^9 N/m^2. Even at such low rigidities, the Love number approximation of $\mu \gg g\rho R$ holds because of the small size and gravity of km-scale near-Earth asteroids.

The despinning timescales for the binary components of these systems are of order 1-10 My for the secondary and of order 100 My to the age of the solar system for the primaries assuming $q = 0.01 - 0.1$, a separation of $4R_p$, and the μQ values found for a 10 My tidal evolution. For smaller separations, the timescales shorten such that, like the main belt binaries, one would expect the secondaries in near-Earth binary systems to have essentially synchronized their rotation to their mean motion in the mutual orbit, but one would not expect the systems to have have reached a fully despun, double synchronous end state. Tidal evolution for a binary system with $q = 0.1$, similar to (66391) 1999 KW$_4$, is shown in Figure 4.5. Even at $q = 0.1$, the tidal contribution of the secondary is barely noticeable as it is quickly synchronized to the orbital mean motion in

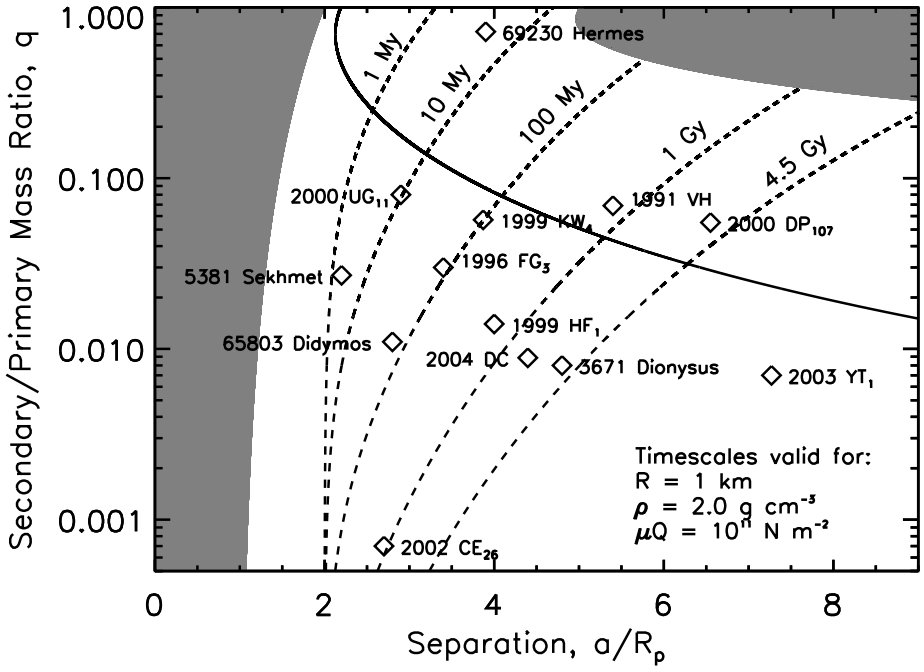

Figure 4.4: Mass ratio q and primary-secondary separation in terms of the primary radius a/R_p for select near-Earth binaries along with the angular momentum limit for $J/J' = 0.5$. Tidal evolution timescales are calculated assuming $\rho_{\mathrm{p,s}} = 2$ g/cm^3, $R_\mathrm{p} = 1$ km, and $\mu_\mathrm{p} Q_\mathrm{p} = \mu_\mathrm{s} Q_\mathrm{s} = 10^{11}$ N/m^2 and allowing tides from both components to contribute over the entire evolution from an initial separation of $2R_\mathrm{p}$. The spread of the binaries across a range of timescales indicates either a range of ages for the binaries, a range of material strengths in terms of μQ, or a combination of both among the near-Earth population.

Table 4.2: Physical properties of select near-Earth binary asteroids with primary radii of order 1 km. Lower and upper bounds on the product of rigidity and the specific tidal dissipation function μQ are given corresponding to primary tides only and primary plus secondary tides, respectively, acting over the 10 My dynamical lifetime of near-Earth asteroids.
† (69230) Hermes is known to be in a fully despun, double synchronous state where tidal evolution has ceased.

	Name	R_p [km]	R_s/R_p	q	ρ [g/cm^3]	a/R_p	J/J'	μQ [N/m^2]	
								Lower	Upper
3671	Dionysus	0.75	0.2	0.008	1.6	4.8	0.397	7.9×10^{7}	9.4×10^{7}
5381	Sekhmet	0.7	0.214	0.0098	2	2.2	0.355	5.1×10^{10}	6.1×10^{10}
35107	1991 VH	0.6	0.417	0.0723	1.6	5.33	0.499	2.4×10^{8}	3.3×10^{8}
65803	Didymos	0.4	0.188	0.0066	1.7	2.75	0.454	9.1×10^{8}	1.1×10^{9}
66391	1999 KW_4	0.66	0.342	0.0402	1.97	3.87	0.392	2.1×10^{9}	2.9×10^{9}
69230	Hermes	0.31	0.898	0.7236	1.8	3.90	0.484	8.5×10^{9}	1.6×10^{10}†
137170	1999 HF_1	1.87	0.214	0.0098	2	3.74	0.415	5.3×10^{9}	6.5×10^{9}
	1996 FG_3	0.7	0.31	0.030	1.4	3.43	0.348	1.7×10^{9}	2.2×10^{9}
	2000 DP_{107}	0.4	0.375	0.0527	1.7	6.55	0.455	2.3×10^{7}	3.2×10^{7}
	2000 UG_{11}	0.12	0.417	0.0723	0.8	2.83	0.402	1.1×10^{8}	1.6×10^{8}
	2002 CE_{26}	1.74	0.086	0.0006	0.9	2.70	0.424	3.9×10^{8}	4.2×10^{8}
	2003 YT_1	0.53	0.189	0.0067	2.01	6.42	0.410	8.8×10^{6}	1.1×10^{7}
	2004 DC	0.17	0.207	0.0089	1.70	4.41	0.402	9.1×10^{6}	1.1×10^{7}

0.1 My. Therefore, one must only be concerned with the contribution of the secondary to orbit expansion when $q \sim 1$ in systems such as (90) Antiope and (69230) Hermes where μQ is not well-constrained. Otherwise, for $q < 1$, the material properties are easily estimated using primary tides only.

For the binary systems like 2004 DC and 2003 YT_1, with μQ of order 10^7 N/m^2, the weakness of the primary is at the border line of Goldreich and Sari's theory of rubble pile structure. For μQ of these systems to be larger, one of the following must be true: the system is older than 10 My, the orbit expansion is aided by another mechanism (BYORP, mass lofting, or close planetary flyby), or the system formed recently in nearly its current configuration leaving μQ unconstrained to justify a more rigid structure than that found through the above tidal evolution scenario. 2004 DC and 2003 YT_1 are also believed to have asynchronous secondaries that have yet to despin to the mean motion as well as having eccentric mutual orbits, placing them in the minority among near-Earth binary systems compared to the more prevalent synchronous secondaries with circularized orbits. Given that the primary dominates the tidal evolution and the secondaries are rapidly despun in $q < 1$ binary systems, finding an asynchronous secondary appears to indicate youth. However, if these systems are younger than the 10 My age assumed, μQ must be even lower to allow the systems to tidally evolve outward in a shorter amount of time unless the binaries formed near the current configuration. μQ could be larger if the binaries are older than 10 My, but then one must explain why the secondaries are not despun over the longer timescale. The eccentric nature of the mutual orbit could be key to understanding why these systems stand out among the rest of the near-Earth binary population. Eccentricities and the case of 2004 DC will be further discussed in Chapters 5 and 7, respectively.

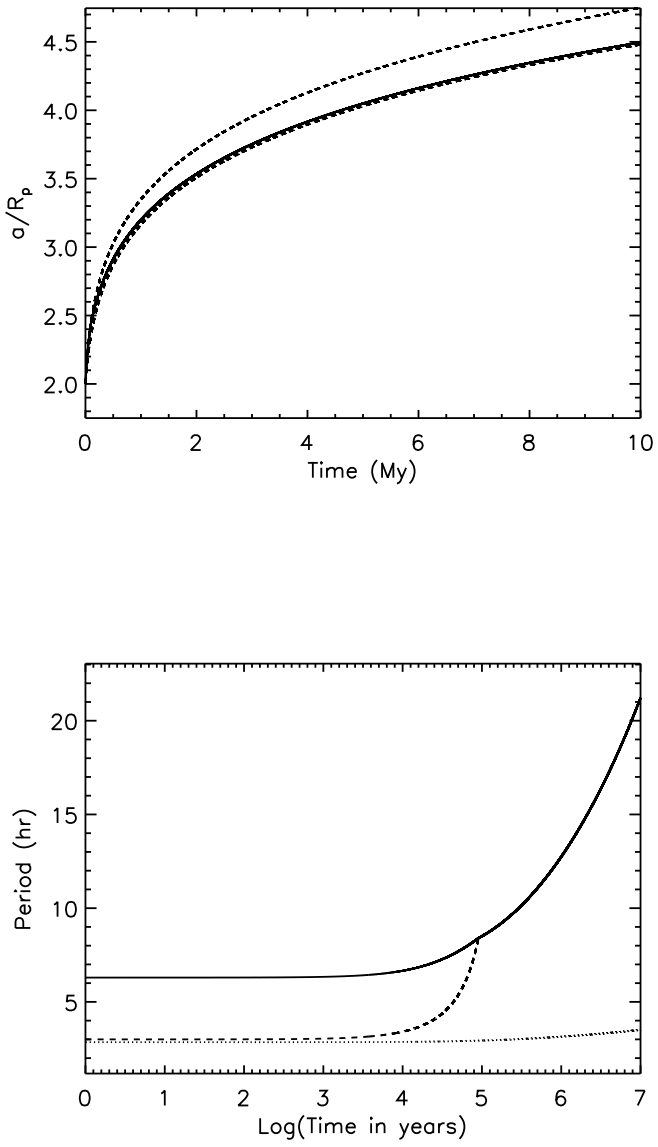

Figure 4.5: Tidal evolution of a near-Earth binary system (R_p = 1 km, ρ = 2 g/cm^3, $\mu_\mathrm{p} Q_\mathrm{p} = \mu_\mathrm{s} Q_\mathrm{s} = 5 \times 10^9$ N/m^2, $J/J' = 0.4$) with $q = 0.1$ in terms of the orbit expansion (top) and the rotation and orbit periods (bottom) over 10 My. The orbit size (solid) doubles over 10 My and closely follows the lower bound for tides on the primary only (dashed) indicating the dominance of the primary in tidal evolution. The secondary (dashed line, bottom) is despun to the orbital period (solid line) in 100,000 years, and the primary is despun by less than one hour.

4.5 Correction for Close Orbits

In Chapter 3 we derived tidal evolution equations applicable to binaries in close orbits by increasing the accuracy to which we reproduce the tidal potentials due to the components. Inside the close orbit regime of $5R_{\rm p}$, higher orders in ℓ must be included such that numerical integration of

$$\begin{aligned}\frac{\mu Q}{\Delta t} &= \frac{8\sqrt{3}}{19}\pi^{3/2}G^{3/2}\rho_{\rm p}^{5/2}R_{\rm p}^{2}q\,(1+q)^{1/2} \\ &\times\left[\int_{2}^{a_{\rm f}/R_{\rm p}}\frac{\left(a/R_{\rm p}\right)^{11/2}}{1+\frac{19}{22}\left(\frac{a}{R_{\rm p}}\right)^{-2}+\frac{380}{459}\left(\frac{a}{R_{\rm p}}\right)^{-4}+\frac{475}{584}\left(\frac{a}{R_{\rm p}}\right)^{-6}+\frac{133}{165}\left(\frac{a}{R_{\rm p}}\right)^{-8}}\mathrm{d}\left(a/R_{\rm p}\right)\right]^{-1} \quad (4.2)\end{aligned}$$

gives the corrected μQ for evolution due to the distorted primary only. Including the contribution of the distorted secondary requires numerical integration of Equation (3.34).

Because the close orbit correction adds terms that enhance the rate of orbit expansion, μQ must increase to provide the same tidal evolution over the same timescale Δt. The increase in μQ from using up to $\ell = 6$ compared to the classical limit of $\ell = 2$ is

$$\frac{\mu Q_{\ell=6}}{\mu Q_{\ell=2}} = \frac{\int_{2}^{a_{\rm f}/R_{\rm p}}\left(\frac{a}{R_{\rm p}}\right)^{11/2}\mathrm{d}\left(a/R_{\rm p}\right)}{\int_{2}^{a_{\rm f}/R_{\rm p}}\frac{\left(a/R_{\rm p}\right)^{11/2}}{1+\frac{19}{22}\left(\frac{a}{R_{\rm p}}\right)^{-2}+\frac{380}{459}\left(\frac{a}{R_{\rm p}}\right)^{-4}+\frac{475}{584}\left(\frac{a}{R_{\rm p}}\right)^{-6}+\frac{133}{165}\left(\frac{a}{R_{\rm p}}\right)^{-8}}\mathrm{d}\left(a/R_{\rm p}\right)} \quad (4.3)$$

and shown as a function of the final separation in Figure 4.6. Evolution from a close initial orbit of $2R_{\rm p}$ to a wide separation of $10R_{\rm p}$ results in only a 1.3% increase in μQ over the classical value of Equation (4.1). Thus, the basic $\ell = 2$ tidal mechanism is sufficient for the main belt binaries that are widely separated. On the other hand, if the final separation is smaller, as is the case for most near-Earth binaries, the correction is

larger, increasing to 5% for evolution from $2R_p$ to $5R_p$ and 15% for evolution from $2R_p$ to $3R_p$. When making a coarse estimate of the bulk material properties of the system, taking the close orbit into account is not that important. Classical tides will easily give order of magnitude estimates for even the closest binaries in our subset.

4.6 Effect of Initial Separation

Because of the strong inverse dependence of the orbital expansion rate on the separation of the components, $\dot{a}/R_p \propto \left(a/R_p\right)^{-11/2}$, the binary rapidly evolves through the region where the close orbit correction is needed. The most significant portion of the tidal evolution timescale Δt is spent near the current value of the separation. Subsequently, the value of μQ calculated for the system is weakly dependent upon the exact value of the initial separation. In fact, to produce a factor of ~2 increase in the estimates of μQ in Tables 4.1 and 4.2, the initial separation must be set to ~90% of the current separation of the components!

In general, for any initial separation a_i/R_p, the estimated μQ for the system compared to the μQ found for $a_i/R_p = 2$ is

$$\frac{\mu Q_i}{\mu Q_2} = \frac{\int_2^{a_f/R_p} \left(\frac{a}{R_p}\right)^{11/2} \mathrm{d}\left(a/R_p\right)}{\int_{a_i/R_p}^{a_f/R_p} \left(\frac{a}{R_p}\right)^{11/2} \mathrm{d}\left(a/R_p\right)} \tag{4.4}$$

and shown in Figure 4.7. Changing the initial separation from $2R_p$ to the contact limit is completely negligible for the main belt binaries that are widely separated. For near-Earth binaries that are not so widely separated, pushing the initial separation inward of $2R_p$ affects the estimate of μQ by less than 1%. Pushing the initial separation outward

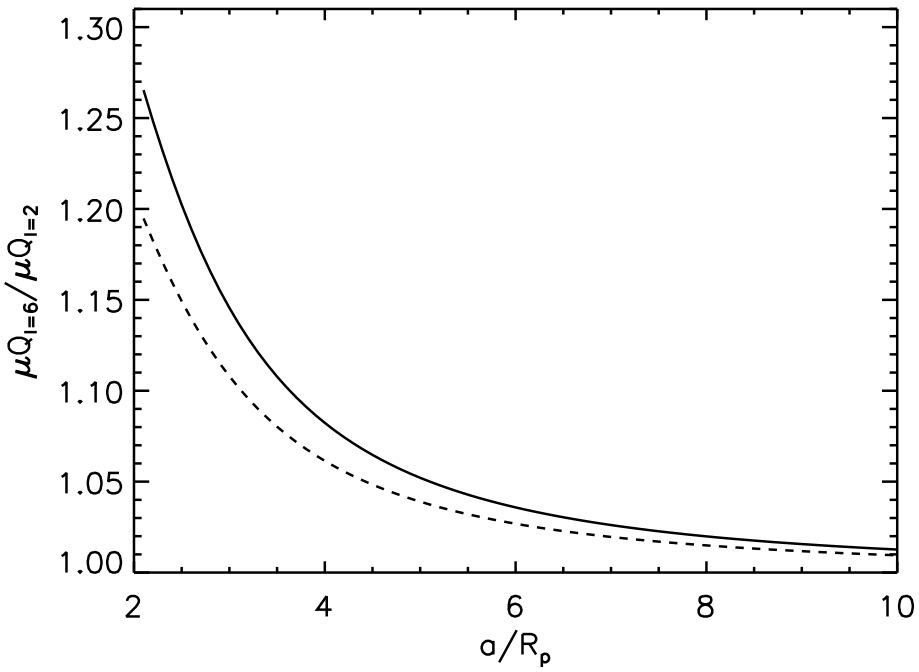

Figure 4.6: In terms of the ratio $\mu Q_{\ell=6}/\mu Q_{\ell=2}$ for tidal evolution from $2R_{\rm p}$ with both components contributing, $q = 0$ (primary tides only) and $q = 1$ share the upper curve and are the most affected by the close orbit correction; the ratio for $q = 0.15$ (dashed curve) is the least affected by the close orbit correction. Overall, the close orbit correction is roughly 20% at $2R_{\rm p}$ and quickly falls off to 5% at $5R_{\rm p}$ and to 1% at $10R_{\rm p}$ for all mass ratios.

to $5R_p$ for main belt binaries currently separated by $\sim 10R_p$ only has a 1% effect on μQ as well. For a binary like (617) Patroclus that may have formed via dynamical capture at a separation greater than $2R_p$, only if the initial separation were $8R_p$ does the estimate of μQ change by $\sim$10%. This illustrates the importance of accurate orbit and size determination at the present epoch for estimating the material properties of a binary system as opposed to needing to accurately know the initial conditions of the system when the binary was first created.

Using the close orbit correction to find the ratio in Equation (4.4) has a negligible effect on these results, but the correction should be applied as dictated in the previous section for finding an explicit value of μQ in a close binary system. Accounting for the contribution from the secondary also has a negligible effect on the ratio. For the classical $\ell = 2$ tides, Equation (4.4) is independent of the mass ratio q, and using the close orbit correction introduces an extremely weak dependence on q.

4.7 Effect of Unequal Component Densities

Often it is assumed that the components of a binary system have similar uniform densities as we have thus far in this chapter in Tables 4.1 and 4.2. If, instead, the secondary is denser than the primary, the mass ratio $q = \rho_s/\rho_p \left(R_s/R_p\right)^3$ will increase accordingly resulting in faster tidal evolution for the same values of μQ: the spin rates will change faster because $\dot{\omega}_p \propto \left(\rho_s/\rho_p\right)^2$ and $\dot{\omega}_s \propto \rho_s/\rho_p$, and the orbit expansion will proceed faster as it varies directly with the mass ratio as $q\,(1+q)^{1/2}$. Since we are assuming a fixed timescale for evolution from an initial configuration to the current configuration, μQ must increase. The components must be mechanically stronger to compensate for or resist the faster tidal evolution implied by an increased mass ratio. Conversely, a less

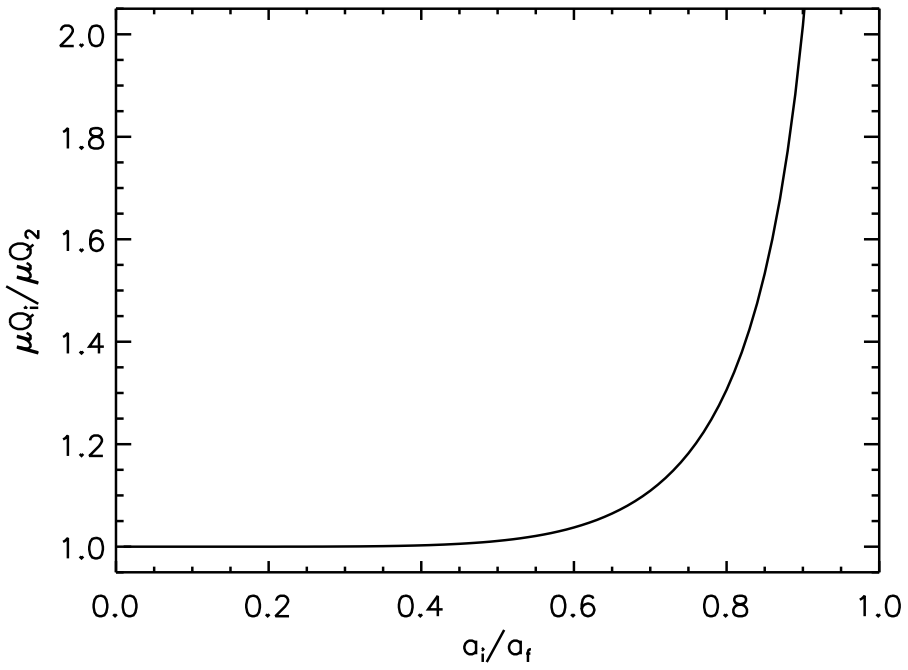

Figure 4.7: The effect of varying the inital separation of the binary on the material properties μQ is very weak unless the initial and final separations are essentially equal, amounting to a factor of ~2 when $a_i = 0.9\,a_f$. The curve shown is Equation (4.4) for $a_f/R_p = 10$ corresponding to the main belt binaries. The curve for near-Earth binaries with $a_f/R_p = 5$ is indistinguishable from the curve shown.

dense secondary allows μQ to decrease for a fixed timescale.

Among our subset of binaries, only 1999 KW_4 has independent estimates of the component densities: 1.97 g/cm^3 for the primary, which we have used for both components to this point, and 2.81 g/cm^3 for the secondary (Ostro et al., 2006). The higher density of the secondary increases the mass ratio by nearly 50% from 0.0402 for equal densities to 0.0573. Therefore, to tidally evolve over the same timescale, the denser secondary requires μQ to increase by 44%. The effect is enhanced for components with similar sizes, but one would not expect having components with different densities to affect μQ by more than a factor of ~2.

4.8 Effect of Solar Tides

Also of concern are solar tides, whose presence are felt through additional tidal distortions raised on each component. The ratio of the $\ell = 2$ tidal amplitudes raised on the primary due to the Sun and the secondary scales as

$$\frac{\zeta_{\mathrm{p},\odot}}{\zeta_{\mathrm{p,s}}} = \frac{M_\odot}{M_\mathrm{s}} \left(\frac{a}{a_\odot} \right)^3 . \tag{4.5}$$

For a typical near-Earth binary system, $M_\odot/M_\mathrm{s} \sim 10^{19}$ and $a/a_\odot \sim 10^{-8}$, and the ratio of tidal amplitudes is 10^{-5} rendering solar tides negligible. Despite their small masses, the secondaries in NEA binary systems are so close to their primaries that they can easily raise the dominant tide on the primary. For a typical main belt binary system, $M_\odot/M_\mathrm{s} \sim 10^{13}$ and $a/a_\odot \sim 10^{-5}$, and the ratio of tidal amplitudes is 10^{-2}, which is still negligible in the scope of this discussion. In this case, the wider separation of the components significantly reduces the tidal amplitude raised by the secondary, but

it still dominates over the tide raised by the Sun. For comparison, in the Earth-Moon system, $\zeta_{\odot}/\zeta_{\rm Moon} \simeq 0.5$, meaning the Earth is distorted by the gravity of the Sun almost as strongly as it is by the gravity of the Moon, and thus solar tides must be accounted for in the tidal evolution of the Moon as explored by Goldreich (1966). Since the mass of the secondary is typically two orders of magnitude less than the primary, the relative strength of the tides on the secondary $\zeta_{\rm s,\odot}/\zeta_{\rm s,p}$ is two orders of magnitude smaller than $\zeta_{\rm p,\odot}/\zeta_{\rm p,s}$, and solar tides on the secondary are negligible for near-Earth and main belt binaries.

4.9 Effect of Unequal Material Properties

If the primary and secondary have the same material properties in terms of μQ, the contribution from the primary dominates the tidal evolution in all cases except when $q \sim 1$. If the secondary is mechanically weaker than the primary, $\mu_{\rm p}Q_{\rm p}/\mu_{\rm s}Q_{\rm s} > 1$, the secondary will despin even faster and reach synchronous rotation sooner than if $\mu_{\rm p}Q_{\rm p}/\mu_{\rm s}Q_{\rm s} = 1$. If the secondary is mechanically stronger than the primary, it will delay the synchronization of the secondary's spin to the mean motion.

While material properties certainly affect the spin rate of the secondary, the evolution of the orbital separation is essentially indifferent to the material properties of the secondary for a circular orbit. The contribution of the secondary to the evolution of the separation is proportional to $\left(R_{\rm s}/R_{\rm p}\right)\left(\mu_{\rm p}Q_{\rm p}/\mu_{\rm s}Q_{\rm s}\right)\,{\rm sign}\,(\omega_{\rm s} - n)$. Although the material properties of the secondary determine the strength of its contribution, the contribution only exists while $\omega_{\rm s} \neq n$, which occurs over a time period $\tau_{\rm s} \propto \dot{\omega}_{\rm s}{}^{-1} \propto \mu_{\rm s}Q_{\rm s}$. For $\mu_{\rm s}Q_{\rm s}$ large, the strength of the secondary's contribution to the orbital evolution is small, but the timescale over which it acts is long, and the opposite is true for $\mu_{\rm s}Q_{\rm s}$ small, such that

the specific value cannot be well-constrained. For synchronized secondaries in circular orbits without considering eccentricity evolution, one may only place an upper limit on $\mu_s Q_s$ such that the secondary will despin in less than 4.5 Gy, which is roughly 10^{14} N/m^2 for a $q = 0.001$ main belt binary.

4.10 Summary of Tidal Evolution in Circular Orbits

We have shown that unless a binary system is made up of components of similar size, tidal evolution is dominated by tides raised on the primary. Use of only primary tides for mass ratios $q < 1$ provides a solid estimate of μQ for the primary component, but cannot immediately constrain the material properties of the secondary in the case of a circular orbit. While $q \sim 1$ binaries are an excellent example of the end state of tidal evolution, the lack of knowledge about the age of the binary prevents a direct estimate of μQ for these systems. Of the effects presented that may change the estimate of μQ for $q < 1$ systems, ignorance of the age of a binary has the greatest effect on the calculation of μQ as changing the age by an order of magnitude changes μQ by an order of magnitude as well. Because tidal evolution is much faster at close separations, the use of the close orbit correction and the choice of initial separation do not have a strong effect on the calculation of μQ, both less than 10% in most cases. Though difficult to measure, a difference in the densities of the components can be the strongest effect other than the age of the binary because the densities directly alter the mass ratio of the system as seen in the case of 1999 KW$_4$ where a roughly 50% difference in density changes μQ by over 40%.

CHAPTER 5

TIDAL EVOLUTION WITH NON-NEGLIGIBLE ECCENTRICITY

We describe the effects of the tidal interaction between the two components in a binary asteroid system when the mutual orbit is eccentric, but uninclined. We build upon the previous work on eccentric orbits by Jeffreys (1961) and Goldreich (1963) and expand to fourth order in eccentricity the rates of change of the semimajor axis and eccentricity of the mutual orbit with time. A higher order expansion in eccentricity is essential for analyzing systems observed among near-Earth binary asteroids such as 2004 DC (Taylor et al., 2008) that have mutual orbits with moderate eccentricities of order a few tenths. Higher order terms in the eccentricity tend to speed the orbit expansion and increase the eccentricity of the mutual orbit as the system tidally evolves. The eccentricity can then be damped once the secondary is synchronized to produce the circular mutual orbits observed among most binary systems via a secondary that is mechanically weaker than the primary or by simply having a rubble pile structure.

5.1 Tidal Evolution to Fourth Order in Eccentricity

Following Jeffreys (1961), suppose a binary system with primary component of mass $M_{\rm p}$ is attended by a secondary component of mass $M_{\rm s}$ with the mutual orbit lying in the equatorial plane of the primary, thus neglecting inclination. In a spherical polar coordinate system (r, θ, ϕ) with radial distance from the center of the primary r, colatitude measured from the pole of the primary θ, and longitude ϕ measured from an arbitrary fixed reference direction in space, the $\ell = 2$ tidal potential from Chapter 3 due to an object a distance d away from the center of the primary is

$$U = -G\frac{M_s R_p^2}{d^3} P_2(\cos\psi) \;=\; -\zeta_{2,p} g_p \left(\frac{d}{a}\right)^{-3} \frac{1}{2}\left(3\cos^2\psi - 1\right). \tag{5.1}$$

Using the definition of the separation angle ψ,

$$\cos\psi \;=\; \cos\theta_p \cos\theta_s + \sin\theta_p \sin\theta_s \cos\left(\phi_p - \phi_s\right), \tag{5.2}$$

reduced to $\cos\theta_p + \sin\theta_p \cos\left(\phi_p - \phi_s\right)$ for an equatorial mutual orbit, the tidal potential due to the secondary on an eccentric path is

$$U = -\zeta_{2,p} g_p \left(\frac{d}{a}\right)^{-3} \left[\frac{3}{4}\sin^2\theta \cos 2(\phi - \nu) + \frac{1}{2}\left(\frac{1}{2} - \frac{3}{2}\cos^2\theta\right)\right], \tag{5.3}$$

where ν is the true longitude of the secondary. The tidal potential above distorts the shape of the primary such that the non-central potential felt at a point at position (r, θ, ϕ) due to the distorted primary is

$$U_{nc}(r,\theta,\phi) \;=\; -k_{2,p}\zeta_p g_p \left(\frac{d}{a}\right)^{-3} \left(\frac{r}{R_p}\right)^{-3} \left[\frac{3}{4}\sin^2\theta \cos 2(\phi - \nu) + \frac{1}{2}\left(\frac{1}{2} - \frac{3}{2}\cos^2\theta\right)\right]. \tag{5.4}$$

Expansions for the separation distance d of the components and the true longitude ν of the secondary in powers of the eccentricity e are well-established (*e.g.*, Brouwer and Clemence (1961), Murray and Dermott (1999)) as extensions of Kepler's equation,

$$\begin{aligned}\frac{d}{a} \;=\;& 1 - e\cos pt + \frac{e^2}{2}(1 - \cos 2pt) + \frac{3e^3}{8}(\cos pt - \cos 3pt) \\ & + \frac{e^4}{3}(\cos 2pt - \cos 4pt) + \ldots\end{aligned} \tag{5.5}$$

where pt is the mean anomaly (in the notation of Jeffreys (1961), trigonometric functions are written in terms of the product of a frequency and time rather than a specific angle), and

$$\begin{aligned} \nu &= nt + 2e\sin pt + \frac{5}{4}e^2 \sin 2pt + e^3\left(\frac{13}{12}\sin 3pt - \frac{1}{4}\sin pt\right) + \\ & \quad e^4\left(\frac{103}{96}\sin 4pt - \frac{11}{24}\sin 2pt\right) + \ldots \end{aligned} \tag{5.6}$$

where nt is the mean longitude.

Further manipulation of the potential using a symbolic manipulator such as *Mathematica* produces a cumbersome amount of terms not easily reproduced here. The steps, however, are as follows. Substituting the expansions of d and ν into the potential due to the distorted primary, Equation (5.4), and expanding to fourth order in the eccentricity produces the approximate potential felt at the point (r, θ, ϕ) as a slew of periodic terms involving linear combinations of pt, nt, θ, and ϕ. Because of friction in the response of the tidal distortion, each periodic term has a lag of $2\epsilon_{\mathrm{i}}$ related to the spin rate of the primary compared to the mean motion assigned according to Table 5.1. Expanding in the small lag angles ϵ_{i} and keeping only the terms containing the lags gives the component of the potential due to friction.

If the point (r, θ, ϕ) is the location of another body in equatorial orbit about the primary, r takes the form of Equation (5.5), $\theta = \pi/2$, and ϕ takes the form of Equation (5.6) except the argument pt is written as $\lambda - \tilde{\omega}$, where λ is the mean longitude and $\tilde{\omega}$ is the longitude of pericenter, to distinguish between the angles related to the perturbing body and the disturbed body. Expanding to fourth order in the eccentricity of the disturbed body produces the potential to fourth order in the eccentricities of the perturbing and disturbed bodies with periodic terms involving linear combinations of p', n', λ, and $\tilde{\omega}$

Table 5.1: For each periodic term in the expansion of the potential due to the distorted component, there is an associated tidal lag due to friction. The first four lags, $\epsilon_0, \epsilon_1, \epsilon_2$, and ϵ_3, are defined in the same way as in Jeffreys (1961) and Goldreich (1963).

Lag Term	Related Periodic Argument	Related Frequency
ϵ_0	$2\phi - 2nt$	$2(\omega - n)$
ϵ_1	$2\phi - 2nt - pt$	$2\omega - 3n$
ϵ_2	$2\phi - 2nt + pt$	$2\omega - n$
ϵ_3	pt	n
ϵ_4	$2\phi - 2nt + 2pt$	ω
ϵ_5	$2\phi - 2nt - 2pt$	$2(\omega - 2n)$
ϵ_6	$2\phi - 2nt + 3pt$	$2\omega + n$
ϵ_7	$2\phi - 2nt - 3pt$	$2\omega - 5n$
ϵ_8	$2\phi - 2nt + 4pt$	$2(\omega + n)$
ϵ_9	$2\phi - 2nt - 4pt$	$2(\omega - 3n)$
ϵ_{10}	$2pt$	$2n$
ϵ_{11}	$3pt$	$3n$
ϵ_{12}	$4pt$	$4n$

with accents indicating the perturbing body. Changes in the orbital parameters of the perturbed body are found from Lagrange's planetary equations (*e.g.*, Murray and Dermott (1999)),

$$\begin{aligned} \dot{a} &= \frac{2(1+q)}{na}\frac{\partial R}{\partial \lambda} \\ \dot{e} &= -(1+q)\frac{\sqrt{1-e^2}}{na^2 e}\left[\left(1-\sqrt{1-e^2}\right)\frac{\partial R}{\partial \lambda} + \frac{\partial R}{\partial \tilde{\omega}}\right], \end{aligned} \tag{5.7}$$

where R is the disturbing function defined as the negative of the perturbing potential. For the secondary perturbed by the tides it raises on the primary, $e' = e$, $a' = a$, $\lambda = nt$, and $p't = \lambda - \tilde{\omega}$, greatly simplifying the expressions. Averaging over the orbit removes the remaining periodic terms leaving the secular changes in the semimajor axis and eccentricity of the mutual orbit due to the tidal distortion of the primary as

$$\begin{aligned}
\frac{\dot{a}_{\rm p}}{a} &= \frac{16\sqrt{3}}{19}\frac{\pi^{3/2}G^{3/2}\rho_{\rm p}^{5/2}R_{\rm p}^2}{\mu_{\rm p}}\,q\,(1+q)^{1/2}\left(\frac{a}{R_{\rm p}}\right)^{-13/2} \\
&\quad\times\left[\epsilon_{0,{\rm p}} - 5e^2\left(\epsilon_{0,{\rm p}} - \frac{147}{40}\epsilon_{1,{\rm p}} - \frac{1}{40}\epsilon_{2,{\rm p}} + \frac{3}{20}\epsilon_{3,{\rm p}}\right)\right. \\
&\quad\left. + \frac{63}{8}e^4\left(\epsilon_{0,{\rm p}} - \frac{41}{4}\epsilon_{1,{\rm p}} - \frac{1}{252}\epsilon_{2,{\rm p}} - \frac{3}{14}\epsilon_{3,{\rm p}} + \frac{1156}{63}\epsilon_{5,{\rm p}} - \frac{3}{7}\epsilon_{10,{\rm p}}\right)\right] \\
\frac{\dot{e}_{\rm p}}{e} &= -\frac{4\sqrt{3}}{19}\frac{\pi^{3/2}G^{3/2}\rho_{\rm p}^{5/2}R_{\rm p}^2}{\mu_{\rm p}}\,q\,(1+q)^{1/2}\left(\frac{a}{R_{\rm p}}\right)^{-13/2}\left[\epsilon_{0,{\rm p}} - \frac{49}{4}\epsilon_{1,{\rm p}} + \frac{1}{4}\epsilon_{2,{\rm p}} + \frac{3}{2}\epsilon_{3,{\rm p}}\right. \\
&\quad\left. - \frac{21}{4}e^2\left(\epsilon_{0,{\rm p}} - \frac{179}{12}\epsilon_{1,{\rm p}} + \frac{1}{84}\epsilon_{2,{\rm p}} - \frac{5}{14}\epsilon_{3,{\rm p}} + \frac{578}{21}\epsilon_{5,{\rm p}} - \frac{9}{7}\epsilon_{10,{\rm p}}\right)\right] \qquad (5.8)
\end{aligned}$$

The secular changes to the semimajor axis and eccentricity due to tides on the secondary follow by switching the p and s subscripts in the potentials, dividing by q (Goldreich, 1963), and setting the lags to $\epsilon_{\rm i,s}$. The coefficients in front of the bracketed lag terms for $\dot{a}_{\rm s}$ and $\dot{e}_{\rm s}$ are the same as for $\dot{a}_{\rm p}$ and $\dot{e}_{\rm p}$, but with an additional factor of $\left(\mu_{\rm p}/\mu_{\rm s}\right)\left(R_{\rm s}/R_{\rm p}\right)$.

5.2 Typical Signs for Lag Terms

The inclusion of eccentricity up to fourth order produces five new lag terms in addition to the one lag term in the circular case. The sign of each lag term depends upon the value of its related frequency in Table 5.1. For any combination of $\omega_{\rm p}$, $\omega_{\rm s}$, n, and J/J',

$$\frac{5}{2}\,\frac{q}{1+q}\,\frac{1}{1+q^{5/3}\left(\omega_{\rm s}/\omega_{\rm p}\right)}\left(\frac{a}{R_{\rm p}}\right)^2 - \frac{5}{2}\,\frac{(1+q)^{7/6}}{1+q^{5/3}\left(\omega_{\rm s}/\omega_{\rm p}\right)}\,(J/J')\left(\frac{a}{R_{\rm p}}\right)^{3/2} + \frac{\omega_{\rm p}}{n} = 0, \quad (5.9)$$

a special condition of which is the synchronous orbit equation from Chapter 3. For a synchronous secondary, $\omega_{\rm s} = n$, the above equation traces out the regions (see Figure 5.1)

where the signs of the frequencies in Table 5.1 change. During the tidal evolution of a $q \sim 0.1$ binary or smaller, all of the lag terms $\epsilon_{i,p}$ will have positive signs for essentially the entire tidal evolution such that, if the $\epsilon_{i,p}$ are comparable, $\dot{e}_p/e > 0$ excites the eccentricity. A similar excitation to the eccentricity results from tides raised on the secondary when $\omega_s > n$. Only for $q \sim 1$ are the signs of the dominant lags, $\epsilon_{1,p}$ and $\epsilon_{5,p}$, negative resulting in a damping of the eccentricity due to tides raised on the primary. Thus, one would not expect to find an equal mass binary with an eccentric mutual orbit if the system is tidally evolved.

Overall, an eccentric orbit tends to expedite the orbit expansion and boosting of the eccentricity for $q < 1$ binaries when the components are not synchronized (or more exactly, when $\omega_{p,s} > n$). When the secondary reaches synchronicity, the signs on the lags reverse, causing tides raised on the secondary to damp the eccentricity, fighting the tides on the primary that excite the eccentricity of the mutual orbit, leading to the eccentricity problem of binary asteroids discussed in the following section. When the primary is synchronized to the mean motion in an eccentric system, the leading term in the orbit expansion goes away, but radial tides due to the changing separation of the components still dissipates energy causing a to decrease in addition to decreasing e to conserve angular momentum.

5.3 The Eccentricity Problem

In the previous chapter we found that when considering circular orbits, it is difficult to constrain the material properties of the secondary. If one considers eccentricity evolution, however, the value of $\mu_s Q_s$ becomes important. To leading order, the eccentricity evolves according to

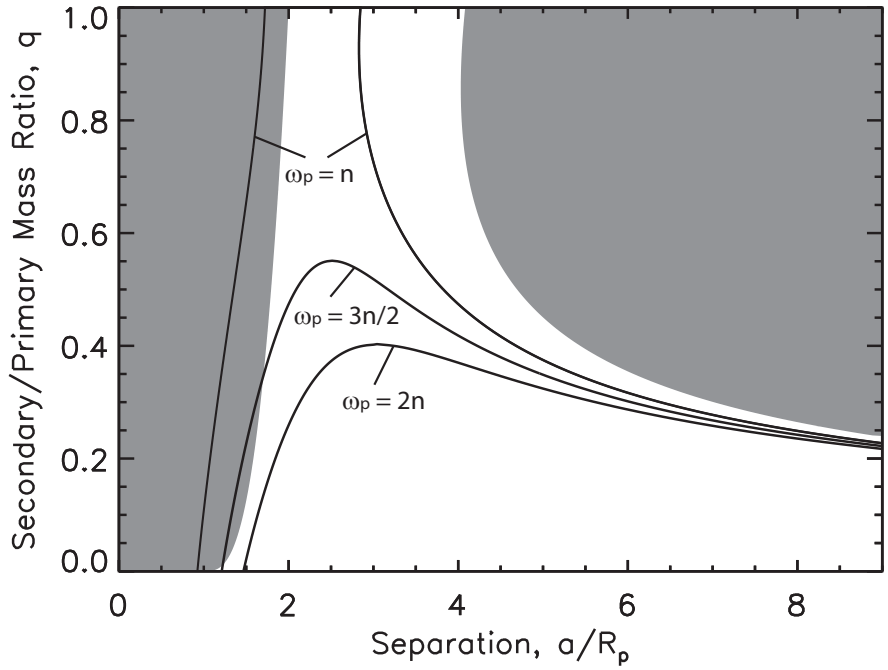

Figure 5.1: Curves representing $\omega_{\rm p} = n$, $\omega_{\rm p} = 3n/2$, and $\omega_{\rm p} = 2n$ for binary systems of mass ratio q, scaled angular momentum $J/J' = 0.45$, and assuming a synchronous secondary. The shaded regions indicate separations that are inaccessible to the binary components. As a $q \sim 0.1$ binary tidally evolves to the right, it passes through regions underneath the $\omega_{\rm p} = 3n/2$ and $\omega_{\rm p} = 2n$ curves where $\omega_{\rm p} > 3n/2$ and $\omega_{\rm p} > 2n$ resulting in excitation of the eccentricity according to $\dot{e}_{\rm p}/e$. In $q \sim 1$ binaries, the primary is despun too rapidly to satisfy $\omega_{\rm p} > 3n/2$. The curve for $\omega_{\rm p} = n/2$ (not shown), related to $\epsilon_{2,{\rm p}}$, surrounds the $\omega_{\rm p} = n$ synchronous curve such that a binary will always satisfy $\omega_{\rm p} > n/2$ when tidally evolving outward.

$$\frac{\dot{e}_{\rm p}}{e} = -\frac{4\sqrt{3}}{19}\frac{\pi^{3/2}G^{3/2}\rho_{\rm p}^{5/2}R_{\rm p}^2}{\mu_{\rm p}}\,q\,(1+q)^{1/2}\left(\frac{a}{R_{\rm p}}\right)^{-13/2}\left[\epsilon_{0,{\rm p}} - \frac{49}{4}\epsilon_{1,{\rm p}} + \frac{1}{4}\epsilon_{2,{\rm p}} + \frac{3}{2}\epsilon_{3,{\rm p}}\right]$$

$$\frac{\dot{e}_{\rm s}}{e} = -\frac{4\sqrt{3}}{19}\frac{\pi^{3/2}G^{3/2}\rho_{\rm p}^{5/2}R_{\rm p}^2}{\mu_{\rm p}}\,q\,(1+q)^{1/2}\left(\frac{a}{R_{\rm p}}\right)^{-13/2}\left(\frac{\mu_{\rm p}}{\mu_{\rm s}}\right)\left(\frac{R_{\rm s}}{R_{\rm p}}\right) \times\left[\epsilon_{0,{\rm s}} - \frac{49}{4}\epsilon_{1,{\rm s}} + \frac{1}{4}\epsilon_{2,{\rm s}} + \frac{3}{2}\epsilon_{3,{\rm s}}\right]. \quad (5.10)$$

Assuming the rotation of the secondary has synchronized to the mean motion and using $\omega_{\rm s} = n$ in the frequency terms from Table 5.1, $\dot{e}_{\rm s}/e$ has the the opposite sign of the mean motion, and thus will damp the eccentricity. The eccentricity evolution due to tides raised on the unsynchronized primary is dominated by the $2\omega_{\rm p} - 3n$ lag term $\epsilon_{1,{\rm p}}$ that excites or damps the eccentricity according to whether or not $\omega_{\rm p} > 3n/2$.

For simplicity, assume that the magnitude of each tidal lag is equal so that $|\epsilon_{\rm i}| = \epsilon = 1/(2Q)$ and $\epsilon_{\rm i}$ has the sign of the respective $i^{\rm th}$ frequency term from Table 5.1. Though simplistic, Touma and Wisdom (1994) find that the exact tidal formulation does not have a strong effect on the overall tidal evolution of a binary system. Taking $\omega_{\rm p} > 3n/2$ such that the eccentricity is excited by tides on the primary, but damped by tides on the synchronous secondary, the net effect on the eccentricity of the mutual orbit (Harris and Ward, 1982) in terms of the semimajor axis evolution (to zeroth order in e) is

$$\frac{de}{e} = \left[\frac{19}{8} - \frac{7\,R_{\rm s}\,\mu_{\rm p}Q_{\rm p}}{2\,R_{\rm p}\,\mu_{\rm s}Q_{\rm s}}\right]\frac{da}{a}. \quad (5.11)$$

One finds that the eccentricity will increase, $de/e > 0$, as the system evolves outward, $da/a > 0$, if

$$q < \left(\frac{19}{28}\frac{\mu_{\rm s}Q_{\rm s}}{\mu_{\rm p}Q_{\rm p}}\right)^3, \quad (5.12)$$

or for all systems with $q < 0.31$ (Weidenschilling et al., 1989; Margot and Brown, 2003), where we have assumed similar densities and material properties of monolithic components. If the damping does not win, the eccentricity will continue to grow until the primary has synchronized.

Aside from (69230) Hermes, (90) Antiope, and (617) Patroclus, all of the binaries in our sample satisfy the $q < 0.31$ condition on the mass ratio, yet we do not observe all of these binaries to have eccentric mutual orbits. By reducing $\mu_s Q_s$, thereby weakening the secondary, the mass ratio for which the eccentricity should increase is supressed. Among the near-Earth binaries, the smallest observed mass ratios are $q \sim 0.001$. To suppress the eccentricity excitation below $q = 0.001$ requires the secondary to be merely a factor of 7 weaker than the primary. Among the main belt binaries, the smallest observed mass ratios are $q \sim 10^{-5}$, which requires the secondary to be a factor of 31 weaker than the primary. Thus, if secondaries tend to be roughly an order of magnitude weaker in terms of μQ than their respective primary, there is no eccentricity problem as these systems should in fact circularize, creating the roughly circular orbits observed among most binary asteroid systems.

The question remains of whether secondaries created through the reaccumulation of matter spun off of a rubble pile primary (in the case of near-Earth binaries) or blasted off the surface of the primary by an impact (in the case of 100 km-scale main belt binaries) should be weaker than the primary itself. Given the smaller masses of the secondaries and the smaller pressures due to gravitational compression among the constituent particles, perhaps an order of magnitude weaker secondary is reasonable, especially among the main belt binaries where the material that composes the secondary is likely the reaccumulated ejecta from a substantial impact compared to a much larger, solid or fractured parent body. A note of caution, however, the above argument for damping the eccen-

tricity has assumed a synchronous secondary. If the secondary is not synchronized and instead has $\omega_s > n$, whether $\mu_s Q_s$ is greater or less than $\mu_p Q_p$ does not matter, the eccentricity should excite as the system tidally evolves.

In Goldreich and Sari (2009)'s formulation of rubble pile structure, the equivalent rigidity of rubble piles compared to monolithic rocks alters the eccentricity condition of Equation (5.11) such that the eccentricity problem does not exist. The eccentricity of the mutual orbit in a rubble pile binary system with a synchronized secondary and identical compositions and Q values for the components will damp no matter what the mass ratio of the system. This provides another method of possibly avoiding the eccentricity problem that is especially appropriate for near-Earth binaries that probably have rubble pile components.

CHAPTER 6

CONTACT BINARY FORMATION AND DISRUPTION

Among near-Earth asteroids, contact binaries are nearly as populous as separated binaries and important to understanding binary formation and evolution. Because the components do not separate we can place an upper limit on the angular momentum of such systems as well as a lower limit on the density. For typical rock densities, one would not expect to find a contact binary rotating with a period shorter than 4 hours. We posit that contact binaries are formed through the absence of a valid, fully despun, double synchronous end state. Such a result may be reached either directly by forming a separated binary in a region of (q, $a/R_{\rm p}$)-space without a synchronous solution or through the removal of angular momentum from the system until a synchronous solution no longer exists, both of which favor the formation of contact binaries with components of similar mass (or size) as have been observed with radar.

6.1 Contact Binary Population

About 11% of near-Earth asteroids larger than 200 m in diameter detected by radar are candidate contact binaries (Benner et al., 2008a) where delay-Doppler images reveal a distinctly bilobated echo and, presumably, a bilobated mass distribution suggestive of two similarly-sized components resting in contact against one another. Combined with a (separated) binary fraction of roughly 16% detected by radar (Margot et al., 2002) and lightcurve photometry (Pravec et al., 2006) among near-Earth asteroids larger than 200 m in diameter, binaries could constitute over one quarter of the near-Earth asteroid population. Thus, our understanding of binary formation and evolution is incomplete without a study of contact binaries.

There is a distinct resolution bias in identifying contact binaries with similar-size components due to the relative ease of detecting a bilobated “peanut” or “snowman” shape with radar compared to two very differently-sized components akin to a pea resting on a beach ball. However, the rate of contact binary detection warrants a discussion of formation processes along with the determination of whether production of contact binaries with similarly-sized $q \sim 1$ components are preferred over $q \ll 1$ components.

6.2 Angular Momentum Content

Suppose two spheres, a larger primary component and a smaller secondary component of radius R_p and R_s, respectively, with similar uniform density ρ and mass ratio $q = M_\mathrm{s}/M_\mathrm{p} = \left(R_\mathrm{s}/R_\mathrm{p}\right)^3$ are in contact with center-to-center separation $R_\mathrm{p} + R_\mathrm{s}$. The two spheres rotate as a single rigid body with moment of inertia I and (non-Keplerian) spin period P as shown in Figure 6.1. The displacement of the center of mass along the line of centers measured from the center of the primary d_p and measured from the center of the secondary d_s satisfy $M_\mathrm{p} d_\mathrm{p} = M_\mathrm{s} d_\mathrm{s}$ and $d_\mathrm{p} + d_\mathrm{s} = R_\mathrm{p} + R_\mathrm{s} = (1 + q^{1/3}) R_\mathrm{p}$ such that

$$\begin{aligned} d_\mathrm{p} &= \frac{q}{1+q}\left(1+q^{1/3}\right)R_\mathrm{p} \\ d_\mathrm{s} &= \frac{1}{1+q}\left(1+q^{1/3}\right)R_\mathrm{p}. \end{aligned} \tag{6.1}$$

The moment of inertia I of the contact binary is given by

$$\begin{aligned} I &= \frac{2}{5}M_\mathrm{p}R_\mathrm{p}^2 + M_\mathrm{p}d_\mathrm{p}^2 + \frac{2}{5}M_\mathrm{s}R_\mathrm{s}^2 + M_\mathrm{s}d_\mathrm{s}^2 \\ &= \left[\frac{2}{5}\left(1+q^{5/3}\right) + \frac{q}{1+q}\left(1+q^{1/3}\right)^2\right]M_\mathrm{p}R_\mathrm{p}^2 \end{aligned} \tag{6.2}$$

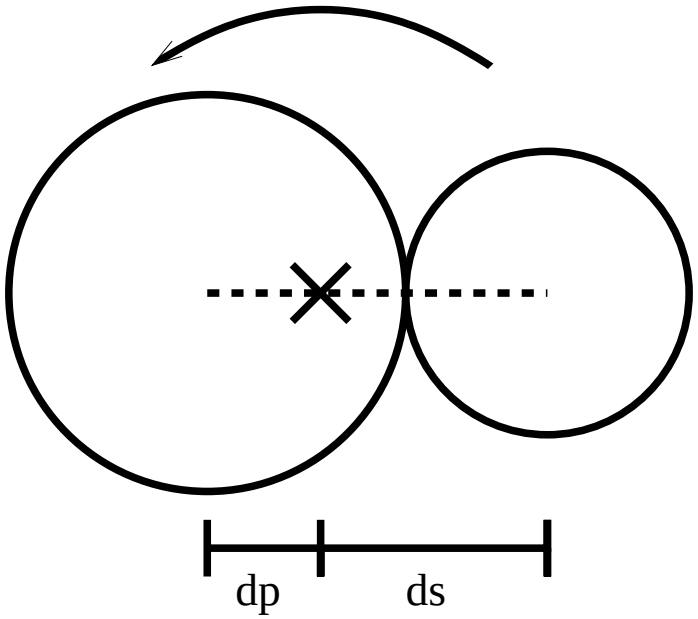

Figure 6.1: A contact binary system where two spherical components rotate as a single rigid body as indicated by the arrow. The center of mass X is displaced along the line connecting the centers of the components (dashed line) a distance d_p from the center of the primary and a distance d_s from the center of the secondary according to the mass ratio of the components.

where the axis of rotation is through the center of mass. The angular momentum J of the system is then $2\pi I/P$. Scaling by $J' = \sqrt{G\left(M_\mathrm{p} + M_\mathrm{s}\right)^3 R_\mathrm{eq}} = (1+q)^{5/3} M_\mathrm{p} R_\mathrm{p}^2 \sqrt{4\pi G\rho/3}$, where $R_\mathrm{eq} = (1+q)^{1/3} R_\mathrm{p}$ is the volumetric equivalent radius if the system were a single sphere, gives the scaled angular momentum of the system,

$$\frac{J}{J'} = \frac{2}{5}\sqrt{\frac{3\pi}{G\rho}}\frac{1}{P}\frac{1+q^{5/3}}{(1+q)^{5/3}}\left[1+\frac{5}{2}\frac{q}{1+q}\frac{\left(1+q^{1/3}\right)^2}{1+q^{5/3}}\right]. \tag{6.3}$$

Ignoring the terms involving q, the leading term is J/J' for a single sphere rotating with period P. For a $q = 1$ contact binary with two equal size components, the terms involving q produce an additional factor of $7/2^{5/3} \sim 2.2$. Thus, if a single rotating sphere and a $q = 1$ contact binary have the same angular momentum content J/J', the contact binary must rotate with a period more than a factor of two longer than the single sphere. If a single body is rotating rapidly with a period of 2-3 hours, a contact binary would rotate with a period of 4.4-6.6 hours.

6.3 Critical Rotation of a Contact Binary

For the contact binary system in Figure 6.1, the components will become separated and enter orbit about the center of mass when the rotation period equals the Keplerian period for a semimajor axis $a = R_\mathrm{p} + R_\mathrm{s} = (1+q^{1/3})R_\mathrm{p}$, which by Kepler's Third Law is

$$P_\mathrm{break} = \sqrt{\frac{3\pi}{G\rho}}\sqrt{\frac{\left(1+q^{1/3}\right)^3}{1+q}}. \tag{6.4}$$

For $q \to 0$, the breakup period is $\sqrt{3\pi/G\rho}$, the familiar result for a critically rotating sphere, and as q increases, the breakup period lengthens monotonically, doubling when

$q \rightarrow 1$, limits noted by Scheeres (2007). At the breakup period of Equation (6.4), the scaled angular momentum becomes a function of the mass ratio q only

$$\frac{J}{J'} = \frac{2}{5} \frac{1}{(1+q^{1/3})^{3/2}} \frac{1+q^{5/3}}{(1+q)^{7/6}} \left[1 + \frac{5}{2} \frac{q}{1+q} \frac{\left(1+q^{1/3}\right)^2}{1+q^{5/3}} \right], \tag{6.5}$$

as shown in Figure 6.2. By the setup of the problem, this value of J/J' corresponds to the angular momentum at which the inner synchronous orbit is at the contact limit. Thus, it is a lower limit on the angular momentum needed to separate the components. For any larger amount of angular momentum, required to overcome inter-component cohesion for instance, the inner synchronous orbit falls within the contact limit and the components would evolve outward upon separation.

6.4 Density Estimation of Contact Binaries

Ignoring cohesion between the components, the maximum J/J' value for a contact binary prior to the components separating is 0.441 for $q = 1$. Thus, one can expect that any observed candidate contact binary must have less angular momentum than $J/J' = 0.441$. For the contact binary to stay intact, the rotational period P must be longer than the breakup period P_{break} of Equation (6.4), producing a lower limit on the density of the system

$$\rho > \frac{10.9}{P^2} \frac{\left(1+q^{1/3}\right)^3}{1+q} \tag{6.6}$$

where ρ is in g/cm^3 and P is in hours. Assuming the components of the binary are equal size, the $q = 1$ lower limit for the density is

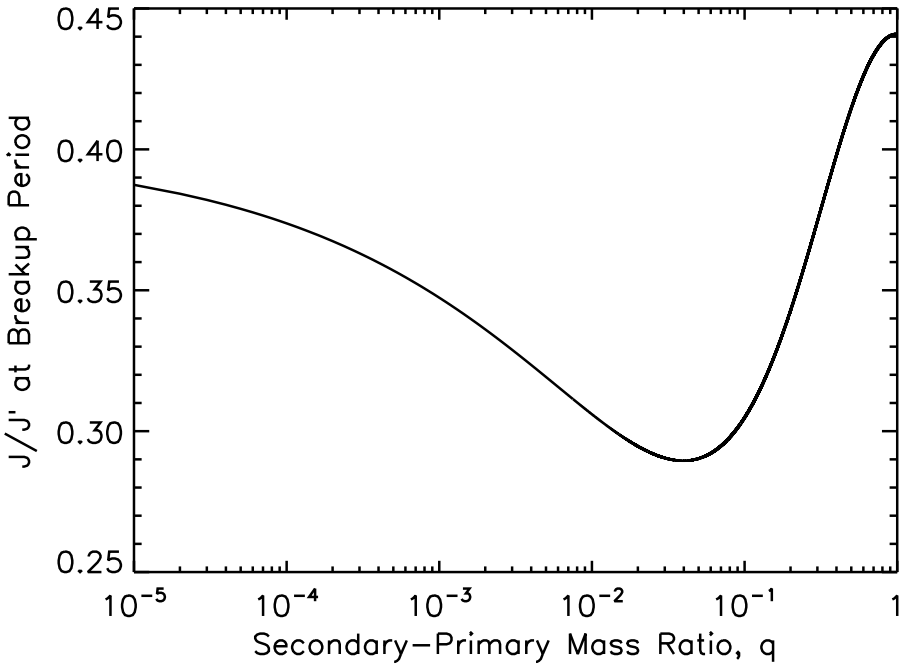

Figure 6.2: Scaled angular momentum of a contact binary system rotating at the breakup period as a function of mass ratio q. $J/J' = 0.4$ for $q = 0$ and decreases to a minimum of $J/J' = 0.290$ at $q = 0.04$ before increasing to $J/J' = 0.441$ at $q = 1$.

$$\rho > \frac{43.6}{P^2}. \tag{6.7}$$

For a period of 4 hours, the density must be greater than 2.73 g/cm^3 for the components to stay in contact and not separate. Thus, the observation of a candidate contact binary with similar size components and a rotation period under 4 hours would either require a density higher than typical rocky asteroids or that the components are not simply resting against each other (*i.e.*, held together with some inter-component tensile strength). If $q < 1$, the lower limit decreases according to Equation (6.6). With the assumption of equal size $q = 1$ components and $q = 0.1$, lower limits on the density of candidate contact binary systems are listed in Table 6.1. Note that the fastest, well-determined, rotation period is that of (4769) Castalia (Hudson and Ostro, 1994; Hudson et al., 1997) at about 4 hours, right at the rough limit one might expect to find a contact binary. Other candidate contact binaries have longer rotation periods than 4 hours, consistent with Equation (6.3).

6.5 Formation Mechanisms

A contact binary will form whenever a separated binary lacks a valid stable synchronous orbit or finds itself within the unstable inner synchronous orbit. As shown in Figure 2.1, the inner synchronous orbit lies within the contact limit in the vast majority of cases making the latter scenario unlikely. Only for small values of J/J' and small q does it seem feasible to form a binary within the inner synchronous orbit at well within $2R_{\rm p}$. Considering our definition of contact binaries as having $q \sim 1$, formation within the inner synchronous orbit is not possible. Instead we explore the lack of a fully despun, double synchonous orbit as the cause of the formation of contact binaries.

Table 6.1: Density requirements for candidate contact binaries to prevent their rotation from separating the components. The systems listed are an update to Table 5 of Benner et al. (2006) (Benner, pers. comm.) where the rotation periods are 20 hours or less. A handful of other candidate contact binaries are believed to have rotation periods on the order of days or weeks making essentially any density allowable without separating the components. Note that if one component is half the size of the other ($q \sim 0.1$), the required density decreases by $\sim 30\%$.

	Candidate	Diameter [km]	Rotation Period [hr]	Density [g/cm^3]	
				$q = 1$	$q = 0.1$
	2004 XL_{14}	0.3	~20	> 0.11	> 0.08
	2002 NY_{40}	0.4	~20	> 0.11	> 0.08
2063	Bacchus	0.6	15.1	> 0.19	> 0.14
179806	2002 TD_{66}	0.3	9	> 0.54	> 0.38
11066	Sigurd	3.0	8.5	> 0.60	> 0.43
	2007 VD_{12}	0.4	7.4	> 0.80	> 0.57
	2005 CR_{37}	1.0	6.5	> 1.03	> 0.74
	2000 YF_{29}	0.4	~6	> 1.21	> 0.86
68346	2001 KZ_{66}	~1	5?	> 1.74	> 1.24
4769	Castalia	1.0	4	> 2.73	> 1.94

6.5.1 No Synchronous Orbit

As seen in Section 2.3 as the uppermost arrow in Figure 2.2, if a binary system has a large enough mass ratio q and small enough angular momentum J/J', requiring slow rotation of the components, the binary can lack a fully despun, double synchronous orbit. The only possible tidal evolution for such a system is for the orbit to decay until the components collide. However, this is not a likely scenario in the near-Earth region where binaries form through spin-up mechanisms such as the YORP effect or close planetary encounters, which result in rapidly-rotating primaries.

A similar instance occurs for oblate and prolate primaries where, for $q \sim 1$ and a primary with a large enough degree of nonsphericity, the system lacks a solution to the synchronous orbit equation because as the shape of the primary deviates from a

sphere, more angular momentum is needed to support a synchronous orbit for the same secondary. For $J/J' = 0.5$, similar to (90) Antiope and (69230) Hermes, the primary needs to have axes in roughly a 2:1 ratio before the synchronous solutions disappear for $q \sim 1$. For $J/J' = 0.45$, the primary must still deviate more from a sphere than the shape of (66391) 1999 KW_4 does (10% oblateness). This mechanism obviously prefers the equal mass binaries that are observed, and if such systems with separated non-spherical components can be formed, they will recollapse on tidal timescales of the order ten thousand years assuming $\mu Q = 5 \times 10^9$ N/m^2 found for near-Earth binaries.

Simple spin-up of a dumbbell shape as in Section 6.3 necessitates a synchronous solution, and thus would form a binary that can sustain separation during tidal evolution. A different mechanism put forth by Holsapple (2007) claims that a body under 10 km size with cohesive strength tends to split into equal size pieces, which become more oblate or elongated during the fracture of the parent body, possibly producing the correct combination of angular momentum and nonsphericity needed to make contact binaries. This suggestion, the testing of which goes well beyond the scope of this discussion, is intriguing as a possible method of forming contact binaries as failed attempts at creating separated binaries using non-spherical components.

6.5.2 Formation Through Spin-Down

Alternatively, a contact binary could be formed from an otherwise typical separated binary through the removal of angular momentum via a spin-down mechanism such as the YORP effect. Because a number of candidate contact binaries have rotation periods on the order of days or weeks, formation through spin-down is an attractive mechanism. Suppose a binary system is formed with enough angular momentum to separate

the components and provide two solutions to the synchronous orbit equation such that tides will evolve the system outward toward the stable outer synchronous orbit solution. As angular momentum is drained from the system, J/J' decreases, and the outer synchronous orbit moves inward, closer to the primary, as illustrated in Figure 2.1. Since tidal evolution wishes to reach the outer synchronous orbit as its end state, the secondary will either continue to evolve outward despite the change in angular momentum or, if the system has already reached the outer synchronous orbit (and the timescale for orbit evolution is shorter than the timescale for spin-down), the secondary will march inward along with the synchronous orbit solution as angular momentum is removed. Eventually, enough angular momentum is removed that a synchronous solution no longer exists for the system, which is evident in Figure 2.1 for $q = 1$ when J/J' falls below 0.44. With no synchronous orbit in which to complete its tidal evolution in, the secondary will continue to evolve closer to the primary in a vain attempt to catch up to the synchronous orbit solution, but it cannot do so, and the system will in time collapse into a contact binary.

For each value of the mass ratio q, there is a value of the angular momentum J/J' for which there is a single solution to Equation (2.8) for the synchronous orbit. For any larger angular momentum value, two synchronous solutions exist and tidal evolution proceeds normally. For any smaller angular momentum value, there is no solution for a synchronous orbit for that mass ratio. Because the synchronous stability condition of Section 2.4 traces out the maxima of the J/J' contours in $(q, a/R_{\rm p})$-space, it represents the case of a single synchronous solution, and the separation $a_{\rm stab}/R_{\rm p}$ of the stability condition from Equation (2.11) represents the synchronous orbit with the smallest angular momentum possible for the desired q. Substituting Equation (2.11) into Equation (2.8) and rearranging gives the minimum angular momentum where a binary system can have a synchronous orbit as

$$\frac{J}{J'} = \frac{4}{3^{3/4}}\alpha_{\rm p}^{3/4}\frac{q^{3/4}}{\left(1+\frac{\rho_{\rm p}}{\rho_{\rm s}}q\right)^{1/6}(1+q)^{7/4}}\left(1+\frac{\alpha_{\rm s}}{\alpha_{\rm p}}\left(\frac{\rho_{\rm p}}{\rho_{\rm s}}\right)^{2/3}q^{5/3}\right)^{1/4}, \tag{6.8}$$

and for spherical components with similar uniform densities,

$$\frac{J}{J'} = \left(\frac{512}{135}\right)^{1/4}\frac{q^{3/4}}{(1+q)^{23/12}}\left(1+q^{5/3}\right)^{1/4}. \tag{6.9}$$

If the angular momentum were any smaller, the mutual orbit would decay until a collision between the components would occur. A gentle collision will produce a contact binary system where the angular momentum is too small to separate the components.

Comparing the angular momentum of the last synchronous orbit to the angular momentum necessary to separate the components of a contact binary in Figure 6.3, it is far easier to recollapse a binary with equal size components than a binary with a much smaller q (Taylor and Margot, 2008). For example, at $q = 1$, it takes $J/J' = 0.441$ to separate the components, but a synchronous orbit only exists for $J/J' > 0.440$, and the loss of merely 0.2% of the angular momentum of the system will allow for the system to recollapse. For a binary with $q = 0.001$, it is evident from Figure 6.3 that over 95% of the angular momentum budget must be drained before the system can collapse back to a contact binary because it requires far more angular momentum to spin the smaller component off the surface of the primary than is necessary to have a stable synchronous orbit.

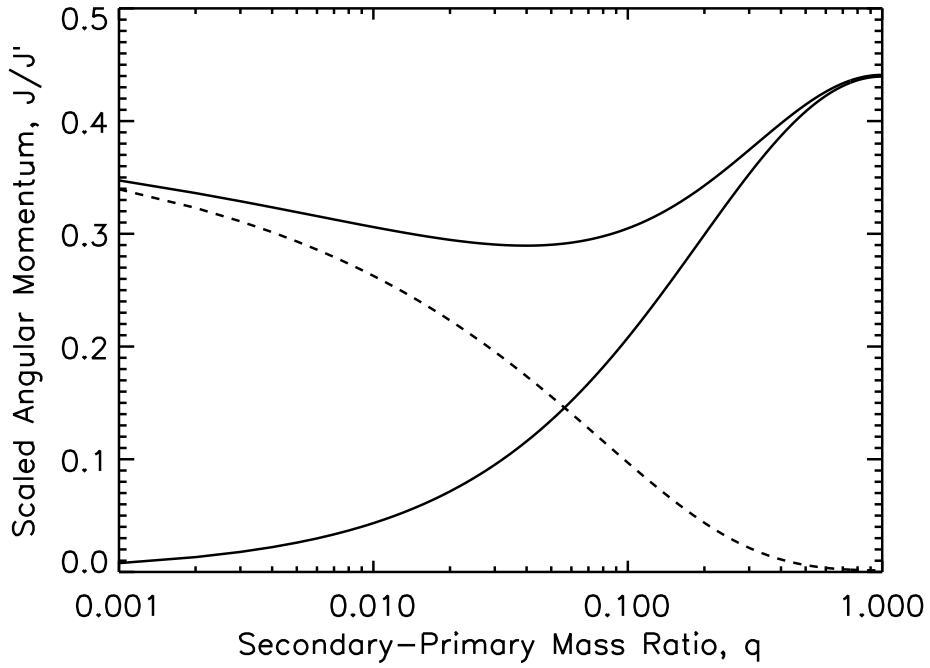

Figure 6.3: Scaled angular momentum required to separate two components of a contact binary system as a function of mass ratio q (upper solid curve) from Figure 6.2 and Equation (6.5), scaled angular momentum below which no synchronous orbit exists (lower solid curve) from Equation (6.9), and the amount of angular momentum that must be removed from the system (dashed curve) by a spin-down mechanism to cause a separated binary system to collapse to a contact binary, which is simply the difference of the solid curves. Clearly, binaries with similar-sized components require the loss of far less angular momentum than binaries with smaller q values to produce a contact binary.

6.6 Timescales for Recollapse

The minimum change in angular momentum $\Delta J/J'$ required to collapse a binary is the difference between the angular momentum required to separate the components from Equation (6.5) and the angular momentum of the last synchronous orbit from Equation (6.9) for the mass ratio q. Suppose this change in angular momentum is caused by the spin-down and subsequent loss of spin angular momentum from the spherical primary component of the binary (brought on by the shape change of the parent body to the primary during binary formation or the re-orientation of the spin axis through collision or close planetary flyby),

$$\frac{\Delta J}{J'} = \frac{1}{5}\sqrt{\frac{3}{\pi}}\frac{1}{\sqrt{G\rho}}\frac{1}{(1+q)^{5/3}}\Delta\omega_{\rm p}. \tag{6.10}$$

The resulting change in spin rate is of order 10^{-4} rad/sec. The YORP effect is observed to act upon (1862) Apollo changing the spin rate at a rate of $\dot{\omega}_{\rm YORP} = 7.1 \times 10^{-18}$ rad/sec^2 (Kaasalainen et al., 2007). The YORP effect acting upon (54509) YORP is two orders of magnitude stronger (Taylor et al., 2007; Lowry et al., 2007) owing to its smaller size than Apollo. Because Apollo is itself a 1-km scale near-Earth binary asteroid, we assume it is a representative value for the near-Earth population at least in terms of magnitude. At this rate, YORP can remove the necessary angular momentum to collapse a binary in merely $\Delta\omega_{\rm p}/\dot{\omega}_{\rm YORP} = 0.1 - 1$ My for $q < 1$ and more rapidly as $q \rightarrow 1$.

For a $q = 1$ equal mass binary with just enough angular momentum to separate, $J/J' = 0.441$, losing angular momentum due to the YORP effect at a rate of $\dot{\omega}_{\rm p} = -7.1 \times 10^{-18}$ rad/sec^2, the components can tidally evolve apart and then recollapse to form a contact binary in less than 50 ky. When the timescale for orbit expansion is

shorter than the spin-down timescale as it is in this case, the evolution is limited by how fast angular momentum can be removed from the system, evidenced in Figure 6.4 by the contrast in slopes between the initial outward evolution (tide dominated), the inward march of the synchronous orbit (spin-down dominated), and the rapid fall back to contact (tide dominated). A similar evolution is expected for any system that crosses the stability limit. If a system is beyond the stability limit, but has a timescale for orbit expansion longer than the spin-down timescale, the outer synchronous orbit will march inward faster than the secondary can, and the system will try to catch up with the synchronous orbit until it crosses the stability limit and collapses.

The final rotation rate of the $q = 1$ contact binary, no matter what the initial angular momentum content (greater than $J/J' = 0.441$), is 4.7 hours for $\rho = 2$ g/cm^3 and assuming no loss of angular momentum in the collision. For less dense bodies, the final rotation period is lengthened to $4.7\sqrt{2/\rho}$ hours according to Equation (6.3). With the exception of (4769) Castalia, the candidate contact binaries in Table 6.1 have rotation periods longer than 4.7 hours. If spin-down continues despite any shape changes from the creation of the contact binary, the observed population of candidate systems would result; if the creation of the contact binary results in YORP spin-up of the system, the components could re-separate. This process of separation, recollapse, and possible re-separation leads to the contact binary cycle first described in terms of asteroid (25143) Itokawa by Scheeres et al. (2007) and Scheeres (2007).

For smaller mass ratios, the timescale for orbit expansion becomes longer than the spin-down timescale. In this case, rather than the binary separating and then marching inward with the outer synchronous orbit as angular momentum is lost, the inner synchronous orbit moves outward and sweeps over the position of the secondary. In doing so, the secondary finds itself now inside the inner synchronous orbit, which requires that

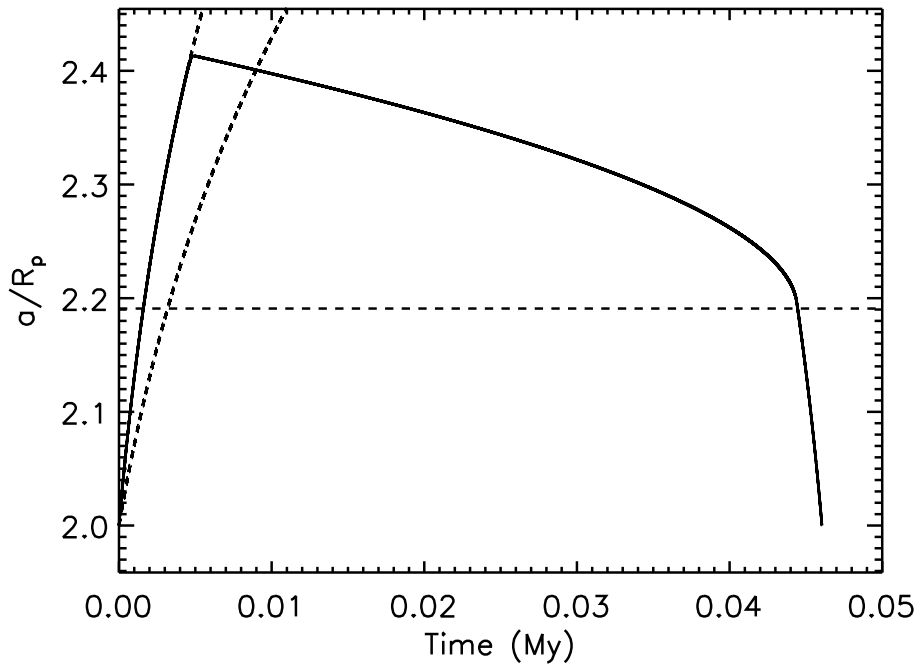

Figure 6.4: Tidal evolution of a near-Earth, equal mass binary system (R_p = 1 km, ρ = 2 g/cm^3, $\mu_s Q_s = \mu_p Q_p = 5 \times 10^9$ N/m^2, $J/J' = 0.441$) while the primary is spun-down at a rate of $\dot{\omega}_p = -7.1 \times 10^{-18}$ rad/sec^2. Because the orbit expansion timescale is shorter than the YORP timescale for this system, the components quickly separate and synchronize. As angular momentum is drained from the system, the synchronous orbit moves inward dragging the secondary inward with it until the system reaches the stability limit (horizontal dashed line). Here, the synchronous orbit disappears, and the system continues to tidally evolve inward back to contact in 46,000 years. The entire process requires the loss of less than 1% of the system's angular momentum.

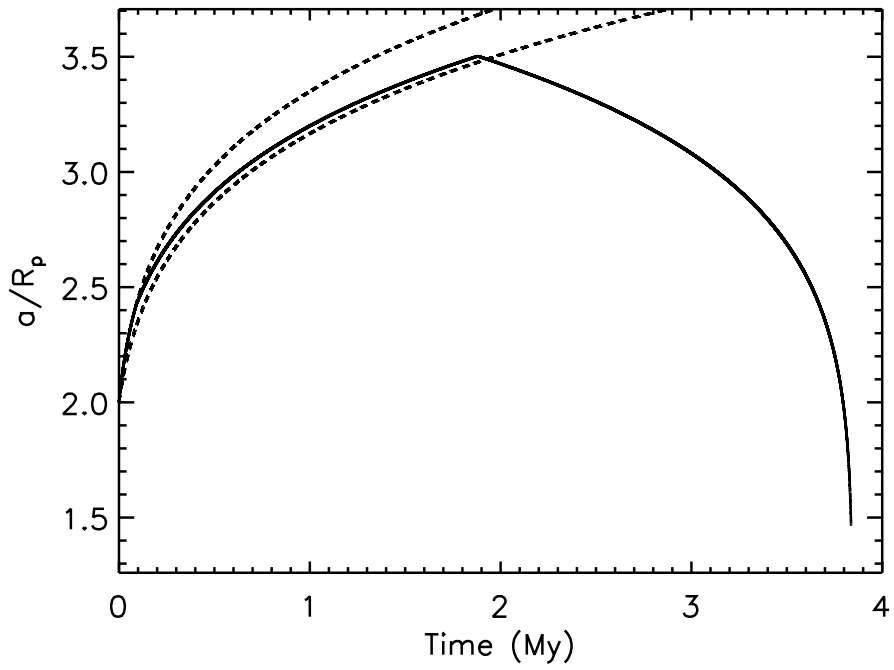

Figure 6.5: Tidal evolution of a $q = 0.1$ near-Earth binary system ($R_p = 1$ km, $\rho = 2$ g/cm^3, $\mu_s Q_s = \mu_p Q_p = 5 \times 10^9$ N/m^2, $J/J' = 0.4$) while the primary is spun-down at a rate of $\dot{\omega}_p = -7.1 \times 10^{-18}$ rad/sec^2. Because the orbit expansion timescale is longer than the YORP timescale for this system, as angular momentum is drained from the system, the inner synchronous orbit moves outward, sweeping over the position of the secondary. Now within the inner synchronous orbit, the secondary must evolve inward to contact. Being limited by the rate of tidal evolution, the timescale to re-collapse is longer than for $q = 1$ at 3.9 My. Note that the system never reaches the stability limit.

the tidal evolution pull the components back together to form a contact binary (*e.g.*, the Mars-Phobos system). An evolution of this type in Figure 6.5 for a $q = 0.1$ binary is characterized by a symmetric orbit evolution where tides dictate the separation and the collapse of the binary with only a cusp to indicate when the inner synchronous orbit sweeps over the position of the secondary. For $q = 0.1$ and $\rho = 2$ g/cm^3, the recollapse of the binary takes 3.8 My; similar evolutionary tracks from an initial separation of $2R_{\rm p}$ with $J/J' = 0.4$ for $q = 0.01, 0.001$, and 0.0001 recollapse in 5.5 My, 10 My, and 60 My, respectively. Equal mass binaries with $J/J' = 0.5$, similar to (90) Antiope and (69230) Hermes, can recollapse in 1.6 My, still more rapidly than $q < 1$ binaries.

Thus, for spin-down from the onset of tidal evolution, equal mass binaries are capable of recollapsing on much shorter timescales than binaries with small secondaries owing to their comparatively rapid tidal evolution. Reducing the rate of spin-down by an order of magnitude increases the timescale for recollapse by an order of magnitude such that only $q \sim 1$ binaries could recollapse during the dynamical lifetime of a near-Earth asteroid. Then, if near-Earth binaries are formed in near-Earth space rather than injected from the main belt, the contact binary population should be dominated by $q = 1$ binaries, which is what is observed. However, a caveat exists that it is difficult to resolve contact binaries with q much different than 1. For instance, the Hayabusa spacecraft showed asteroid (25143) Itokawa to have a shape reminiscent of a contact binary of mass ratio $q \sim 0.2$ (Demura et al., 2006) in contrast to pre-Hayabusa shape reconstructions by lightcurve (Kaasalainen et al., 2003) and radar (Ostro et al., 2004) inversion, which revealed only an elongated shape without clear evidence of a bifurcation or concavities.

CHAPTER 7

PHYSICAL CHARACTERIZATION OF NEAR-EARTH BINARY ASTEROID 2004 DC

Arecibo S-band (2380 MHz, 13 cm) and Goldstone X-band (8560 MHz, 3.5 cm) radar observations from May 29 to June 6, 2006 show that near-Earth asteroid 2004 DC is a binary system. The mutual orbit has a semimajor axis of 4.4 primary radii, an eccentricity of 0.24, and is uninclined to the equator of the primary. The <6.5-h rotation period of the secondary is not synchronized to the 23.2-h mutual orbit period. The 2.57-h lightcurve period of the primary and the total angular momentum of the system suggest the binary formed via spin-up. Shape modeling reveals an oblate shape for the primary with an equivalent spherical diameter of 337 m reminiscent of the 1999 KW_4 primary including a pronounced circular equatorial belt and polar flattening. The shape of the secondary is less constrained as a 70-m diameter roughly spherical body if it is not tumbling due to the moderate eccentricity of the mutual orbit. To have both an eccentricity and an asynchronous secondary, the 2004 DC binary likely formed with essentially its current separation and eccentricity and has not evolved significantly due to tides.

7.1 Radar Observations

During a radar experiment, either a circularly polarized continuous wave or coded waveform is transmitted for roughly the round-trip time it takes for light to reach the target, echo, and return to the receiver, then the echo is recieved for a similar length of time. Continuous wave (cw) or Doppler-only spectra are shifted by the bulk motion of the target along the line of sight, providing important astrometric information, as well as broadened by the rotation of the target, providing constraints on its spin state. Analyzing

the received signal from transmission of a time-dependent coded waveform according to arrival time provides complementary astrometric data in terms of a precise distance measurement to the target and produces delay-Doppler images that resolve the radar echo in two orthogonal dimensions, distance (time delay) from the observer and Doppler shift due to rotation, that constrain the shape of the target with resolution unparalleled by other ground-based techniques. The time increment τ used in the transmitted signal yields a range resolution $c\tau/2$, where c is the speed of light. The highest resolution achieved is 7.5 m using $\tau = 0.05\,\mu s$.

2004 DC, an Apollo near-Earth asteroid (heliocentric a = 1.64 AU, e = 0.40, I = 19.4°), was observed in 2006 from May 29 to June 6 with the 305-m antenna and 900 kW, 13-cm wavelength transmitter at Arecibo and the 70-m antenna and 450 kW, 3.5-cm wavelength transmitter at Goldstone (see Table 7.1). The binary nature of 2004 DC was unambiguously determined from high-resolution delay-Doppler images from June 2 at Arecibo shown in Figure 7.1. Although not visible in delay-Doppler images from Goldstone on May 29 and 30 prior to its closest approach, subsequent Goldstone images with higher signal-to-noise clearly show the secondary as well as a mutual event on June 3 described in Section 7.4.

Unlike most binary asteroids observed with radar, the cw spectra of 2004 DC (see Figures 7.2 and 7.3) do not show clear evidence that the system has two components. Most near-Earth binaries produce a characteristic echo consisting of the broad echo of the larger, rapidly-rotating primary with a strong, skinny echo spike from the smaller, slowly-rotating, likely synchronized secondary superimposed upon it (*e.g.*, 2000 DP_{107} in Margot et al. (2002)). The lack of a clear secondary peak is a hint that the secondary may not be rotating slowly and, hence, its echo is smeared out and blended into the echo of the primary.

Table 7.1: The first column indicates the telescope: Arecibo (A) or Goldstone (G). Date is the UT date of the observation. MJD is the modified Julian date of the observation. Eph is the ephemeris solution number used. RTT is the round trip light-time to the target in seconds. PTX is the transmitter power in kilowatts. Baud and res are the delay (range) and frequency resolution in microseconds and Hz, respectively, of the processed data. Delay resolution in μs translates to range resolution in meters via a factor of 150 making the best Goldstone resolution 18.75 m and the best Arecibo resolution 7.5 m. Code is the length of the pseudo-random code used for ranging and delay-Doppler imaging. The timespan of the received data are listed by the UT start time of the first receive cycle and stop time of the last receive cycle. Runs is the number of transmit-receive cycles completed.

Tel	Date	MJD	Eph	RTT	PTX	Baud	Res	Code	Start-Stop	Runs
	yyyy-mm-dd			s	kW	μs	Hz		hhmmss-hhmmss	
G	2006-05-29	53884	31	47	425	cw	1.25	none	073155-075609	16
					425	10	11.2	127	081824-082347	4
					438	11	12.3	127	084447-085557	6
					415	1	8.20	127	091849-093454	10
			33		431	1	8.20	127	094328-102322	26
			35	46	427	0.125	0.75	127	104757-134318	108
					444	cw	1.25	none	135940-143007	20
G	2006-05-30	53885	35	40	442	cw	1.25	none	122417-124215	15
					425	0.125	0.75	127	132845-151440	80

Table 7.1 (Continued)

Tel	Date yyyy-mm-dd	MJD	Eph	RTT s	PTX kW	Baud μs	Res Hz	Code	Start-Stop hhmmss-hhmmss	Runs
			37	39	418	0.125	0.75	127	153929-172613	76
					432	0.5	5.02	127	173650-174848	10
					445	cw	1.25	none	180521-183517	23
A	2006-06-02	53888	37	27	717	cw	0.25	none	105350-110340	11
					518	0.05	0.05	65535	110812-125649	113
A	2006-06-03	53889	39	26	725	cw	0.25	none	103956-104904	11
						0.05	0.05	65535	105329-110812	17
G	2006-06-03	53889	39	26	447	cw	1.25	none	123437-124457	12
					430	0.125	0.75	127	131956-133108	13
					425	0.125	0.75	127	133435-152818	126
					425	0.125	0.75	127	154758-184731	180
					450	cw	1.25	none	190405-190951	7
A	2006-06-04	53890	47	26	650	cw	0.25	none	111116-111855	9

Table 7.1 (Continued)

Tel	Date yyyy-mm-dd	MJD	Eph	RTT s	PTX kW	Baud μs	Res Hz	Code	Start-Stop hhmmss-hhmmss	Runs
G	2006-06-05	53891	41	28	420	cw	1.25	none	114735-115800	11
					422	0.125	0.75	127	121434-122359	10
				29	427	0.125	0.75	127	122523-133543	71
						0.125	0.75	127	140050-141515	15
					430	cw	1.25	none	141823-142949	12
G	2006-06-06	53892	41	32	447	cw	1.25	none	131632-132653	10
				33	440	0.125	0.75	127	134532-151250	80
					453	0.125	0.75	127	152030-153052	10
					457	cw	1.25	none	153542-154458	9

7.2 Reflection Properties

The equivalent radius R of the system, found by adding the equivalent spherical radii of the components (0.168 km and 0.035 km, determined by radar data inversion described in Section 7.7) in quadrature, is 0.172 km. The geometric visible albedo in terms of the absolute magnitude H (Fowler and Chillemi, 1992) is

$$\log p_{\mathrm{v}} = 5.645 - 2\log R - 0.4H. \tag{7.1}$$

For $H = 18.0 \pm 0.6$ (Jet Propulsion Laboratory Small Body Database), the albedo of the 2004 DC system is $0.92^{+0.69}_{-0.39}$, easily the highest albedo of any known asteroid if the absolute magnitude is correct. Any brighter absolute magnitude would result in an unphysical albedo greater than 1.

Normal reflection of a circularly polarized wave by a plane mirror completely reverses the polarization of the wave (opposite-sense circular, OC), but a wave reflected by a surface rough on the scale of the wavelength of the wave can retain a degree of its original polarization (same-sense circular, SC) through multiple scatterings (Ostro, 1993). The degree of decimeter-scale near-surface roughness is quantified by the circular polarization ratio SC/OC, defined as the ratio of the same-sense radar cross section to the opposite-sense radar cross section. In Table 7.2, the circular polarization ratio at X-band (3.5 cm) is 1.03, indicated by the similar echo strengths of the OC and SC polarizations in the Goldstone spectra from Figures 7.2 and 7.3. A circular polarization ratio greater than one implies an extremely rough surface on centimeter scales. At S-band (13 cm), the circular polarization ratio is slightly lower at 0.80. The average circular polarization ratio of 0.92 is in the top 5% among near-Earth asteroids compiled in Benner et al. (2008b). The radar albedo of 2004 DC, the combined

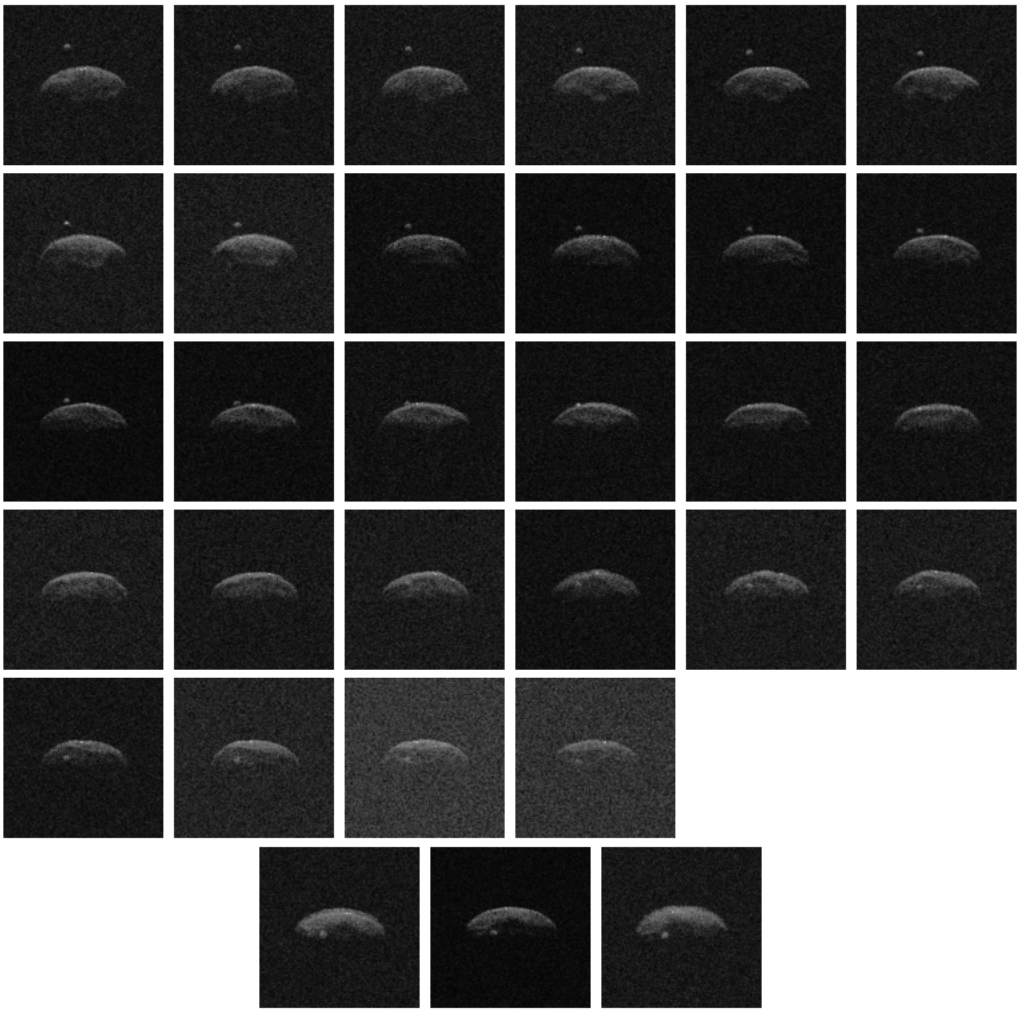

Figure 7.1: Arecibo high-resolution delay-Doppler images from 2006 June 2 (top) and June 3 (bottom) covering over 250° of rotation of the primary. Range increases downward with 7.5 m resolution and frequency increases to the right with 0.05 Hz resolution in each frame, which is itself the average of 4 transmit-receive cycles, so the primary appears to rotate counter-clockwise. The similarity in position of the secondary in the final images of June 2 and the images from June 3 implies an orbital period of roughly 24 hours.

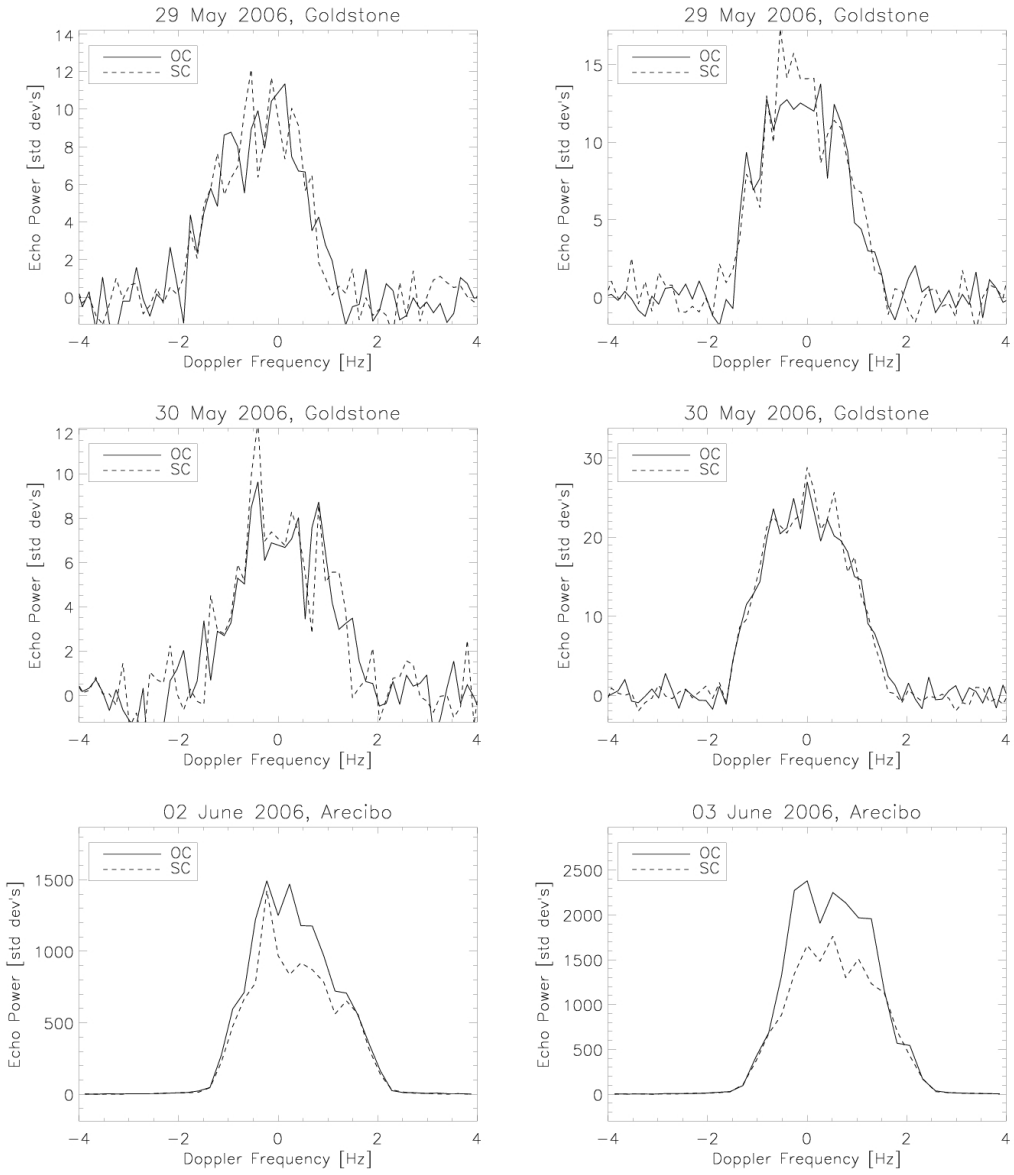

Figure 7.2: Sums of Doppler-only spectra for each cw data set in Table 7.1 with echo power measured in standard deviations of the off-target noise. *OC* is the radar echo with the opposite circular polarization of the transmitted signal, and SC is the echo with the same circular polarization as the transmitted signal. Goldstone X-band measurements are scaled to the Arecibo S-band radar frequency by a factor of 2380/8560 for easier comparison. The S-band frequency resolution is then 0.35 Hz for the Goldstone data and 0.25 for the Arecibo data. The presence of the secondary is not obvious in these data, but its relative position in the spectra can be inferred from its position in delay-Doppler images.

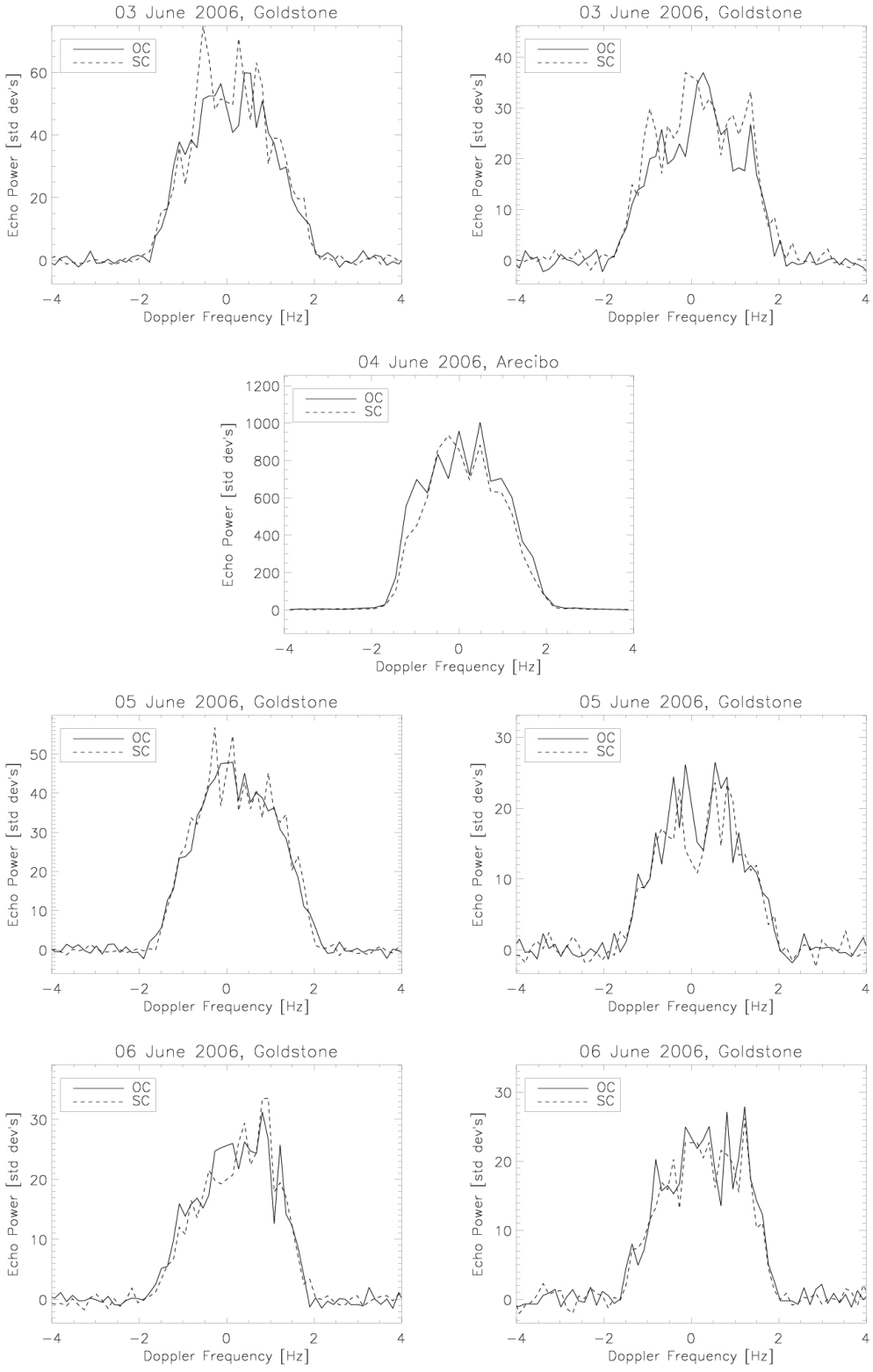

Figure 7.3: See Figure 7.2

radar cross-section of both polarizations scaled by the equivalent cross-sectional area of the primary, of 0.26 is also among the highest recorded for a near-Earth asteroid (http://echo.jpl.nasa.gov/~lance/asteroid_radar_properties/nea.radaralbedo.html).

The spectral class of 2004 DC has not been determined. However, Benner et al. (2008b) showed a clear link between circular polarization ratio, and thus near-surface, radar-wavelength (decimeter) scale roughness, and spectral class. With H = 18.0 and SC/OC = 0.92, 2004 DC falls amongst known members of spectral class E (Benner et al., 2008b, Figure 1). E class asteroids are a subset of the spectrally degenerate X class that also includes M and P class asteroids. The classes are separated by optical albedo with E class asteroids having the highest albedos and P class asteroids having the lowest albedos of roughly 0.5 and 0.05, respectively (Binzel et al., 2002). A survey by Fornasier et al. (2008) of 13 E class asteroids finds a typical albedo of $p_v = 0.5 \pm 0.1$. Thus, if 2004 DC is in fact an E class asteroid as its circular polarization ratio suggests, a high albedo of roughly 0.5 would be reasonable. If the absolute magnitude of 2004 DC is incorrect, and is instead skewed to the fainter end of its uncertainty range, the albedo of 2004 DC would fall below 0.6, the rough upper bound on the albedos of E class asteroids.

7.3 Mutual Orbit

The similar positions of the secondary at the end of the imaging sequence on June 2 and the images from June 3 point toward an orbital period of roughly 24 hours or possibly 12 hours. Subsequent Goldstone delay-Doppler images provide further positions necessary for mutual orbit determination. The relative positions of the components in the delay-Doppler images and cw spectra over more than 90° of sky motion produce a best-fit

Table 7.2: Radar reflection properties of 2004 DC. Date corresponds to the epoch for the cw runs given in Table 7.1. λ and β are the ecliptic coordinates of the line of sight. Res is the frequency resolution of the spectra. Bandwidth is the limb-to-limb bandwidth of the radar echo measured at a signal threshold of 2 standard deviations of the off-source noise for the sum of all runs on the date. Goldstone X-band frequencies are translated to Arecibo S-band frequencies by a factor of 2380/8560. $\hat{\sigma}$ is the radar albedo assuming an equivalent radius of 168 m. SC/OC is the circular polarization ratio. The uncertainties on $\hat{\sigma}$ and SC/OC are the RMS of the values from the daily sums with 25% and 10% uncertainties, respectively, being typical based on variability in pointing and system parameters.

Tel	Date yyyy-mm-dd	λ deg	β deg	Runs	Res Hz	Bandwidth Hz	$\hat{\sigma}$	SC/OC
G	2006-05-29	42	59	16	0.35	2.86	0.14	1.06
				20	0.35	3.12	0.14	1.11
G	2006-05-30	34	54	15	0.35	3.63	0.31	1.00
				23	0.35	3.57	0.33	1.01
A	2006-06-02	16	29	11	0.25	3.96	0.31	0.78
A	2006-06-03	10	15	11	0.25	4.15	0.40	0.73
G	2006-06-03	9	12	12	0.35	3.78	0.31	1.01
				7	0.35	3.94	0.14	0.97
A	2006-06-04	5	0	9	0.25	3.94	0.22	0.90
G	2006-06-05	359	-15	11	0.35	3.95	0.27	1.02
				12	0.35	3.94	0.20	1.08
G	2006-06-06	355	-26	10	0.35	4.14	0.33	1.00
				9	0.35	3.87	0.30	1.01
						Average:	0.26 ± 0.09	1.03 ± 0.04 (X) 0.80 ± 0.09 (S)

mutual orbit with $a = 0.74 \pm 0.02$ km, $e = 0.24 \pm 0.03$, a 23.22 ± 0.07-h orbit period, a retrograde orbit normal of $(\lambda, \beta) = (272^\circ, -11^\circ)$ in ecliptic coordinates, and a reduced χ^2 parameter of 0.346. The next best solution has a nearly identical orbit with a reduced χ^2 parameter of 0.383, but the orbit normal is prograde with $(\lambda, \beta) = (285^\circ, 53^\circ)$.

7.4 Mutual Event

In the Goldstone delay-Doppler images on June 3, a mutual event is detected where the secondary passes through the radar shadow of the primary (see Figure 7.4) such that the primary blocks the radar signal from reaching the secondary for a period of roughly 80 minutes from 154758-170803 (hhmmss) UT. We note that the first image where the secondary has disappeared is also the first image after a 20 minute break in receiving used to recalibrate the pointing of the telescope, so the mutual event could be up to 20 minutes longer. The mutual orbits determined in Section 7.3 both predict a mutual event from 152000-172000 using 20 minute timesteps. The slight discrepancy between the mutual event timing, especially if the event began several minutes prior to resumption of datataking, could be due to the assumption of sizes for and spherical shapes of the components in determining when the secondary is in the radar shadow, but the overall agreement lends credence to the accuracy of the orbit solutions.

7.5 Spin States of the Components

The Doppler broadening of the radar echo due to the rotation of the target is

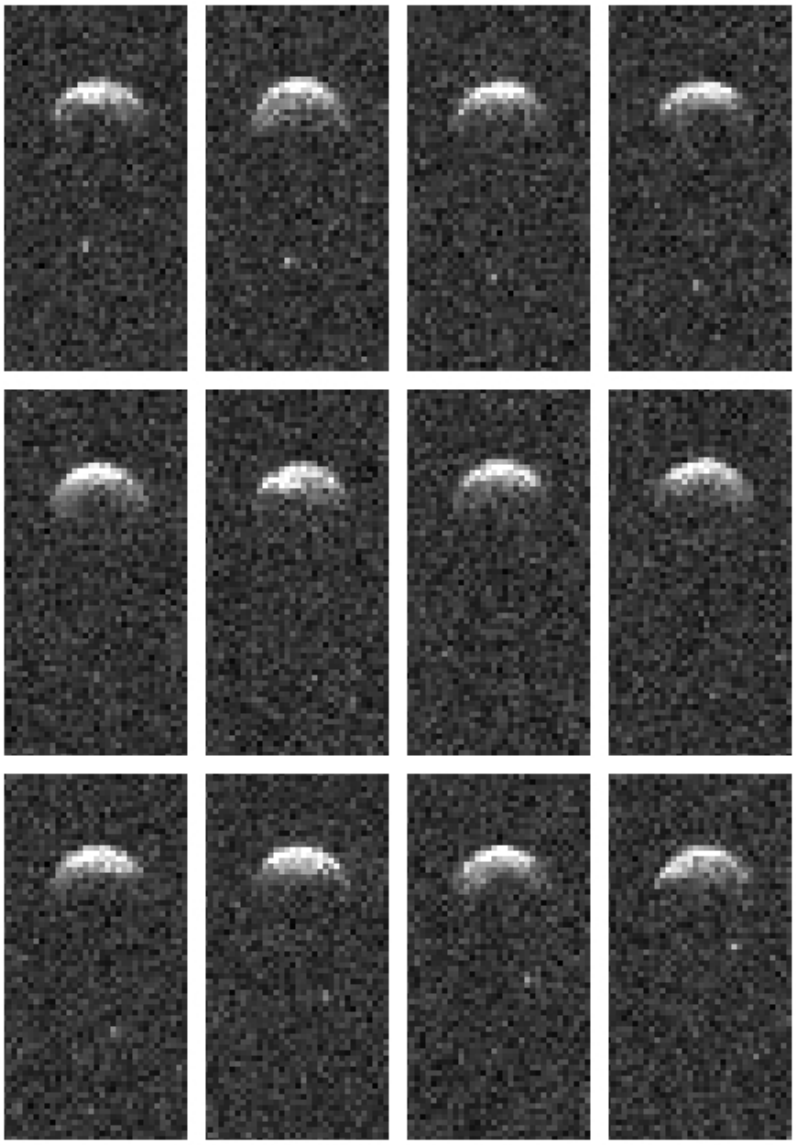

Figure 7.4: Delay-Doppler images from Goldstone on 2006 June 3 spanning over five hours from 133435-184731 (hhmmss) UT recorded the 2004 DC secondary passing through the radar shadow of the primary. Range increases downward with 18.75 m resolution and frequency increases to the right with 0.75 Hz resolution in each frame, which is itself the average of 10 transmit-receive cycles. The secondary begins beyond the primary along the line of sight and moving away (top row) before disappearing behind the primary (middle row) such that the primary blocks the radar signal from reaching the secondary for at least 80 minutes. Then the secondary emerges from the radar shadow of the primary (bottom row) moving toward the radar along the line of sight.

$$B = \frac{4\pi D}{\lambda P} \sin\delta \tag{7.2}$$

where B is the limb-to-limb bandwidth of the echo, D is the target diameter producing the Doppler shift at the current viewing geometery and rotation phase, λ is the radar wavelength, P is the spin period of the target, and δ is the inclination of the target's spin axis with respect to the line of sight. The bandwidth of the primary echo (Table 7.2) increases over the first two Goldstone tracks before leveling out at ~4 Hz in S-band for the remainder of the observations indicating a roughly constant sub-radar latitude from June 2 to 6. To constrain the pole location of the primary, a grid search over the entire celestial sphere with 5° resolution is completed where for each pole position an oblate shape for the primary is fit to the summed echoes from each set of cw data in Table 7.2 assuming a (lightcurve) rotation period of 2.57 h (R. Behrend, pers. comm.). The grid search finds 4 possible pole regions, two of which are shown in Figure 7.5, the other two being poles pointed in the opposite direction because the cw echoes contain a north-south ambiguity. The best-fit spin pole falls nearly atop the best-fit mutual orbit normal at $(272°, -11°)$. The second possible pole region in Figure 7.5 corresponds to the second best mutual orbit normal, but pointed in the opposite direction. Although the precise rotation pole for the primary is undetermined by this method as all four regions are capable of producing the observed bandwidths of the cw echoes, the best pole solutions from the observed radar bandwidths of the primary are in excellent agreement with the best fit mutual orbit normals, suggesting an equatorial orbit for the secondary.

The synodic period measured by a lightcurve differs from the intrinsic sidereal rotation period of the target due to an apparent rotation caused by the sky motion of the target during observations. For the best-fit poles of the 2004 DC primary, the sky motion should cause less than a 0.005 h (18 second) difference between the 2.57-h lightcurve

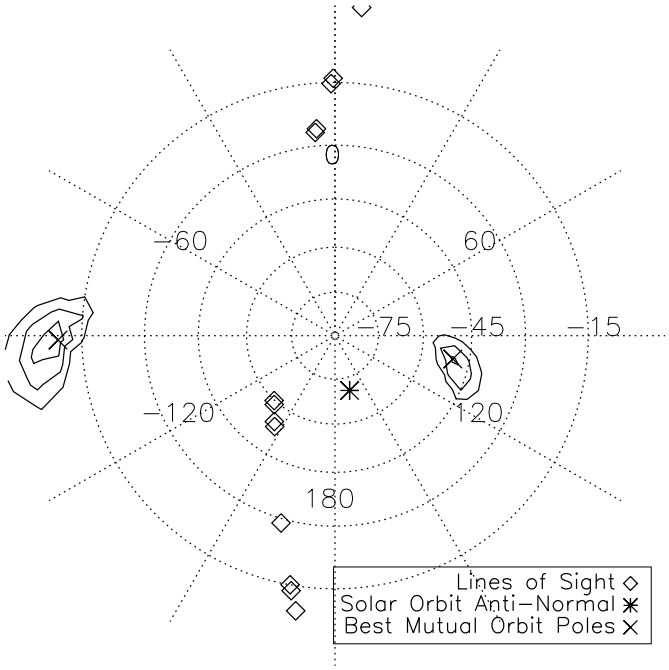

Figure 7.5: Looking down on the south ecliptic pole, the contours represent the 1σ, 2σ, and 3σ confidence intervals of the best-fit spin poles for the 2004 DC primary found by fitting the cw echoes from Table 7.2. The overall best-fit pole region (at left) corresponds to the best-fit orbit normal. The region at right corresponds to the second best-fit orbit normal, but oppositely directed. Two prograde regions pointed in the opposite direction of the regions shown fit the data equally well. All possible solutions lie far from both the lines of sight and the heliocentric orbit normal of (345°, 70°).

period and the sidereal period. Using the best-fit system mass of 3.432×10^{10} kg found during mutual orbit fitting and the effective volumetric radius of the system, 169 m, the density of the 2004 DC system is 1.70 g/cm^3. At this density, the rubble pile breakup period (Harris, 1996) is 2.53 h, less than 2% faster than the lightcurve period. The rapid rotation of the primary near the rubble pile breakup limit plus the total angular momentum of the system of $J/J' = 0.406$, 96% of which is contained in the spin of the primary, suggest formation of the binary system through mass shedding from a spin-up mechanism such as the YORP effect. The equatorial orbit of the secondary is also an indication of formation by spin-up as material lofted from the equator into orbit about the primary coalesces into a secondary.

Evolution for a single body with finite thermal conductivity due to the YORP effect tends to push the spin pole direction to an obliquity of 0° or 180° with respect to the heliocentric orbit normal (Capek and Vokrouhlický, 2004) as seen for (54509) YORP (Taylor et al., 2007). Capek and Vokrouhlický (2004) also find that a 90° obliquity is attainable in of order 10% of cases for random Gaussian spheroid test shapes. In the case of 2004 DC, the best spin pole candidates lie far from the heliocentric orbit normal, but (272°, -11°) and its prograde counterpart (92°, 11°) have obliquities of 95° and 85°, respectively. The other two best pole solutions have obliquities of roughly 30° and 150°. The rapid rotation of the primary and the near-90° obliquity of the best spin pole and mutual orbit normal to the heliocentric orbit normal are consistent with a YORP-evolved asteroid with timescales for YORP spin-up and obliquity change of order 0.1–1 My.

Because the presence of the secondary is difficult to uncover in the cw spectra, the high resolution delay-Doppler images are used to show the secondary has a bandwidth of 6 pixels or 0.3 Hz. For a body 70 m in diameter with the same spin pole as the

primary and the orbit normal, the secondary must have a period of roughly 6 hours. If the secondary is actually synchronized to the 23.2-h mutual orbit period, the product $D \sin\delta$ must increase by a factor of almost 4 to keep the bandwidth fixed. Over the course of the radar observations $\sin\delta$ ranges between 0.87 and 1 and cannot get any larger by moving the spin axis of the secondary from $(272^\circ, -11^\circ)$. Thus, the size of the secondary would have to account for the entire increase in period to keep the bandwidth fixed. A secondary over 200 m in diameter is irreconcilable with the echo depth seen in the high resolution delay-Doppler images; therefore, definitively, the spin of the secondary is not synchronized with the orbital motion. Not being able to fit the bandwidth of secondary over several dates as was done with the primary, we cannot constrain the spin pole and may only say that the spin period of the secondary must satisfy $P < 4\pi D/\lambda B = 6.5$ hours during the observations since $\sin\delta \leq 1$ for any choice of spin pole.

7.6 Is the Secondary Tumbling?

The eccentric mutual orbit of 2004 DC and the inability to constrain the spin pole and spin period of the secondary lead one to ask whether the secondary could be tumbling like the saturnian moon Hyperion (Wisdom et al., 1984). As the rotation rate and orbital distance of the secondary evolve due to tidal evolution, the secondary may be captured in a spin-orbit resonance where the spin rate and orbital mean motion are commensurate as is the case of Mercury, which is in a 3:2 spin-orbit resonance about the Sun (Pettengill and Dyce, 1965; Colombo, 1965). With a spin period faster than 6.5 hours and an orbital period of 23.2 hours, the secondary of 2004 DC cannot be locked in a low-order spin-orbit resonance. Regardless, in spin-orbit coupling, the strength of the resonance depends on the eccentricity of the orbit and the shape of the secondary (Goldreich and Peale, 1966) in the form of the factor $(B - A)/C$, where A, B, and C are the principal

moments of inertia in increasing order. For a principal axis rotator in its minimum energy rotation state, the spin axis is parallel to the short axis of the rotator's shape, the axis of maximum inertia. For moderate eccentricities and shape asymmetries, the spin-orbit resonances begin to overlap, allowing the secondary's spin state to become chaotic because an object cannot simultaneously occupy two resonances. Upon entering a chaotic region of spin-orbit phase space, the spin state of the secondary is not fixed (on timescales much shorter than tides can alter the spin state); the spin rate becomes variable and the spin axis is free to tumble through all possible orientations.

The resonance overlap condition (Chirikov, 1979), as described by Wisdom et al. (1984), says that the 1:1 (synchronous orbit) and 3:2 spin-orbit resonances, the widest resonances in the spin-orbit coupling problem, overlap if

$$\omega_0 \geq \frac{1}{2 + \sqrt{14e}}, \tag{7.3}$$

where $\omega_0^2 = 3(B - A)/C$. Thus, if ω_0 is too large, meaning the shape of the secondary deviates too far from that of a sphere, the secondary will tumble due to the severe overlap between the spin-orbit resonances. In the case of 2004 DC, the eccentricity of the mutual orbit is $e = 0.24$ such that if the shape of the secondary satisfies $\omega_0 \geq 0.26$, it should tumble chaotically. This is equivalent to saying the secondary will tumble unless its equatorial axes are within 2.2% of each other. From the high-resolution delay-Doppler images, the radar echo of the secondary appears roughly spherical but producing a three-dimensional shape model from the inversion of the radar data can improve the constraints on the shape of the secondary. If the secondary is tumbling, it will not synchronize as in a conventional tidally-evolved binary.

7.7 Shape Model

The shape modeling process (Hudson, 1993; Magri et al., 2007) produces a three dimensional model of the asteroid by minimizing the weighted squared residuals between the synthetic model and the one or two dimensional radar data sets. Three models of increasing complexity may be produced, typically in sequential order: (i) triaxial ellipsoid, described by the major axis length and axial ratios, (ii) harmonic, described by a spherical harmonic expansion of surface displacements, and (iii) vertex, described by a polygon with triangular facets. The final vertex model of the primary is 1148 vertices and 2292 facets with 6° resolution, comparable to the rotational smearing of the high-resolution delay-Doppler images from Arecibo, and fit to said Arecibo images and the full complement of cw spectra.

The four best spin pole regions for the 2004 DC primary are tested with the best-fit pole $(272°, -11°)$ consistently producing the best fits to the data (see Figure 7.6) with the roughly oblate 358 m $\times$ 353 m $\times$ 335 m shape model displayed in Figure 7.7. Modeling suggests the shape of the 2004 DC primary is reminiscent of the 1999 KW_4 primary (Ostro et al., 2006) including a pronounced circular equatorial belt, sloped sides, and flattened poles. Such a shape is indicative of a binary formation process such as the YORP effect that spins up the primary, redistributes regolith to the potential low at the equator, and causes material to be shed into an equatorial orbit about the primary (Walsh et al., 2008).

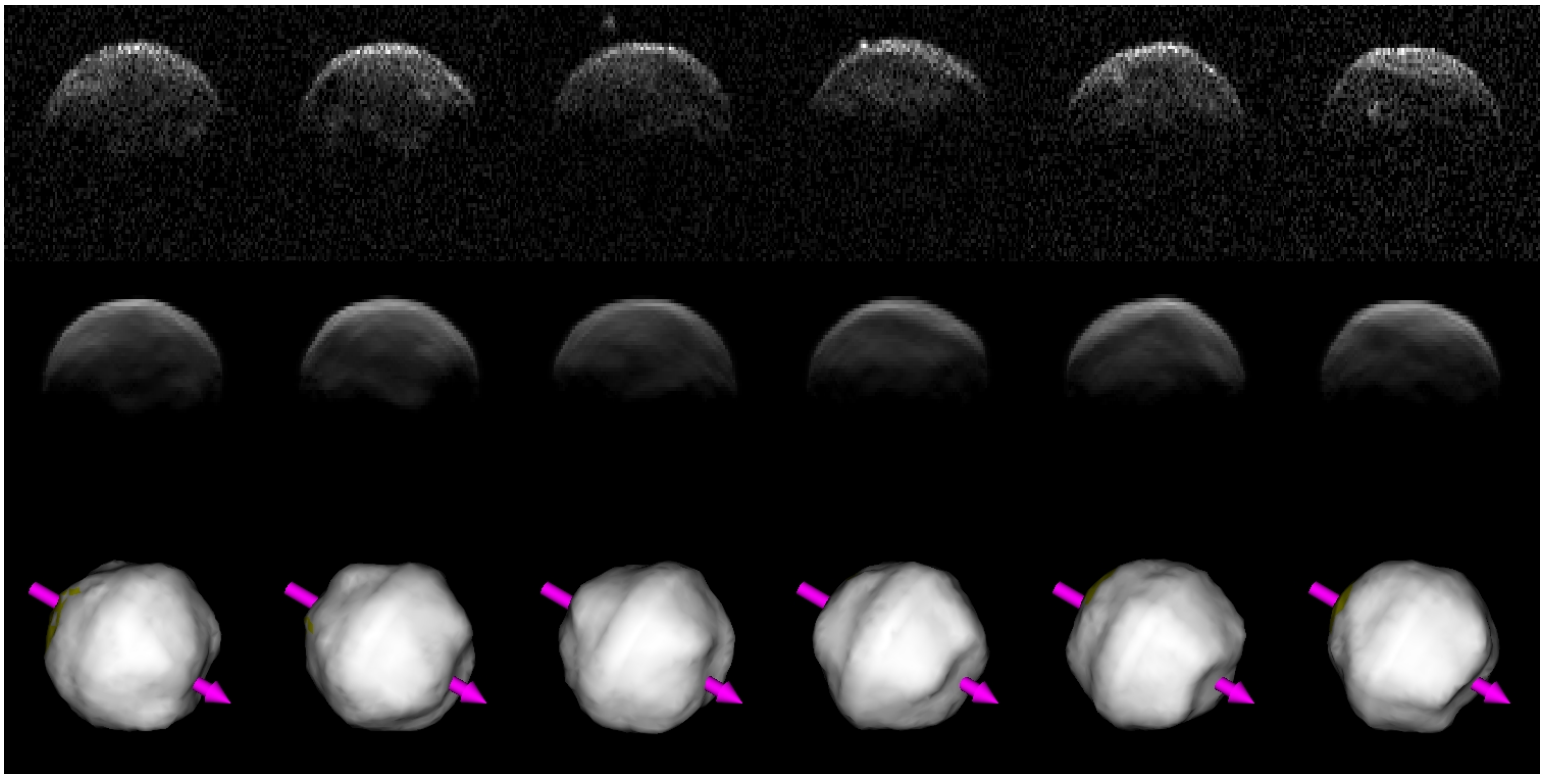

Figure 7.6: Subset of delay-Doppler images with 7.5 m $\times$ 0.05 Hz resolution, simulated radar images produced by the shape model, and plane-of-sky projections of the shape model (with spin vector) covering 225° of rotation. Range increases downward and frequency increases to the right giving the illusion of counter-clockwise rotation. The secondary drifts across the image of the primary, but is masked out during the shape modeling process to avoid affecting the shape of the primary.

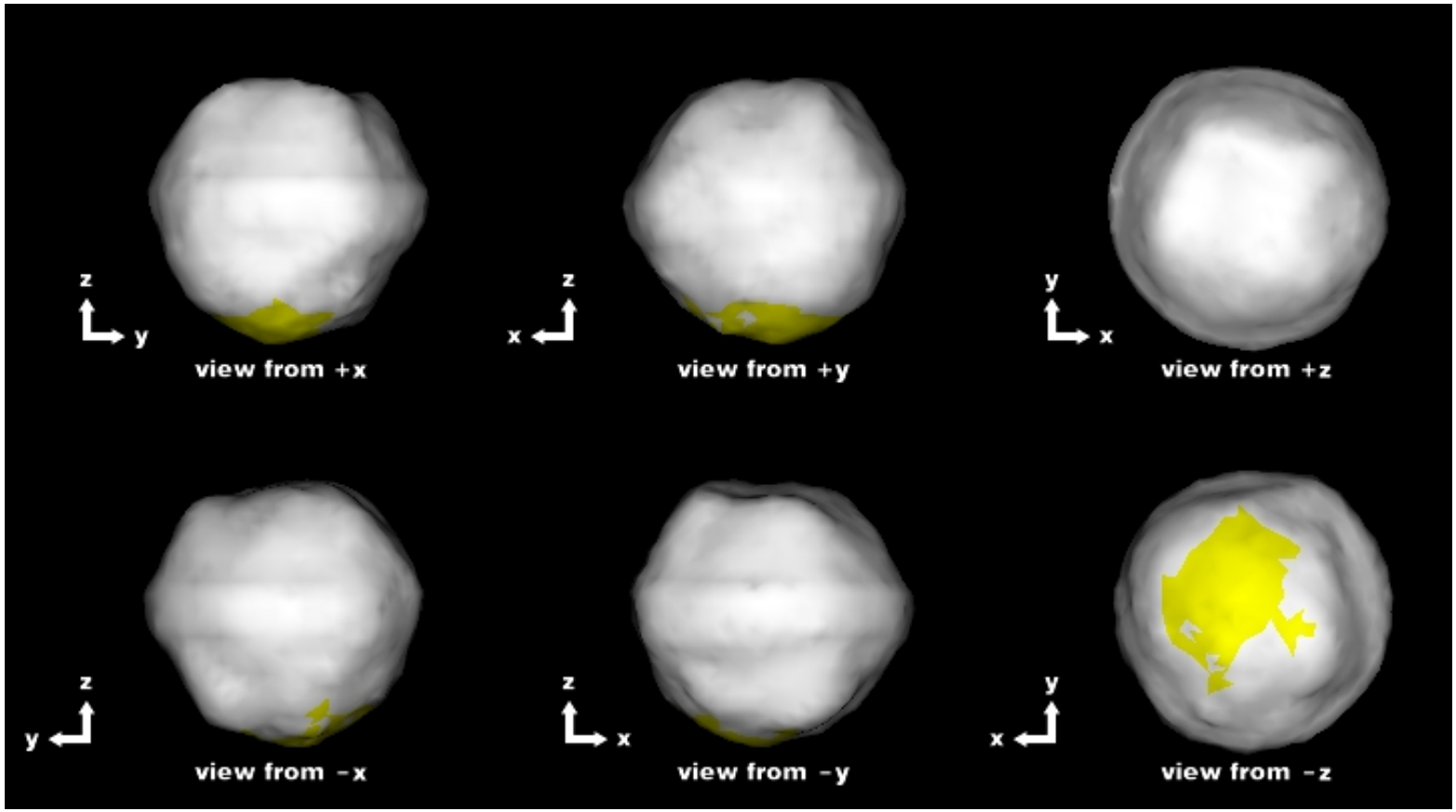

Figure 7.7: Equatorial and polar views of the shape model for the primary component of 2004 DC. The ~355-m diameter circular belt at the equator and flattened poles are similar to those seen on 1999 KW_4. The rapid rotation causes material to flow from the poles to the equator giving the shape its flat-topped appearance and bulging midsection. The oblateness of the primary is less than that of 1999 KW_4 at $\gamma = 0.94$. Yellow shading indicates regions either hidden from view of the radar or have radar reflection angles greater than 60°.

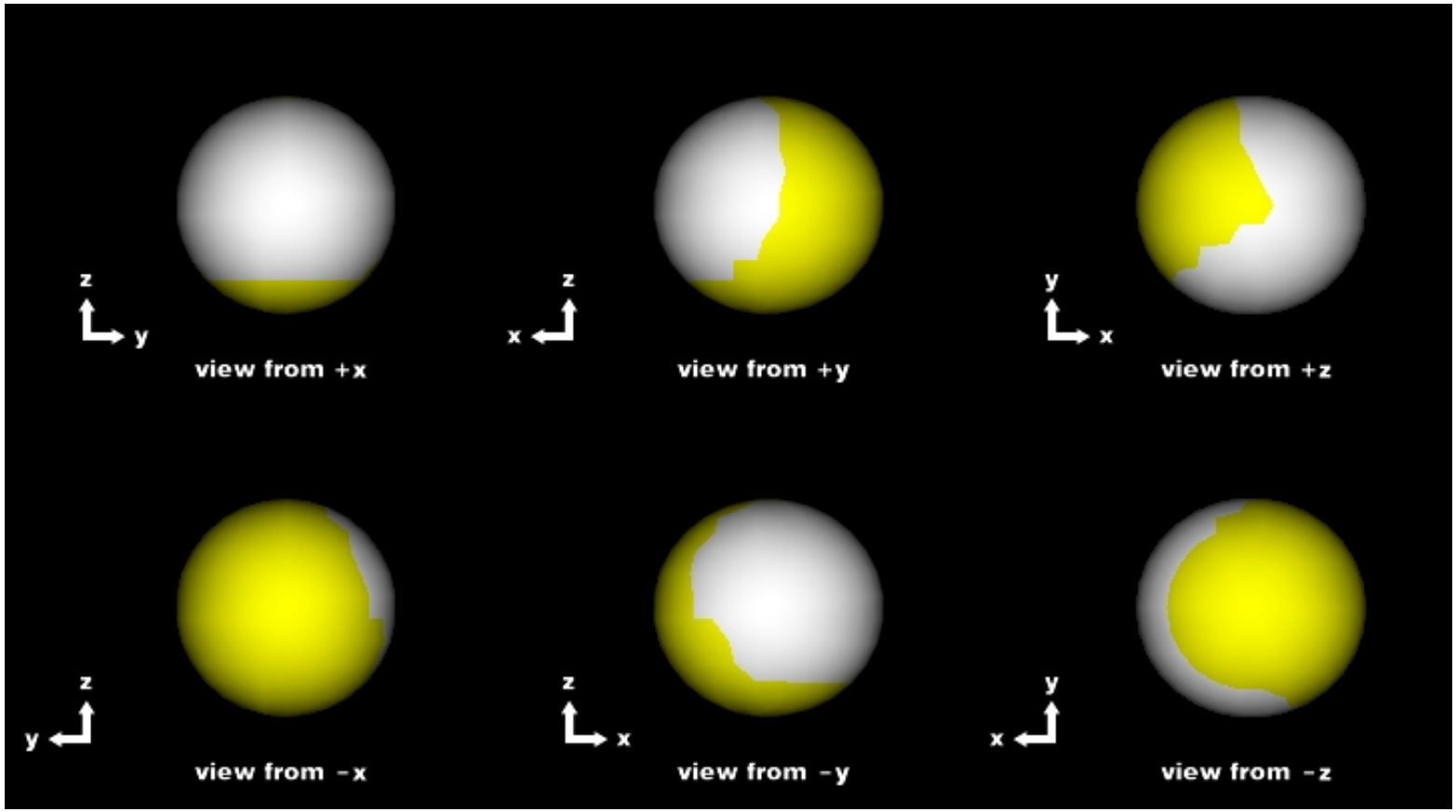

Figure 7.8: Equatorial and polar views of the essentially spherical shape model for the secondary component of 2004 DC. Yellow shading indicates regions either hidden from view, mostly due to the limited rotational coverage from the small number of usable high resolution images, or have radar reflection angles greater than 60°. The shape model is invalid if the secondary is tumbling.

The secondary is modeled as an ellipsoid, which is realized as a 288 vertex, 572 facet shape assuming the secondary is not tumbling; tumbling would render shape modeling ineffective from the inability to correctly model the spin state of the body. Only the high-resolution delay-Doppler images from Arecibo are usable as the secondary fits within a few pixels in the Goldstone imagery. Several images from Arecibo must also be discarded because of the overlap between the primary and secondary. While the secondary can be masked out and leave enough data for fitting the primary, the primary cannot be similarly masked out from behind the secondary. The resulting shape model, assuming the same spin pole as the primary and a spin period of 6.4 hours, in Figure 7.8 is slightly prolate with dimensions of 72 m $\times$ 69 m $\times$ 69 m.

The limited timebase over which the high-resolution delay-Doppler images of the secondary are available hinders the shape modeling process. However, we can still estimate the shape of the secondary as roughly spherical. The equatorial axes differ by 3 meters or less than 5%. Although the deviation from a sphere is small, it is more than the 2.2% threshold for preventing the onset of chaos. The necessity of an extremely spherical secondary to prevent resonance overlap makes a tumbling state very difficult to avoid.

7.8 Tidal Evolution

In Chapter 4, we found that for 2004 DC to tidally evolve from $2R_{\rm p}$ to its current separation of $4.4R_{\rm p}$ in 10 My requires an extremely weak primary with a μQ of order 10^7 N/m^2. At a separation of $4.4R_{\rm p}$, using the close orbit correction allows for μQ to increase by merely 7%. Even if the binary formed further from the primary at $4R_{\rm p}$, μQ can only increase by a factor of 2 for a 10 My evolution. Therefore, if the 2004 DC

system has tidally evolved at all in the last 10 My, the primary must have an extremely weak internal structure at the limit of Goldreich and Sari (2009)'s theory of rubble pile structure. If the 2004 DC binary is much older than 10 My, perhaps by forming in the inner main belt, to evolve from $2R_p$ to $4.4R_p$, μQ must still be less than 5×10^9 N/m^2, far less than the monolithic 100-km scale main belt binaries.

Ignoring the effects of an eccentric mutual orbit, the tidal evolution of the 2004 DC system in Figure 7.9 shows the rapid despinning of the secondary in well under 100 ky making it difficult to reconcile tidal evolution with the observed asynchronous secondary if the system is tidally evolved. If the system formed with nearly its current semimajor axis, the despinning timescale lengthens to of order 1 My. Because of its rapid despinning timescale, either the 2004 DC system is young enough that the secondary has not had time to tidally despin or the eccentricity of the mutual orbit has caused the secondary to tumble, preventing the secondary from synchronizing. Different scenarios for the past and future evolution of the 2004 DC system depend on which method of preventing the secondary from synchronizing holds true:

- The system is too young for tides to have synchronized the secondary —
  - For $\mu_s Q_s = \mu_p Q_p$, the system must have formed near its current separation and the eccentricity is left over from formation because the system cannot tidally evolve outward very far nor can the tides of Chapter 5 excite the eccentricity very much prior to despinning the secondary. μQ is not well-constrained if the initial and current separation are essentially equal (within much less than 10%). Once the secondary synchronizes, in terms of the monolithic eccentricity problem of Section 5.3 with $q = 0.0089$, tides on the secondary cannot damp out the eccentricity, and the eccentricity continues to build. For Goldreich and Sari's rubble piles, the eccentricity will damp

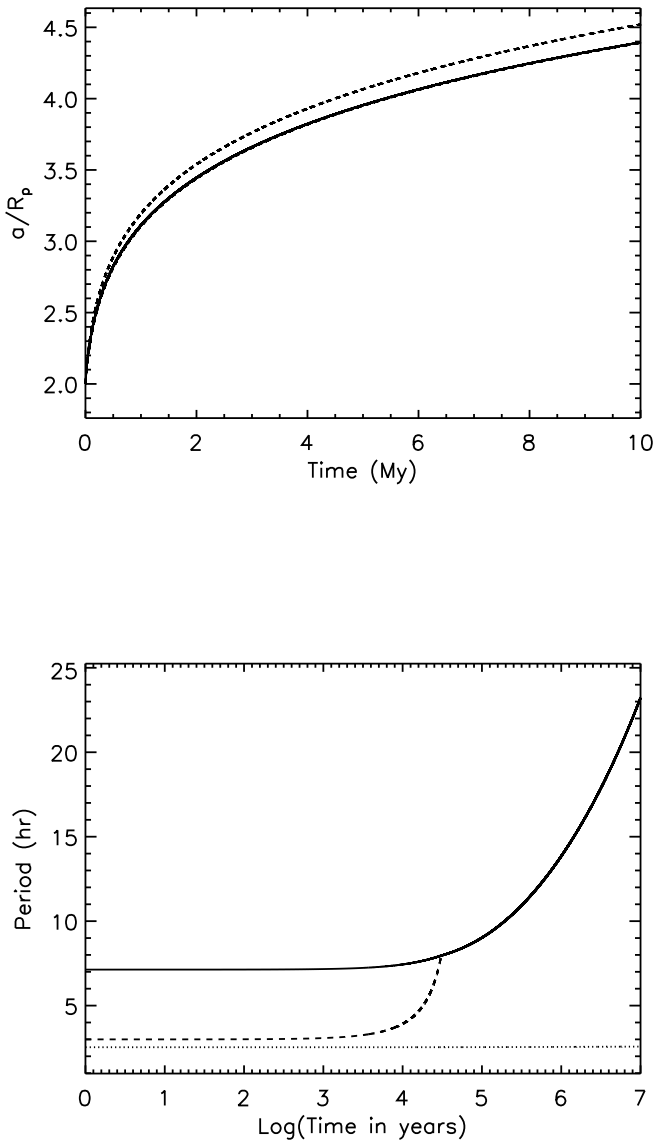

Figure 7.9: Tidal evolution of 2004 DC (q = 0.00887, R_p = 0.168 km, ρ = 1.70 g/cm^3, $\mu_s Q_s = \mu_p Q_p = 9.1 \times 10^6$ N/m^2) in terms of the orbit expansion (top) and the rotation and orbit periods (bottom) over 10 My. The orbit (solid, top) evolves to the current separation of 4.4 R_p dominated by tides on the primary, the primary despins slightly from the rubble pile breakup period to a 2.57-h spin period, but the secondary despins in tens of thousands of years, leaving a synchronized secondary contrary to what is observed today.

out over time after the secondary synchronizes.

  - For $\mu_s Q_s < \mu_p Q_p$ by an order of magnitude or more, the system evolves similarly to the $\mu_s Q_s = \mu_p Q_p$ case with a shorter despinning time, but, in terms of the monolithic eccentricity problem, the eccentricity will damp after the secondary synchronizes.

  - For $\mu_s Q_s > \mu_p Q_p$, the despinning timescale is lengthened allowing for more evolution of the semimajor axis and eccentricity prior to synchronizing the secondary. However, the synchronized secondary cannot damp out the eccentricity and the eccentricity continues to build for monolithic components. If $\mu_s Q_s$ is larger than $\mu_p Q_p$ by a factor of 100, the system can evolve from $2R_p$ and produce an eccentric orbit of ~ 0.3 before reaching the current separation of $4.4R_p$, but without a damping mechanism, the eccentricity will continue to grow. This situation would likely require the secondary to be a solid boulder while the primary is a rubble pile.

- The secondary is tumbling — If the secondary enters a tumbling state, the binary system no longer has a method of damping the eccentricity until the primary despins, which is much longer than the dynamical lifetime of an asteroid in the near-Earth region. Tumbling also removes any evidence that the binary is younger than the despinning time of the secondary.

  - If the secondary begins to tumble prior to synchronizing, the binary must have formed in essentially its present configuration, and the eccentricity must be left over from the formation of the binary as described above for similar μQ values.

  - If a growing eccentricity can pull the secondary out of a synchronous state and into a tumbling state, $\mu_s Q_s$ must be greater than $\mu_p Q_p$ to allow the eccen-

tricity to increase despite a synchronous secondary in terms of the monolithic eccentricity problem. Such an evolution could not occur with Goldreich and Sari's rubble piles.

- Other methods of orbit expansion are at work in addition to tides – BYORP cannot act without a synchronized secondary, so it has not affected the mutual orbit of 2004 DC. One cannot rule out a close planetary flyby from inducing an eccentricity or further separating the components. Mass lofting may occur given the rapid rotation of the primary and similarities to the 1999 KW_4 system that was used by Fahnestock and Scheeres (2008) to demonstrate the lofting process. Orbit expansion by non-tidal means has the effect of reducing μQ of the system as our tidal evolution scenario is accounting for a more rapid orbit expansion than it is actually responsible for.

The common theme to these evolution scenarios, with the exception of when $\mu_s Q_s \gg \mu_p Q_p$, is that the 2004 DC must have formed near its present configuration as the semimajor axis and the eccentricity of the mutual orbit cannot evolve much without the secondary synchronizing. If the system has barely tidally evolved at all, μQ cannot be well-constrained. Thus, μQ for 2004 DC could be much larger than 10^7 N/m^2 yet still be less than the monolithic main belt primaries as one would expect for an asteroid showing all the physical characteristics of a rubble pile. It is unclear at this time whether the secondary is tumbling, though according to the resonance overlap criterion, widespread chaos may exist in the spin-orbit phase space of the secondary making it very difficult to avoid entering a tumbling state. The uniqueness of the $\mu_s Q_s \gg \mu_p Q_p$ scenario of a boulder orbiting a rubble pile is intriguing and may deserve future attention to determine how easily a boulder could exist on, and be placed in orbit from, the surface of a rubble pile.

CHAPTER 8

DISCUSSION

For over 100 years, tidal interactions in binary systems, specifically the planets and their satellites, have hinted at the internal structures and material properties of the bodies. With the discovery of binary asteroids, the rich history of study of tidal interactions has been extended to minor planets. Here, we have expanded the current knowledge of tidal interactions by extending the evolutionary equations to include both close orbits and moderate eccentricities. Where the classical tidal evolution equations truncate the expansion of the potential between the two components to order $\ell = 2$ leaving the approximate potential accurate to 1% only for separations of more than $5R_{\rm p}$, we generalized the expansion of the potential and the resulting equations for the changes in spin rate of the components and the change in semimajor axis of the mutual orbit to arbitrary order ℓ. We also extended the equations of semimajor axis and eccentricity evolution to fourth order in the eccentricity, allowing more accurate description of systems with moderate eccentricities of a few tenths, an improvement over the classical equations for negligible eccentricity. Accounting for close orbits and moderate eccentricities both tend to speed up the expansion of the mutual orbit. Higher order terms in the eccentricity also tend to increase the eccentricity until the secondary is synchronized.

The effect of a non-spherical primary was also examined. The increased moment of inertia of an oblate or prolate body compared to a sphere makes it more difficult for a binary with a non-spherical primary with the same angular momentum content as a binary with a spherical primary to support a secondary in a fully despun, double synchronous tidal end state. Without a stable end state to complete tidal evolution in, the system must collapse to contact. This is one of three methods presented for the formation of contact binaries that led to our supposition that contact binary systems are the result of

the collapse of a binary system that lacks a stable, fully despun, double synchronous end state. A similar method arises from a binary system that forms with spherical primary, but too little angular momentum to support a stable end state. Both methods favor the collapse of equal mass binaries, but the non-spherical case may require combinations of low angular momenta and high degrees of non-sphericity yet to be observed in equal mass binaries, and the spherical case requires slow rotation of the components with respect to the mean motion in the mutual orbit, which is not expected among near-Earth asteroids formed by spin-up. The third method, of removal of angular momentum from the system via a spin-down mechanism like the YORP effect, is more attractive because it begins with a normal binary system and uses the loss of angular momentum to eliminate the stable end state. Not only does this method prefer the collapse of equal mass binaries to contact, but spin-down supports the long rotation periods of several hours up to several days of roughly equal mass contact binaries observed by radar.

Using tidal evolution and an assumption of the age of binary systems in the main belt and near-Earth regions, we placed limits on the material properties of the asteroids. Main belt binaries with 100-km scale primaries tidally evolving over the age of the solar system are consistent with having the material properties of monolithic or fractured rock as one would expect of systems produced through subcatastrophic collisions in the early solar system. Because of tides being the dominant method of orbit expansion for systems in the main belt, the dominance of tides on the primary, the wide separation of the components, and the weak dependence on initial separation, μQ of the primary is reliably determined by the classical tidal equations.

For near-Earth asteroids to tidally evolve over a 10 My dynamical lifetime, μQ must be orders of magnitude weaker than for the main belt binaries as one would expect of a rubble pile, but in some cases, such as for 2004 DC, μQ may be too low to reconcile with

Goldreich and Sari's theory of rubble pile structure. μQ can increase if a binary is older than 10 My having been injected from the main belt already as a binary, by forming near its current configuration and not having tidally evolved much, or if another orbit expansion mechanism is acting such as BYORP, mass lofting, or close planetary flybys. Clearly, it is far more difficult to accurately estimate μQ of a near-Earth binary than a main belt binary. The uncertainty in the age of binary systems is the leading source of uncertainty in the determination of μQ. Although important in accurately reproducing the potential felt by the components in a binary system, the close orbit correction does not have a significant effect on the calculation of μQ because of the relatively short amount of time spent at close separations during tidal evolution.

Near-Earth binary asteroid 2004 DC shows all of the hallmarks of a binary formed through the spin-up of a rubblized parent body: the rapid rotation near the rubble pile breakup limit, the circular belt of material around the midsection of the primary, the perfect amount of angular momentum corresponding to a parent body able to lose material due its rapid spin, and the equatorial orbit of the secondary. This litany of properties leads one to believe that 2004 DC, along with 1999 KW_4, are the prototypical near-Earth binary asteroids. If the 2004 DC system has tidally evolved at all, the material properties indicate the structure of the primary is much weaker than solid rock as one would expect for a rubble pile both intuitively and according to Goldreich and Sari (2009). However, to account for the eccentricity and the asynchronous secondary of 2004 DC, the system likely formed in nearly its current configuration and has not tidally evolved significantly making estimation of μQ difficult.

With an eccentricity of 0.24, it appears difficult for the secondary in the 2004 DC binary system to avoid entering a state of chaotic tumbling similar to the saturnian satellite Hyperion. Since the majority of binary systems have synchronous secondaries and

circularized mutual orbits, most binaries must form with negligibly eccentric orbits to synchronize their secondary without the eccentricity of the mutual orbit being large enough to cause tumbling. If the eccentricity starts at a few tenths or is able to grow that large during tidal evolution (difficult due to the short despinning timescales of secondaries unless $\mu_s Q_s \gg \mu_p Q_p$), the secondary likely tumbles and cannot synchronize or damp out the eccentricity. An analysis of the likelihood of a tumbling state for the secondary in a binary asteroid system similar to that done by Wisdom et al. (1984) for Hyperion is necessary to better understand whether eccentric binary asteroid systems are prone to tumbling, and, hence, prevent the secondary from synchronizing.

APPENDIX A

INTEGRALS FOR SYNCHRONOUS ORBITS ABOUT NON-SPHERICAL PRIMARIES

The series of steps for solving the integrals in Section 2.7 for the synchronous orbit condition for oblate and prolate primaries are as follows (integrated via *Mathematica*). In the oblate case,

$$
\begin{aligned}
J/J' &= \sqrt{\frac{3}{2}}\frac{\gamma^{1/2}}{(1+q)^{7/6}}\left[\frac{q}{1+q}\bar{a}^2+\frac{2}{5}\left(\gamma^{-2/3}+q^{5/3}\right)\right]\left[\int_{\gamma^{2/3}\bar{a}^2-1}^{\infty}\frac{\mathrm{d}u'}{(1+u')^2\left(\gamma^2+u'\right)^{1/2}}\right]^{1/2} \\
&= \sqrt{\frac{3}{2}}\frac{\gamma^{1/2}}{(1+q)^{7/6}}\left[\frac{q}{1+q}\bar{a}^2+\frac{2}{5}\left(\gamma^{-2/3}+q^{5/3}\right)\right] \\
&\quad \times\left[\frac{u'+\gamma^2}{(1+u')(1-\gamma^2)}+\frac{\tan^{-1}\sqrt{\frac{u'+\gamma^2}{1-\gamma^2}}}{(1-\gamma^2)}\Bigg|_{\gamma^{2/3}\bar{a}^2-1}^{\infty}\right]^{1/2} \\
&= \sqrt{\frac{3}{2}}\frac{\gamma^{1/2}}{(1+q)^{7/6}}\left[\frac{q}{1+q}\bar{a}^2+\frac{2}{5}\left(\gamma^{-2/3}+q^{5/3}\right)\right] \\
&\quad \times\left[\frac{\pi/2}{(1-\gamma^2)^{3/2}}-\frac{\sqrt{\gamma^{2/3}\bar{a}^2+\gamma^2-1}}{\gamma^{2/3}\bar{a}^2(1-\gamma^2)}-\frac{\tan^{-1}\sqrt{\frac{\gamma^{2/3}\bar{a}^2+\gamma^2-1}{1-\gamma^2}}}{(1-\gamma^2)^{3/2}}\right]^{1/2} \\
&= \frac{\sqrt{3/2}}{(1+q)^{7/6}}\left(\frac{\gamma}{1-\gamma^2}\right)^{1/2}\left[\frac{q}{1+q}\bar{a}^2+\frac{2}{5}\left(\gamma^{-2/3}+q^{5/3}\right)\right] \\
&\quad \times\left[\frac{1}{(1-\gamma^2)^{1/2}}\left(\frac{\pi}{2}-\tan^{-1}\sqrt{\frac{\gamma^{2/3}\bar{a}^2+\gamma^2-1}{1-\gamma^2}}\right)-\frac{\sqrt{\gamma^{2/3}\bar{a}^2+\gamma^2-1}}{\gamma^{2/3}\bar{a}^2}\right]^{1/2} \qquad \text{(A.1)}
\end{aligned}
$$

Other simplifications and substitutions included in the above integral, but not belabored upon in the text include the integrand $r^2-\alpha_1^2=a^2-\alpha_1^2$ reduced by α_1^2 when u is replaced by $u'=u/\alpha_1^2$ leading to $a^2/\alpha_1^2-1=\bar{a}^2R_{\mathrm{p}}^2/\alpha_1^2-1=\gamma^{2/3}\bar{a}^2-1$ because $\alpha_1/R_{\mathrm{p}}=\alpha_1/\left(\alpha_1\alpha_2\alpha_3\right)^{1/3}=\alpha_1/\left(\alpha_1^2\alpha_3\right)^{1/3}=\left(\alpha_1/\alpha_3\right)^{1/3}=\gamma^{-1/3}$ and the leading $\gamma^{1/2}$ that comes from the combination of $R_{\mathrm{p}}^{3/2}$ divided by the $\alpha_1^{3/2}$ pulled out of the square root of

the integral upon defining u'.

For a prolate primary where the secondary lies along the longest principal axis α_1, the synchronous orbit condition is

$$\begin{aligned}
J/J' &= \sqrt{\frac{3}{2}}\frac{\gamma}{(1+q)^{7/6}}\left[\frac{q}{1+q}\vec{a}^2+\frac{2}{5}\left(\frac{1+\gamma^2}{2\gamma^{4/3}}+q^{5/3}\right)\right]\left[\int_{\gamma^{4/3}\vec{a}^2-1}^{\infty}\frac{\mathrm{d}u'}{(1+u')^{3/2}(\gamma^2+u')}\right]^{1/2} \\
&= \sqrt{\frac{3}{2}}\frac{\gamma}{(1+q)^{7/6}}\left[\frac{q}{1+q}\vec{a}^2+\frac{2}{5}\left(\frac{1+\gamma^2}{2\gamma^{4/3}}+q^{5/3}\right)\right] \\
&\quad\times\left[-\frac{2}{\sqrt{1+u'}\,(\gamma^2-1)}-\frac{2\tan^{-1}\left(\frac{\sqrt{1+u'}}{\sqrt{\gamma^2-1}}\right)}{(\gamma^2-1)^{3/2}}\Bigg|_{\gamma^{4/3}\vec{a}^2-1}^{\infty}\right]^{1/2} \\
&= \sqrt{\frac{3}{2}}\frac{\gamma}{(1+q)^{7/6}}\left[\frac{q}{1+q}\vec{a}^2+\frac{2}{5}\left(\frac{1+\gamma^2}{2\gamma^{4/3}}+q^{5/3}\right)\right] \\
&\quad\times\left[\frac{\pi}{(\gamma^2-1)^{3/2}}+\frac{2}{\gamma^{2/3}\bar{a}\,(\gamma^2-1)}+\frac{2\tan^{-1}\left(\frac{\gamma^{2/3}\bar{a}}{\sqrt{\gamma^2-1}}\right)}{(\gamma^2-1)^{3/2}}\right]^{1/2} \\
&= \frac{\sqrt{3}}{(1+q)^{7/6}}\frac{\gamma}{(1-\gamma^2)^{1/2}}\left[\frac{q}{1+q}\vec{a}^2+\frac{2}{5}\left(\frac{1+\gamma^2}{2\gamma^{4/3}}+q^{5/3}\right)\right] \\
&\quad\times\left[\frac{\tanh^{-1}\left(\frac{\sqrt{1-\gamma^2}}{\gamma^{2/3}\bar{a}}\right)}{(1-\gamma^2)^{1/2}}-\frac{1}{\gamma^{2/3}\bar{a}}\right]^{1/2} . \qquad \text{(A.2)}
\end{aligned}$$

The integrand $r^2-\alpha_1^2 = a^2-\alpha_1^2$ is reduced by α_1^2 when u is replaced by $u' = u/\alpha_1^2$ leading to $a^2/\alpha_1^2-1 = \bar{a}^2R_\mathrm{p}^2/\alpha_1^2-1 = \gamma^{4/3}\bar{a}^2-1$ because $\alpha_1/R_\mathrm{p} = \alpha_1/(\alpha_1\alpha_2\alpha_3)^{1/3} = \alpha_1/\left(\alpha_1\alpha_3^2\right)^{1/3} = (\alpha_1/\alpha_3)^{2/3} = \gamma^{-2/3}$ and the leading γ comes from the combination of $R_\mathrm{p}^{3/2}$ divided by the $\alpha_1^{3/2}$ pulled out of the square root of the integral upon defining u'.

If the secondary lies along the intermediate axis α_2, the synchronous orbit condition is

$$
\begin{aligned}
J/J' &= \sqrt{\frac{3}{2}}\frac{\gamma}{(1+q)^{7/6}}\left[\frac{q}{1+q}\bar{a}^2+\frac{2}{5}\left(\frac{1+\gamma^2}{2\gamma^{4/3}}+q^{5/3}\right)\right]\left[\int_{\gamma^{4/3}\bar{a}^2-\gamma^2}^{\infty}\frac{\mathrm{d}u'}{(1+u')^{1/2}\left(\gamma^2+u'\right)^2}\right]^{1/2} \\
&= \sqrt{\frac{3}{2}}\frac{\gamma}{(1+q)^{7/6}}\left[\frac{q}{1+q}\bar{a}^2+\frac{2}{5}\left(\frac{1+\gamma^2}{2\gamma^{4/3}}+q^{5/3}\right)\right] \\
&\quad\times\left[\frac{\sqrt{1+u'}}{(u'+\gamma^2)(\gamma^2-1)}+\frac{\tan^{-1}\left(\frac{\sqrt{1+u'}}{\sqrt{\gamma^2-1}}\right)}{(\gamma^2-1)^{3/2}}\Bigg|_{\gamma^{4/3}\bar{a}^2-\gamma^2}^{\infty}\right]^{1/2} \\
&= \sqrt{\frac{3}{2}}\frac{\gamma}{(1+q)^{7/6}}\left[\frac{q}{1+q}\bar{a}^2+\frac{2}{5}\left(\frac{1+\gamma^2}{2\gamma^{4/3}}+q^{5/3}\right)\right] \\
&\quad\times\left[-\frac{\pi/2}{(\gamma^2-1)^{3/2}}-\frac{\sqrt{1+\gamma^{4/3}\bar{a}^2-\gamma^2}}{\gamma^{4/3}\bar{a}^2(\gamma^2-1)}-\frac{\tan^{-1}\left(\frac{\sqrt{1+\gamma^{4/3}\bar{a}^2-\gamma^2}}{\sqrt{\gamma^2-1}}\right)}{(\gamma^2-1)^{3/2}}\right]^{1/2} \\
&= \frac{\sqrt{3/2}}{(1+q)^{7/6}}\frac{\gamma}{(1-\gamma^2)^{1/2}}\left[\frac{q}{1+q}\bar{a}^2+\frac{2}{5}\left(\frac{1+\gamma^2}{2\gamma^{4/3}}+q^{5/3}\right)\right] \\
&\quad\times\left[\frac{\sqrt{1+\gamma^{4/3}\bar{a}^2-\gamma^2}}{\gamma^{4/3}\bar{a}^2}-\frac{\tanh^{-1}\left(\sqrt{\frac{1-\gamma^2}{1+\gamma^{4/3}\bar{a}^2-\gamma^2}}\right)}{(1-\gamma^2)^{1/2}}\right]^{1/2}. \qquad \text{(A.3)}
\end{aligned}
$$

Because the secondary lies along α_2, the integrand $r^2-\alpha_2^2 = a^2-\alpha_2^2$ becomes $\gamma^{4/3}\bar{a}^2-\gamma^2$ when scaled by α_1^2.

The final simplifications in each prolate case, which may not be obvious, stem from the terms with $\left(\gamma^2-1\right)^{1/2}$ and $\left(\gamma^2-1\right)^{3/2}$, which are necessarily complex since $0<\gamma<1$. Their manipulation is based on the rules of algebra with complex numbers that can easily lead to sign errors. The imaginary part of terms such as $\left(\gamma^2-1\right)^{3/2}$ are easily extracted by any number of means, including

$$
\frac{1}{(\gamma^2-1)^{3/2}} = \frac{1}{\left[(-1)^{3/2}(1-\gamma^2)^{3/2}\right]} = \frac{1}{i^3(1-\gamma^2)^{3/2}}
$$

$$= \frac{1}{-i\left(1-\gamma^2\right)^{3/2}} = \frac{i}{\left(1-\gamma^2\right)^{3/2}}$$

or

$$\frac{1}{\left(\gamma^2-1\right)^{3/2}} = \frac{\left(\gamma^2-1\right)^{1/2}}{\left(\gamma^2-1\right)^2} = \frac{i\left(1-\gamma^2\right)^{1/2}}{\left(1-\gamma^2\right)^2} = \frac{i}{\left(1-\gamma^2\right)^{3/2}}. \qquad \text{(A.4)}$$

An important point is the sign difference between the above and $\left(1/\left(\gamma^2-1\right)\right)^{3/2}$,

$$\left(\frac{1}{\gamma^2-1}\right)^{3/2} = \left(\frac{1}{(-1)\left(1-\gamma^2\right)}\right)^{3/2} = \left(\frac{1}{-1}\right)^{3/2}\left(\frac{1}{1-\gamma^2}\right)^{3/2}$$
$$= (-1)^{3/2}\left(\frac{1}{1-\gamma^2}\right)^{3/2} = \frac{-i}{\left(1-\gamma^2\right)^{3/2}} \qquad \text{(A.5)}$$

where the second and third steps are allowed because both terms are real. The difference in the order of operations picks up a sign difference between raising to a power then inverting compared to inverting then raising to a power. *Mathematica* tends to output equations in the latter form, and this can easily lead to sign confusion if one naively expects the two syntaxes to be equivalent. The term $1/\sqrt{\gamma^2-1}$ also appears and is simply $-i/\sqrt{1-\gamma^2}$.

In both prolate cases, the inverse tangent term reduces to the form $i\tan^{-1}(-iz)$, which is simply $\tanh^{-1} z$. Also, in these cases, the argument z of the $\tanh^{-1} z$ function is always greater than one. When $z > 1$, the $\tanh^{-1} z$ function has an imaginary component that exactly cancels the purely imaginary term with π in the numerator. Thus, one can simply write $\mathrm{Re}[\tanh^{-1} z]$ in place of both terms. Rather than writing the real part of a function, one can write

$$\mathrm{Re}\left[\tanh^{-1} z\right] = \tanh^{-1}\left(\frac{1}{z}\right), \qquad \text{(A.6)}$$

which is purely real. Thus, all imaginary parts have been cancelled and the expression for the angular momentum is greatly reduced for the prolate cases. No similar simplifications can be done for the oblate case since only terms with $\left(1-\gamma^2\right)^{m/2}$ where m is an integer appear, and these terms are strictly real for $0 < \gamma < 1$. With the proper diligence, we arrive at the final equations for the oblate and prolate cases in Section 2.7.

BIBLIOGRAPHY

H. R. Aggarwal and V. R. Oberbeck. Roche Limit of a Solid Body. *Astrophysical Journal*, 191:577–588, July 1974.

L. A. M. Benner, M. C. Nolan, J. L. Margot, M. Brozovic, S. J. Ostro, M. K. Shepard, C. Magri, J. D. Giorgini, and M. W. Busch. Arecibo and Goldstone Radar Imaging of Contact Binary Near-Earth Asteroids. In *AAS/Division for Planetary Sciences Meeting Abstracts*, volume 40 of *AAS/Division for Planetary Sciences Meeting Abstracts*, September 2008a.

L. A. M. Benner, M. C. Nolan, S. J. Ostro, J. D. Giorgini, D. P. Pray, A. W. Harris, C. Magri, and J.-L. Margot. Near-Earth Asteroid 2005 CR37: Radar Images and Photometry of a Candidate Contact Binary. *Icarus*, 182:474–481, June 2006.

L. A. M. Benner, S. J. Ostro, C. Magri, M. C. Nolan, E. S. Howell, J. D. Giorgini, R. F. Jurgens, J. L. Margot, P. A. Taylor, M. W. Busch, and M. K. Shepard. Near-Earth Asteroid Surface Roughness Depends on Compositional Class. *Icarus*, 198:294–304, December 2008b.

R. P. Binzel, D. Lupishko, M. di Martino, R. J. Whiteley, and G. J. Hahn. Physical Properties of Near-Earth Objects. *Asteroids III*, pages 255–271, 2002.

W. F. Bottke and H. J. Melosh. Binary Asteroids and the Formation of Doublet Craters. *Icarus*, 124:372–391, December 1996a.

W. F. Bottke and H. J. Melosh. The Formation of Asteroid Satellites and Doublet Craters by Planetary Tidal Forces. *Nature*, 381:51–53, May 1996b.

W. F. Bottke, D. Vokrouhlický, D. P. Rubincam, and M. Broz. The Effect of Yarkovsky Thermal Forces on the Dynamical Evolution of Asteroids and Meteoroids. *Asteroids III*, pages 395–408, 2002.

D. T. Britt, D. Yeomans, K. Housen, and G. Consolmagno. Asteroid Density, Porosity, and Structure. *Asteroids III*, pages 485–500, 2002.

D. Brouwer and G. M. Clemence. *Methods of Celestial Mechanics*. New York: Academic Press, 1961.

N. Button. On the Compactibility of Snow Into Spheres. *Physics Review S*, 1:1, December 2008.

R. M. Canup. A Giant Impact Origin of Pluto-Charon. *Science*, 307:546–550, January 2005.

D. Capek and D. Vokrouhlický. The YORP Effect with Finite Thermal Conductivity. *Icarus*, 172:526–536, December 2004.

S. Chandrasekhar. *Ellipsoidal Figures of Equilibrium*. New Haven, CT: Yale University, 1969.

C. R. Chapman, J. Veverka, P. C. Thomas, K. Klaasen, M. J. S. Belton, A. Harch, A. McEwen, T. V. Johnson, P. Helfenstein, M. E. Davies, W. J. Merline, and T. Denk. Discovery and Physical Properties of Dactyl a Satellite of Asteroid 243 Ida. *Nature*, 374:783–785, April 1995.

B. V. Chirikov. A Universal Instability of Many-Dimensional Oscillator Systems. *Physics Reports*, 1979.

J. W. Christy and R. S. Harrington. The Satellite of Pluto. *Astronomical Journal*, 83: 1005–1008, August 1978.

G. Colombo. Rotational Period of the Planet Mercury. *Nature*, 208:575, 1965.

M. Ćuk and J. A. Burns. Effects of Thermal Radiation on the Dynamics of Binary NEAs. *Icarus*, 176:418–431, August 2005.

G. H. Darwin. On the Bodily Tides of Viscous and Semi-Elastic Spheroids, and on the Ocean Tides upon a Yielding Nucleus. *Philosophical Transactions of the Royal Society of London*, 170:1–35, 1879.

G. H. Darwin. On the Secular Changes in the Elements of the Orbit of a Satellite Revolving about a Tidally Distorted Planet. *Proceedings of the Royal Society of London*, 30:1–10, 1880.

H. Demura, S. Kobayashi, E. Nemoto, N. Matsumoto, M. Furuya, A. Yukishita, N. Muranaka, H. Morita, K. Shirakawa, M. Maruya, H. Ohyama, M. Uo, T. Kubota, T. Hashimoto, J. Kawaguchi, A. Fujiwara, J. Saito, S. Sasaki, H. Miyamoto, and N. Hirata. Pole and Global Shape of 25143 Itokawa. *Science*, 312:1347–1349, June 2006.

P. Descamps and F. Marchis. Angular Momentum of Binary Asteroids: Implications for Their Possible Origin. *Icarus*, 193:74–84, January 2008.

P. Descamps, F. Marchis, T. Michalowski, F. Vachier, F. Colas, J. Berthier, M. Assafin, P. B. Dunckel, M. Polinska, W. Pych, D. Hestroffer, K. P. M. Miller, R. Vieira-Martins, M. Birlan, J.-P. Teng-Chuen-Yu, A. Peyrot, B. Payet, J. Dorseuil, Y. Léonie, and T. Dijoux. Figure of the Double Asteroid 90 Antiope from Adaptive Optics and Lightcurve Observations. *Icarus*, 187:482–499, April 2007.

D. D. Durda, W. F. Bottke, B. L. Enke, W. J. Merline, E. Asphaug, D. C. Richardson, and Z. M. Leinhardt. The Formation of Asteroid Satellites in Large Impacts: Results from Numerical Simulations. *Icarus*, 170:243–257, July 2004.

E. G. Fahnestock and D. J. Scheeres. Primary Surface Particle Motion as a Mechanism for YORP-Driven Binary Asteroid Evolution. In *AAS/Division for Planetary Sci-*

ences Meeting Abstracts, volume 40 of *AAS/Division for Planetary Sciences Meeting Abstracts*, September 2008.

S. Fornasier, A. Migliorini, E. Dotto, and M. A. Barucci. Visible and Near Infrared Spectroscopic Investigation of E-type Asteroids, Including 2867 Steins, a Target of the Rosetta Mission. *Icarus*, 196:119–134, July 2008.

J. W. Fowler and J. R. Chillemi. IRAS Asteroid Data Processing. *The IRAS Minor Planet Survey*, pages 17–43, 1992.

B. Gladman, P. Michel, and C. Froeschlé. The Near-Earth Object Population. *Icarus*, 146:176–189, July 2000.

B. J. Gladman, F. Migliorini, A. Morbidelli, V. Zappala, P. Michel, A. Cellino, C. Froeschle, H. F. Levison, M. Bailey, and M. Duncan. Dynamical Lifetimes of Objects Injected into Asteroid Belt Resonances. *Science*, 277:197–201, 1997.

P. Goldreich. On the Eccentricity of Satellite Orbits in the Solar System. *Monthly Notices of the Royal Astronomical Society*, 126:257–268, 1963.

P. Goldreich. History of the Lunar Orbit. *Reviews of Geophysics and Space Physics*, 4: 411–439, 1966.

P. Goldreich and S. Peale. Spin-orbit Coupling in the Solar System. *Astronomical Journal*, 71:425–438, August 1966.

P. Goldreich and R. Sari. Tidal Evolution of Rubble Piles. *Astrophysical Journal*, 691: 54–60, January 2009.

P. Goldreich and S. Soter. Q in the Solar System. *Icarus*, 5:375–389, July 1966.

V. Guibout and D. J. Scheeres. Stability of Surface Motion on a Rotating Ellipsoid. *Celestial Mechanics and Dynamical Astronomy*, 87:263–290, November 2003.

A. W. Harris. The Rotation Rates of Very Small Asteroids: Evidence for 'Rubble Pile' Structure. In *Lunar and Planetary Institute Conference Abstracts*, page 493, March 1996.

A. W. Harris, E. G. Fahnestock, and P. Pravec. Regulation of Primary Spin Rate of Asynchronous Binary Asteroids by "Tidal Saltation". In *AAS/Division of Dynamical Astronomy Meeting*, volume 39 of *AAS/Division of Dynamical Astronomy Meeting*, May 2008.

A. W. Harris and W. R. Ward. Dynamical Constraints on the Formation and Evolution of Planetary Bodies. *Annual Review of Earth and Planetary Sciences*, 10:61–108, 1982.

K. A. Holsapple. Formation of Binary Asteroids by Spin Fission. In *Lunar and Planetary Institute Conference Abstracts*, volume 38 of *Lunar and Planetary Inst. Technical Report*, page 2440, March 2007.

R. S. Hudson. Three-Dimensional Reconstruction of Asteroids from Radar Observations. *Remote Sensing Reviews*, 8:195–203, 1993.

R. S. Hudson and S. J. Ostro. Shape of Asteroid 4769 Castalia (1989 PB) from Inversion of Radar Images. *Science*, 263:940–943, February 1994.

R. S. Hudson, S. J. Ostro, and A. W. Harris. Constraints on Spin State and Hapke Parameters of Asteroid 4769 Castalia Using Lightcurves and a Radar-Derived Shape Model. *Icarus*, 130:165–176, November 1997.

H. Jeffreys. The Effect of Tidal Friction on Eccentricity and Inclination. *Monthly Notices of the Royal Astronomical Society*, 122:339–343, 1961.

M. Kaasalainen, T. Kwiatkowski, M. Abe, J. Piironen, T. Nakamura, Y. Ohba, B. Dermawan, T. Farnham, F. Colas, S. Lowry, P. Weissman, R. J. Whiteley, D. J. Tholen,

S. M. Larson, M. Yoshikawa, I. Toth, and F. P. Velichko. CCD Photometry and Model of MUSES-C Target (25143) 1998 SF36. *Astronomy and Astrophysics*, 405:L29–L32, July 2003.

M. Kaasalainen, J. Ďurech, B. D. Warner, Y. N. Krugly, and N. M. Gaftonyuk. Acceleration of the Rotation of Asteroid 1862 Apollo by Radiation Torques. *Nature*, 446: 420–422, March 2007.

W. M. Kaula. Tidal Dissipation by Solid Friction and the Resulting Orbital Evolution. *Reviews of Geophysics*, 2:661–685, 1964.

A. E. H. Love. *A Treatise on the Mathematical Theory of Elasticity*. New York : Dover, 1944.

S. C. Lowry, A. Fitzsimmons, P. Pravec, D. Vokrouhlický, H. Boehnhardt, P. A. Taylor, J. L. Margot, A. Galád, M. Irwin, J. Irwin, and P. Kusnirák. Direct Detection of the Asteroidal YORP Effect. *Science*, 316:272–274, April 2007.

G. J. F. MacDonald. Tidal Friction. *Reviews of Geophysics and Space Physics*, 2:467–541, 1964.

C. Magri, S. J. Ostro, D. J. Scheeres, M. C. Nolan, J. D. Giorgini, L. A. M. Benner, and J. L. Margot. Radar Observations and a Physical Model of Asteroid 1580 Betulia. *Icarus*, 186:152–177, January 2007.

F. Marchis, P. Descamps, M. Baek, A. W. Harris, M. Kaasalainen, J. Berthier, D. Hestroffer, and F. Vachier. Main Belt Binary Asteroidal Systems with Circular Mutual Orbits. *Icarus*, 196:97–118, July 2008a.

F. Marchis, P. Descamps, J. Berthier, D. Hestroffer, F. Vachier, M. Baek, A. W. Harris, and D. Nesvorný. Main Belt Binary Asteroidal Systems with Eccentric Mutual Orbits. *Icarus*, 195:295–316, May 2008b.

F. Marchis, D. Hestroffer, P. Descamps, J. Berthier, A. H. Bouchez, R. D. Campbell, J. C. Y. Chin, M. A. van Dam, S. K. Hartman, E. M. Johansson, R. E. Lafon, D. Le Mignant, I. de Pater, P. J. Stomski, D. M. Summers, F. Vachier, P. L. Wizinovich, and M. H. Wong. A Low Density of 0.8 g cm^{-3} for the Trojan Binary Asteroid 617 Patroclus. *Nature*, 439:565–567, February 2006.

J. L. Margot and M. E. Brown. A Low-Density M-type Asteroid in the Main Belt. *Science*, 300:1939–1942, June 2003.

J. L. Margot, M. C. Nolan, L. A. M. Benner, S. J. Ostro, R. F. Jurgens, J. D. Giorgini, M. A. Slade, and D. B. Campbell. Binary Asteroids in the Near-Earth Object Population. *Science*, 296(5572):1445–1448, May 2002.

J. L. Margot, P. Pravec, M. C. Nolan, E. S. Howell, L. A. M. Benner, J. D. Giorgini, Jurgens R. F., S. J. Ostro, M. A. Slade, C. Magri, P. A. Taylor, P. D. Nicholson, and D. B. Campbell. Hermes as an Exceptional Case Among Binary Near-Earth Asteroids. In *IAU General Assembly*, 2006.

W. J. Merline, L. M. Close, C. Dumas, J. C. Shelton, F. Menard, C. R. Chapman, and D. C. Slater. Discovery of Companions to Asteroids 762 Pulcova and 90 Antiope by Direct Imaging. In *Bulletin of the American Astronomical Society*, volume 32 of *Bulletin of the American Astronomical Society*, page 1017, October 2000a.

W. J. Merline, L. M. Close, J. C. Shelton, C. Dumas, F. Menard, C. R. Chapman, D. C. Slater, and W. M. Keck II Telescope. Satellites of Minor Planets. *IAU Circulars*, 7503:3, October 2000b.

W. J. Merline, S. J. Weidenschilling, D. D. Durda, J. L. Margot, P. Pravec, and A.D. Storrs. Asteroids Do Have Satellites. *Asteroids III*, pages 289–312, 2002.

T. Michałowski, P. Bartczak, F. P. Velichko, A. Kryszczyńska, T. Kwiatkowski, S. Breiter, F. Colas, S. Fauvaud, A. Marciniak, J. Michałowski, R. Hirsch, R. Behrend, L. Bernasconi, C. Rinner, and S. Charbonnel. Eclipsing Binary Asteroid 90 Antiope. *Astronomy and Astrophysics*, 423:1159–1168, September 2004.

W. H. Munk and G. J. F. MacDonald. *The Rotation of the Earth*. Cambridge University Press, 1960.

C. D. Murray and S. F. Dermott. *Solar System Dynamics*. Cambridge University Press, 1999.

M. C. Nolan, E. S. Howell, and G. Miranda. Radar Images of Binary Asteroid 2003 YT1. In *Bulletin of the American Astronomical Society*, volume 36 of *Bulletin of the American Astronomical Society*, page 1132, November 2004.

K. S. Noll, W. M. Grundy, E. I. Chiang, J.-L. Margot, and S. D. Kern. *Binaries in the Kuiper Belt*, pages 345–363. The Solar System Beyond Neptune, 2008.

S. J. Ostro. Planetary Radar Astronomy. *Rev. Modern Phys.*, 65:1235–1279, 1993.

S. J. Ostro, L. A. M. Benner, M. C. Nolan, C. Magri, J. D. Giorgini, D. J. Scheeres, S. B. Broschart, M. Kaasalainen, D. Vokrouhlický, S. R. Chesley, J.-L. Margot, R. F. Jurgens, R. Rose, D. K. Yeomans, S. Suzuku, and E. M. de Jong. Radar Observations of Asteroid 25143 Itokawa (1998 SF36). *Meteoritics and Planetary Science*, 39:407–424, March 2004.

S. J. Ostro, J.-L. Margot, L. A. M. Benner, J. D. Giorgini, D. J. Scheeres, E. G. Fahnestock, S. B. Broschart, J. Bellerose, M. C. Nolan, C. Magri, P. Pravec, P. Scheirich, R. Rose, R. F. Jurgens, E. M. De Jong, and S. Suzuki. Radar Imaging of Binary Near-Earth Asteroid (66391) 1999 KW4. *Science*, 314:1276–1280, November 2006.

J.-M. Petit and O. Mousis. KBO binaries: How Numerous were They? *Icarus*, 168: 409–419, April 2004.

J. J. Petrovic. Mechanical Properties of Ice and Snow. *Journal of Materials Science*, 38:1–6, January 2003.

G. H. Pettengill and R. B. Dyce. A Radar Determination of the Rotation of the Planet Mercury. *Nature*, 206:1240, 1965.

P. Pravec and A. W. Harris. Binary Asteroid Population 1. Angular Momentum Content. *Icarus*, 190:250–259, September 2007.

P. Pravec, A. W. Harris, and B. D. Warner. NEA Rotations and Binaries. In G. B. Valsecchi, D. Vokrouhlický, and A. Milani, editors, *IAU Symposium*, volume 236 of *IAU Symposium*, pages 167–176, 2007.

P. Pravec, P. Scheirich, P. Kušnirák, L. Šarounová, S. Mottola, G. Hahn, P. Brown, G. Esquerdo, N. Kaiser, Z. Krzeminski, D. P. Pray, B. D. Warner, A. W. Harris, M. C. Nolan, E. S. Howell, L. A. M. Benner, J.-L. Margot, A. Galád, W. Holliday, M. D. Hicks, Y. N. Krugly, D. Tholen, R. Whiteley, F. Marchis, D. R. Degraff, A. Grauer, S. Larson, F. P. Velichko, W. R. Cooney, R. Stephens, J. Zhu, K. Kirsch, R. Dyvig, L. Snyder, V. Reddy, S. Moore, Š. Gajdoš, J. Világi, G. Masi, D. Higgins, G. Funkhouser, B. Knight, S. Slivan, R. Behrend, M. Grenon, G. Burki, R. Roy, C. Demeautis, D. Matter, N. Waelchli, Y. Revaz, A. Klotz, M. Rieugné, P. Thierry, V. Cotrez, L. Brunetto, and G. Kober. Photometric Survey of Binary Near-Earth Asteroids. *Icarus*, 181:63–93, March 2006.

D. C. Richardson, W. F. Bottke, and S. G. Love. Tidal Distortion and Disruption of Earth-Crossing Asteroids. *Icarus*, 134:47–76, July 1998.

D. C. Richardson and K. J. Walsh. Binary Minor Planets. *Annual Review of Earth and Planetary Sciences*, 34:47–81, May 2006.

D. P. Rubincam. Radiative Spin-up and Spin-down of Small Asteroids. *Icarus*, 148: 2–11, November 2000.

D. J. Scheeres. Relative Equilibria for General Gravity Fields in the Sphere-Restricted Full 2-Body Problem. *Celestial Mechanics and Dynamical Astronomy*, 94:317–349, March 2006.

D. J. Scheeres. Rotational Fission of Contact Binary Asteroids. *Icarus*, 189:370–385, August 2007.

D. J. Scheeres, M. Abe, M. Yoshikawa, R. Nakamura, R. W. Gaskell, and P. A. Abell. The Effect of YORP on Itokawa. *Icarus*, 188:425–429, June 2007.

D. J. Scheeres, E. G. Fahnestock, S. J. Ostro, J.-L. Margot, L. A. M. Benner, S. B. Broschart, J. Bellerose, J. D. Giorgini, M. C. Nolan, C. Magri, P. Pravec, P. Scheirich, R. Rose, R. F. Jurgens, E. M. De Jong, and S. Suzuki. Dynamical Configuration of Binary Near-Earth Asteroid (66391) 1999 KW4. *Science*, 314:1280–1283, November 2006.

D. C. Stephens and K. S. Noll. Detection of Six Trans-Neptunian Binaries with NICMOS: A High Fraction of Binaries in the Cold Classical Disk. *Astronomical Journal*, 131:1142–1148, February 2006.

P. A. Taylor and J. L. Margot. Tidal Evolution of Solar System Binaries. In *AAS/Division for Planetary Sciences Meeting Abstracts*, volume 39 of *AAS/Division for Planetary Sciences Meeting Abstracts*, October 2007.

P. A. Taylor and J. L. Margot. Tidal Evolution of Binary Asteroids: Eccentric Mutual Orbits and Contact Binary Formation. In *AAS/Division for Planetary Sciences Meet-*

ing Abstracts, volume 40 of *AAS/Division for Planetary Sciences Meeting Abstracts*, September 2008.

P. A. Taylor, J. L. Margot, M. C. Nolan, L. A. M. Benner, S. J. Ostro, J. D. Giorgini, and C. Magri. The Shape, Mutual Orbit, and Tidal Evolution of Binary Near-Earth Asteroid 2004 DC. *LPI Contributions*, 1405:8322, 2008.

P. A. Taylor, J. L. Margot, D. Vokrouhlický, D. J. Scheeres, P. Pravec, S. C. Lowry, A. Fitzsimmons, M. C. Nolan, S. J. Ostro, L. A. M. Benner, J. D. Giorgini, and C. Magri. Spin Rate of Asteroid (54509) 2000 PH5 Increasing due to the YORP Effect. *Science*, 316:274–277, April 2007.

J. Touma and J. Wisdom. Evolution of the Earth-Moon System. *Astronomical Journal*, 108:1943–1961, November 1994.

K. J. Walsh and D. C. Richardson. Binary Near-Earth Asteroid Formation: Rubble Pile Model of Tidal Disruptions. *Icarus*, 180:201–216, January 2006.

K. J. Walsh and D. C. Richardson. A Steady-State Model of NEA Binaries Formed by Tidal Disruption of Gravitational Aggregates. *Icarus*, 193:553–566, February 2008.

K. J. Walsh, D. C. Richardson, and P. Michel. Rotational Breakup as the Origin of Small Binary Asteroids. *Nature*, 454:188–191, July 2008.

S. J. Weidenschilling, P. Paolicchi, and V. Zappalà. Do Asteroids Have Satellites? In R. P. Binzel, T. Gehrels, and M. S. Matthews, editors, *Asteroids II*, pages 643–660. University of Arizona Press, 1989.

J. Wisdom, S. J. Peale, and F. Mignard. The Chaotic Rotation of Hyperion. *Icarus*, 58: 137–152, May 1984.

C. F. Yoder. Effect of Resonance Passage on the Tidal Evolution of Phobos' Orbit. In *Bulletin of the American Astronomical Society*, volume 13 of *Bulletin of the American Astronomical Society*, page 710, June 1981.